LIPID NANOPARTICLES IN THERMORESPONSIVE GEL FOR TOPICAL APPLICATION

LIM QIAN YING

FACULTY OF SCIENCE
UNIVERSITY OF MALAYA
KUALA LUMPUR

2018

LIPID NANOPARTICLES IN THERMORESPONSIVE GEL FOR TOPICAL APPLICATION

LIM QIAN YING

DISSERTATION SUBMITTED IN FULFILMENT OF THE REQUIREMENTS FOR THE DEGREE OF MASTER OF SCIENCE

DEPARTMENT OF CHEMISTRY
FACULTY OF SCIENCE
UNIVERSITY OF MALAYA
KUALA LUMPUR

2018

UNIVERSITY OF MALAYA
ORIGINAL LITERARY WORK DECLARATION

Name of Candidate: Lim Qian Ying

[redacted]

Matric No: SGR150063

Name of Degree: Master of Science (Except Mathematics and Science Philosophy)

Title of Project Paper/Research Report/Dissertation/Thesis ("this Work"):

"LIPID NANOPARTICLES IN THERMORESPONSIVE GEL FOR TOPICAL APPLICATION"

Field of Study: Physical Chemistry

I do solemnly and sincerely declare that:

(1) I am the sole author/writer of this Work;
(2) This Work is original;
(3) Any use of any work in which copyright exists was done by way of fair dealing and for permitted purposes and any excerpt or extract from, or reference to or reproduction of any copyright work has been disclosed expressly and sufficiently and the title of the Work and its authorship have been acknowledged in this Work;
(4) I do not have any actual knowledge nor do I ought reasonably to know that the making of this work constitutes an infringement of any copyright work;
(5) I hereby assign all and every rights in the copyright to this Work to the University of Malaya ("UM"), who henceforth shall be owner of the copyright in this Work and that any reproduction or use in any form or by any means whatsoever is prohibited without the written consent of UM having been first had and obtained;
(6) I am fully aware that if in the course of making this Work I have infringed any copyright whether intentionally or otherwise, I may be subject to legal action or any other action as may be determined by UM.

Candidate's Signature [redacted] Date: 26/12/2017

Subscribed and solemnly declared before,

[redacted]

Date: 26-12-2017

Name: PROFESSOR DR. MISNI BIN MISRAN

Designation: Supervisor

Dr. Misni Misran
Professor
Department of Chemistry
University of Malaya, Lembah Pantai
50603 Kuala Lumpur, Malaysia

ABSTRACT

Medicated topical gel having thermoresponsive feature is advantageous with respect to spreadability and drug delivery. However, gels are restricted by insolubility due to the hydrophobic drug compounds used and chemical degradation of active compounds in an aqueous system. Therefore, lipid nanoparticles are incorporated as a carrier for the active ingredients. In present work, *alpha*-tocopherol and hydroquinone were loaded in lecithin-fatty acid nanoparticles which was then incorporated into a thermoresponsive gel, consisting of carboxymethyl cellulose (CMC) and *iota*-carrageenan (*ι*-C). Temperature and Ca^{2+} ions effect on the rheological behavior of the prepared gel mixture was investigated. The nanostructured lipid carrier (NLC) was evaluated for its mean particle size, zeta potential, morphology, encapsulation efficiency and *in vitro* release. Physicochemical characterization showed that both *alpha*-tocopherol and hydroquinone loaded NLCs being stored at 4 ˚C were stable for 30 days, while the encapsulation efficiency was different more than 30% due to the distinct hydrophobicity. *In vitro* release studies showed that NLC had the capability to slow release both the hydrophobic and hydrophilic active ingredients. Meanwhile, a gel system was formulated to transform from gel-like to liquid-like consistency in the vicinity of body temperature. NLC gave advantages to the pure gel system as the NLC-gel showed slightly higher elasticity, indicating contribution of NLC to rigidity of the gel system. Nevertheless, the effect of NLC on gelling point was negligible. These results suggest that gel mixture of CMC and *ι*-C is likely to be developed as a thermoresponsive gel while NLC is a potential active ingredient carrier system in topical application.

ABSTRAK

Gel topikal berubat yang peka terhadap suhu amat berguna dalam keupayaan untuk menyebar dan pengangkutan ubat. Walau bagaimanapun, kegunaan gel selalu terhad oleh masalah kelarutan ubat hidrofobik dan degradasi bahan aktif secara kimia dalam sistem akueus. Oleh itu, lipid zarah nano diperkenalkan sebagai pembawa untuk bahan aktif ini. Dalam kajian ini, *alfa*-tokoferol dan hidrokuinon dimuatkan dalam zarah nano yang diperbuat daripada lecitin dan asid lemak dan seterusnya diperkenalkan ke dalam gel peka suhu yang mengandungi karboksimetil selulosa (CMC) dan *iota*-karagenan (*ι*-C). Kesan suhu dan kation pada kelakuan reologi gel campuran yang disediakan disiasati. Purata saiz, keupayaan Zeta, morfologi, kecekapan pengkapsulan dan pelepasan *in vitro* bagi pembawa lipid berstruktur-nano (NLC) dinilaikan. Pencirian fizikokimia menunjukkan bahawa kedua-dua NLC yang dimuatkan oleh *alfa*-tokoferol dan hidrokuinon adalah stabil selama 30 hari apabila disimpan pada suhu 4 ˚C, namun kecekapan pengkapsulan berbeza lebih daripada 30% disebabkan oleh sifat hidrofobik yang berbeza. Kajian pelepasan *in vitro* membuktikan bahawa NLC berupaya untuk melepaskan kedua-dua bahan aktif hidrofobik dan hidrofilik secara perlahan. Sementara itu, satu sistem gel yang berubah daripada gel ke cecair pada suhu di sekitar suhu badan telah diformulasikan. NLC memberikan kelebihan kepada sistem gel tulen memandangkan NLC-gel menunjukkan kekenyalan yang lebih tinggi, menyatakan sumbangan NLC terhadap ketegaran sistem gel. Walau bagaimanapun, kesan NLC pada suhu pembentukan gel boleh diabaikan. Keputusan tersebut mencadangkan bahawa gel campuran CMC dan *ι*-C adalah berkemungkinan untuk dibangunkan sebagai gel peka suhu manakala NLC merupakan sistem pembawa bahan aktif yang berpotensi dalam aplikasi topikal.

ACKNOWLEDGEMENTS

I would like to express my deepest gratitude to my supervisor, Prof. Dr. Misni Misran for his patient guidance and useful comments on this project. He had been sharing his experiences and knowledge to his students liberally and his willingness to give his precious time generously was greatly appreciated.

I am also grateful for the valuable and constructive suggestions given by the members of Colloid and Surfaces Laboratory including Dr. Anita Marlina, Mr. Vicit Rizal Eh Suk, Dr. Yew Han Choi, Ms. Premanarayani Menon, Ms. Tiew Shu Xian, Mrs. Sumaira Naeem, Mr. Tang Nyiak Tao, Ms. Rabi'Atul'Adawiyah, Ms. Farhanim and others. Advices given by them had been a great help in planning and development of this research work. Furthermore, my special thanks are extended to the Ministry of Science, Technology and Innovation (MOSTI) and University of Malaya that have provided financial support for the entire project. Also thanks to the staff of Department of Chemistry, University of Malaya for their kind assistance throughout the study period.

Finally, I am particularly appreciative of the continuous support from my beloved family and friends who have been encouraging and inspiring me throughout my study.

TABLE OF CONTENTS

LIST OF FIGURES

LIST OF TABLES

LIST OF SYMBOLS AND ABBREVIATIONS

BEMT	:	Bis-ethylhexyloxyphenol methoxyphenyl triazine
CMC	:	Carboxymethyl cellulose
CoQ10	:	Coenzyme-Q_{10}
DLS	:	Dynamic light scattering
DSC	:	Differential scanning calorimetry
FESEM	:	Field emission scanning electron microscope
HLB	:	Hydrophilic-lipophilic balance
LCST	:	Low critical solution temperature
LVR	:	Linear viscoelastic region
NIBS	:	Non-invasive backscatter
NLC	:	Nanostructured lipid carriers
o/w	:	Oil-in-water
OCT	:	2-Ethylhexyl-2-cyano-3,3-diphenylacrylate
OMC	:	2-Ethylhexyl trans-4-methoxycinnamate
OPM	:	Optical Polarizing Microscope
PAA	:	Poly(acrylic acid)
PBS	:	Phosphate buffer saline
PDEAAm	:	Poly(*N,N*-diethylacrylamide)
PDI	:	Polydispersity index
PLI	:	Power-Law index
PMAA	:	Poly(methacrylic acid)
PNIPAM	:	Poly(*N*-isopropylacrylamide)
SLN	:	Solid lipid nanoparticles
SPF	:	Sun protector factor

TEM	:	Transmission electron microscope
UCST	:	Upper critical solution temperature
UV	:	Ultraviolet
UV-vis	:	Ultraviolet-visible
w/o	:	Water-in-oil
ι-C	:	*iota*-Carrageenan
$\dot{\gamma}$	:	Shear rate
ΔH	:	Melting enthalpy
ΔHf_{298}	:	Bond dissociation energy
$\Delta T_{1/2}$	:	Peak width at half minimum
C_1	:	Stress constant
C_2	:	Strain constant
f	:	Frequency
G'	:	Storage modulus
G''	:	Loss modulus
n	:	Power-Law index
r	:	Diameter of measuring geometry cone and plate
R^2	:	Coefficient of determination
$R^2_{adj.}$	:	Adjusted coefficient of determination
T	:	Temperature
T_c	:	Crossover temperature
T_m	:	Melting point
γ_c	:	Critical strain
δ	:	Phase angle
η	:	Viscosity
θ	:	Angular displacement

θ_G	:	Cone angle of measuring geometry cone and plate
λ	:	Wavelength
$\boldsymbol{\sigma}$	:	Shear stress
σ_y	:	Yield stress
τ	:	Torque
ω	:	Angular velocity
γ	:	Shear strain

CHAPTER 1: INTRODUCTION

1.1 General introduction

Personal appearance is always related to first impression, self-esteem and self-confidence although it is an often disregarded part of communication skills. As such, people today are more concerned about taking care of their appearance. This has allowed a rapid growth in the cosmetic industry in the last 20 years, where the global beauty market had grown by 4.5% a year on average, proving its ability to achieve stable and continuous growth, even in unfavorable economic conditions (Lopaciuk & Loboda, 2013). In order to design an appropriate cosmetic formulation, understanding how the skin functions is necessary. Being the largest organ of our body, the skin interfaces with the environment and protects the body against pathogens and excessive water loss, making it vital in guarding muscles, bones, ligaments and internal organs. There are many skin types, ranging from dry to oily, providing a diverse habitat for various bacteria, which causes skin problems and diseases. The outer most layer of skin, known as epidermis, has no blood vessels and is nourished by diffusion of liquid and nutrients from the dermis. Therefore, topical application is important to nourish the skin from the exterior (Souto & Müller, 2008).

Semisolid formulations have been in use in topical application since the ancient times. Both cream and gel systems are well established for topical delivery of drugs and active ingredients to supplement the skin in pharmaceutical and cosmetic industries. During the development of novel topical formulations, stability and shelf life become the main concern. Gel formulations are considered superior to cream formulations, which are always limited by potential separation problems. Moreover, the absence of greasiness and residue upon application on haired skin adds credit to the gel formulations (Beaurline *et al.*, 1999; Richter & Steiger, 1999). Nonetheless, gels are

restricted by insolubility or degradation of active ingredients in the aqueous system and, in some cases, poor spreadability on skin upon usage. For a gel system with good spreadability and stability, the gel has to remain as a solid at room temperature and easily flow when applied to the skin. Therefore, a thermoresponsive material falls in the priority of choices to produce a gel system with such properties. Alternatively, a carrier system can be incorporated into the gel system to deliver hydrophobic active ingredients, while at the same time protecting the active ingredients from chemical degradation by the surrounding dispersion medium.

Solid lipid nanoparticles (SLN), an alternative carrier system to emulsions, liposomes and polymeric nanoparticles, were developed at the beginning of 1990s-, by replacing the liquid lipid of an emulsion with solid lipids (Lucks & Muller, 1998). While most colloidal carrier systems are designed to modify the release profile of the loaded drug, SLN has the added advantage that it has a minimum risk of toxicity as organic solvents are not involved in the production. Moreover, incorporation of a drug into the solid lipid matrix can prevent chemical degradation of the active compound, caused by the dispersing aqueous medium where the drug is easily diffused and being degraded. However, the crystalline state of nanoparticles which tends to transform into a more stable modification is associated with the risk of gelation, particle growth and potential expulsion of active compounds during storage (Freitas & Müller, 1999; Liu *et al.*, 2007; zur Mühlen *et al.*, 1998). The second generation of lipid nanoparticles, known as nanostructured lipid carriers (NLC), was developed to minimize the limitations of SLN by introducing liquid lipids into the solid lipid matrix to reduce its crystallinity (Mehnert & Mäder, 2001; Mueller *et al.*, 2000). This difference in structure increases the loading capacity of nanoparticles for active compounds. Both SLN and NLC are useful in topical application for their excellent tolerability and occlusive properties. In comparison, with direct addition of active compounds, which are sensitive to light and oxidation,

enhancement of the chemical stability of the active compounds can be achieved by loading into the lipid nanoparticles before incorporation into the semisolid formulation (Pardeike *et al.*, 2009).

Vitamin E is a lipid-soluble compound essential for health. By acting against oxidation, which is linked to numerous diseases, especially cancer and ageing, vitamin E has been merchandised for its antioxidant properties (Albanes *et al.*, 1995; Podda & Grundmann-Kollmann, 2001). Besides being taken as dietary supplements, vitamin E can be applied topically to delay ageing by nourishing the skin and protecting the cells from damaging effects caused by free radicals (Rizvi *et al.*, 2014). However, vitamin E is sensitive to light and water-insoluble, posing a problem to the formulators. In order to enhance its stability and shelf-life, vitamin E can be loaded into lipid nanoparticles for topical use.

Hydroquinone is a ubiquitous ingredient used in the cosmeceutical field for depigmentation purposes. There are various mechanisms suggested for its action, including inhibition of tyrosinase synthesis, prohibition of tyrosinase effects, which are responsible for melanin production and destruction of melanocytes. Nonetheless, it was known to cause undesirable side effects when used excessively such as ochronosis, post-inflammatory pigmentation, discoloration of nails and contact dermatitis (Agorku *et al.*, 2016; Couteau & Coiffard, 2016). In addition, formulation of hydroquinone is limited by its oxidation instability and poor skin penetration due to the hydrophilic structure. As such, a carrier system is required to load the active compound into the aqueous dispersing medium to provide an effective treatment of hydroquinone, while minimizing the dosage (Ghanbarzadeh *et al.*, 2015).

In present study, the ability of NLC to carry active ingredients with different water solubility, which were *alpha*-tocopherol (a type of Vitamin E) and hydroquinone, was

investigated. The materials used to prepare the NLC were fatty acid and lecithin that had been studied extensively to produce a stable NLC system besides their low cost and easy availability. The loaded NLC was then incorporated into a thermoresponsive gel, which exhibited flow behavior in the vicinity of body temperature. Carboxymethyl cellulose (CMC) and *iota*-carrageenan (ι-C) were chosen as the gelling polymers for their temperature-dependent gelling properties with good sensorial during application. The rheological properties and *in vitro* release profile of the samples were evaluated.

1.2 Objectives of research

1. To formulate a thermoresponsive gel system.
2. To prepare fatty acid-lecithin lipid nanoparticles for loading active ingredients *alpha*-tocopherol and hydroquinone.
3. To study *in vitro* release of active ingredients and rheology of nanolipid incorporated thermoresponsive gel.

CHAPTER 2: LITERATURE REVIEW

2.1 Topical delivery

Topical formulations are no longer simple emulsions or lotions to deliver plant extracts to nourish our skin. Actives delivery technologies are extensively developed as formulation approaches that improve stability and efficacy, while reducing irritation in a meaningful way. Topical delivery has always been the first choice, either for cosmetic or treatment of localized disease purposes, due to its convenience and pain-free self-administration. It is also considered safer and generally inexpensive compared to the other administration route such as oral and intravenous (Paudel *et al.*, 2010). Nonetheless, the main function of our skin as protection barrier has become the major disadvantage in topical application, causing poor penetration and ineffectiveness of active compounds.

Structurally, skin is made of two primary layers, known as the epidermis and dermis. The outermost sub-layer of epidermis, stratum corneum, provides protection against the intrusion of external substances into our body. Various approaches have been developed to weaken the skin barrier, so that active ingredients, drugs or even toxins may penetrate across the barrier layer. One of these approaches is the use of semisolid formulations, such as creams and gels, by targeting skin appendages that are surrounded by capillary networks, such as hair follicles and sweat glands (Zhang *et al.*, 2014). Depending on the designed delivery system, the extent and rate of transportation of active compounds can be variable due to physicochemical properties of the drugs and constituent components of the vehicle (Weiss, 2011). At the meanwhile, deep penetration into dermis layer is not desired for general topical formulations as the contacting compounds may bring adverse effects on dermal structure and more seriously systemic toxicity.

2.2 Gels

A gel system is generally defined as a network of one phase dispersed in another continuous phase, forming a three-dimensional network by either chemical covalent bonds or non-covalent interactions. To be more specific, a gel system can be defined both from structural features, based on the connectivity of the system, and also from a rheological behavior, where the system does not flow. This is characterized by the presence of a plateau region of storage modulus, *G'* and the low tan phase angle, δ at an angular frequency range from 10^{-3} to 10^{2} rad s^{-1}. There are two mechanisms of gelation, classified as chemical and physical. Chemical gelation is irreversible, whereby the weight average molecular weight diverges to infinity, while physical gelation formed by hydrogen bonds or hydrophobic interactions is a reversible transformation (Nishinari, 2009; Winter, 1987).

Hydrogels are ubiquitous biopolymers widely used in the food, cosmetic, pharmaceutical and medical sectors for their emulsifying and thickening properties. In addition, their high water content and soft consistency, similar to natural tissue, contribute to their biocompatibility (Janaswamy & Youngren, 2012; Peppas *et al.*, 2000). In topical applications, release of active compounds can be manipulated with respect to the viscosity of hydrogel. A gelled solution enhances the drug flux when the solvent or liquid phase evaporates, leaving high concentrations of drug in the evaporating vehicle, while a highly viscous gel sustains drug release by trapping the drug molecules in the porous gel network scaffold, causing hindered diffusion of the drug molecules (Aulton & Taylor, 2013). The nature of side groups of the gel molecules can also be utilized to manage the property of the gel under different environmental conditions such as pH, temperature, ionic strength and UV-irradiation. Therefore, a gel formulation can be designed to change their properties under certain conditions to serve different purposes.

2.2.1 Thermoresponsive gels

Thermoresponsive hydrogels like poly(*N*-isopropylacrylamide) (PNIPAM), poly(*N,N*-diethylacrylamide) (PDEAAm), poly(acrylic acid) (PAA) and poly(methacrylic acid) (PMAA) exhibit different gelling behavior in response to temperature changes. There are two types of thermoresponsive behavior in which gel with low critical solution temperature (LCST) becomes insoluble above a certain temperature, while gel with upper critical solution temperature (UCST) becomes soluble upon heating.

In previous years, studies for biomedical applications were mainly focused on thermoresponsive hydrogels which are liquid at ambient temperature and transform into gel at physiological temperature. This transition provides a user-friendly means for drug delivery, cell encapsulation and tissue engineering. Hydrogels with LCST are able to squeeze out the loaded drug below the LCST, due to gel collapsed by pressure generated at high temperature (Bromberg & Ron, 1998; Jeong *et al.*, 2012). In cell culture substrates, the cells attach to the hydrophobic surfaces at temperature above LCST and detach the hydrophilic surfaces at temperature below LCST (Klouda & Mikos, 2008). Similarly, a combination of deacetylated chitosan and glycerol phosphate disodium salt was investigated for its potential in tissue engineering. The formulation was reported to form gel in the vicinity of 37 ˚C and was able to maintain the bioactivity of loaded bone protein and viability of entrapped cells, then release them in the body (Chenite *et al.*, 2000). The proposed mechanisms for these reversible physical crosslinking of the polymer chains include micelle packing and coil to helix transition. The response of hydrogels towards temperature changes by swelling or contracting recently have also found its application in catalysis. The catalyst is induced to move in and out of the reactant layer according to the temperature applied, and as such playing a role as a chemical reaction on/off switch (Hapiot *et al.*, 2013).

In topical applications, a thermorsensitive poloxamers gel system was developed as a vehicle for an antifungal drug, fluconazole, which is delivered topically on to the affected area (Gandra *et al.*, 2015). The gel was formulated to transform from Newtonian (liquid-like) behavior at 20 ˚C to non-Newtonian (solid-like) behavior at 37 ˚C. Sustained release of fluconazole from the gel matrix at 37 ˚C was reported in the study. On the other hand, a method utilizing thermoresponsive hydrogel for sustained delivery of a drug to an ocular organ was invented (Fedorchak *et al.*, 2014). A liquid thermoresponsive hydrogel comprising drug loaded polymer microparticles was topically delivered to the ocular surface, wherein the drug was sustainably released for five days. *In-situ* gelation occurred in the lower fornix of the eye and therein the loaded drug was released.

Typical pharmaceutical and cosmetic formulations involve a wide range of ingredients, including electrolytes, co-solvent and surfactants. The effect of these additives on the thermoresponsive behavior of hydrogel should be taken into consideration, as the interactions between solvent and polymer directly affect the hydrophobic/hydrophilic balance within the polymer molecules, where hydrophobic interaction promotes gelation while hydrophilic interaction enhances solubility in solvent. Therefore, the extent of shifted transition temperature can be counted in (Schmaljohann, 2006).

Despite the concepts of thermoresponsive hydrogels being sound in research to date, the practical application in industry is not common due to its slow response time and poor biocompatibility. Hence, natural polysaccharides that have a rapid response to temperature changes are preferred. In contrast to polymers used in biomedical applications, a rigid hydrogel which flows as liquid at body temperature is desired for topical applications (Qiu & Park, 2001).

2.2.2 *iota*-Carrageenan (*ι*-C)

Carrageenan is one of the popular natural polysaccharides that possess thermoresponsive properties. In general, it gels at low temperature and dissolve in water upon heating. Carrageenan had been widely used as thickening or gelling agent in food, cosmetic and pharmaceutical industries due to its economic benefits and easy availability. This polymer is comprised of alternate units of d-galactose and 3, 6-anhydro-galactose joined by α-1, 3 and β-1, 4-glycosidic linkage and can be obtained by extraction from certain species of red seaweeds of the *Rhodophyceae* class. The three main types of carrageenan, *kappa* (κ-), *iota* (ι-) and *lambda* (λ-) are, distinguished by the number of sulfate groups per repeat unit of disaccharide, one, two and three, respectively (Janaswamy & Chandrasekaran, 2005). The primary differences in the degree of sulfation and position of the sulfate groups influences the polymer properties. For instance, higher levels of ester sulfate gives lower solubility temperature and weaker gel strength (Necas & Bartosikova, 2013). Therefore, κ-carrageenan forms the strongest gel while λ-carrageenan does not form gel at any concentration.

Alternatively, ι-C in aqueous solution can be reversibly transformed from an ordered conformation at low temperature to a random coil conformation at high temperature. This disorder-order transition was observed by using a semi-empirical method which correlated the optical rotation with the conformations at glycosidic linkage (Rees *et al.*, 1982). X-ray investigation also confirmed the double helix conformation in solid state and its dissociation into single strands when the interchain hydrogen bonds in the double helix were broken at high temperature (Janaswamy & Chandrasekaran, 2002). Nevertheless, the gelation behavior of ι-C strongly depends on the types of counter ions and its concentration. It was reported that the divalent cations, especially Ca^{2+} ions, affect more on the ι-C gel system compared to monovalent cations (Kara *et al.*, 2007; Yuguchi *et al.*, 2003).

2.3 Colloidal carrier systems

In the past few decades, colloidal carrier systems have been employed to deliver drugs or active ingredients through various administration routes, such as parenteral, oral, topical and intravenous. Among these particulate carriers, liposomes, micelles, microemulsions and polymeric nanoparticles possess the most appropriate characteristics for encapsulation of drugs and active ingredients. As well as being encapsulated in the core of particles, drug molecules can be covalently attached or adsorbed onto the surface of nanocarriers.

Microemulsions are thermodynamically stable droplet type dispersion of oil and water that is stabilized by surfactants (Lawrence & Rees, 2000). They are normally transparent or translucent in appearance due to the small droplet size, typically less than 140 nm. Basically, there are two types of microemulsions, oil-in-water (o/w) to encapsulate hydrophobic drugs and water-in-oil (w/o) to load hydrophilic drugs. Even though microemulsions can be designed to slow or enhance release of the loaded drug, high amounts of surfactants used are not favorable in body use.

Another famous nanocarrier is liposomes, which are spherical vesicles formed by one or more phospholipid bilayers enclosing an aqueous compartment (Akbarzadeh *et al.*, 2013). Ideally, liposomes are able to encapsulate both hydrophobic and hydrophilic drugs concurrently, making their use in drug delivery particularly attractive. Liposomes were designed to mimic red blood cells in term of shape, size, surface charge and material composition for intravenous application (Doshi *et al.*, 2009; Naeem *et al.*, 2015). In spite of these advantages, liposomes are limited by potential systemic toxicity as an organic solvent is required to dissolve the lipids. The fluidity of liposomes is also possible to affect its stability in semisolid formulations, especially emulsions in which the lipid content may fuse with the phospholipid bilayer of liposomes.

Polymeric nanoparticles are either nanospheres (solid matrix particles) with lower loading capacity or nanocapsules (vesicular systems surrounded by solid material shell) with higher loading capacity (Rao & Geckeler, 2011). Nanocapsules are preferred compared to nanospheres for their higher encapsulation and protection ability in polymer shells against degradation activities. Nevertheless, production of polymeric nanoparticles mostly involves organic solvents and thus lower biocompatibility.

2.3.1 Solid lipid nanoparticles (SLN)

Lipid nanoparticles was developed as an alternative drug carrier to microemulsions, liposomes and polymeric nanoparticles, that combines their advantages including modified release and protection of loaded ingredients, which are sensitive to light, oxidation and hydrolysis, while at the same time avoiding their drawbacks. Lipid nanoparticles possesses lower risk of toxicity and are biocompatible under physiological conditions. Moreover, they meet industrial needs, such as low cost and high feasibility for large scale production. The first generation, known as SLN, is a colloidal particle composed of a solid lipid core which is stabilized by surfactants, ranging in size between 10 nm to 1000 nm (Puri *et al.*, 2009).

In general, SLN has a similar structure to a lipid nanoemulsions, with the exception of the replacement of liquid lipid by solid lipid. As shown in Figure 2.1, controlled release of the loaded drug is achievable as the mobility of the drug in solid lipid should be lower compared to liquid lipid (Garud *et al.*, 2012; Mehnert & Mäder, 2001). SLN can also protect the loaded drug against chemical degradation caused by the dispersing medium as the drug molecules in lipid nanoemulsions easily diffuse through the interfacial film of the droplet and enter the dispersing medium, where degradation activities occur. Enhancement of stability and sustained release of labile compounds in SLN were reported by many studies in the literature, for instances clotrimazole (Souto

et al., 2004), frankincense and myrrh oil (Shi *et al.*, 2012), coenzyme-Q_{10} (CoQ10) (Teeranachaideekul *et al.*, 2007), neem oil (Vijayan *et al.*, 2013), retinoid (Jenning & Gohla, 2001) and vitamin E (Shylaja & Mathew, 2016). However, not all encapsulated drugs show slow release properties, a burst release of active compound can also occur. Both burst release and slow release are of interest as burst release improves the penetration of active compounds whilst sustained release controls the release of irritating ingredients (Müller *et al.*, 2000).

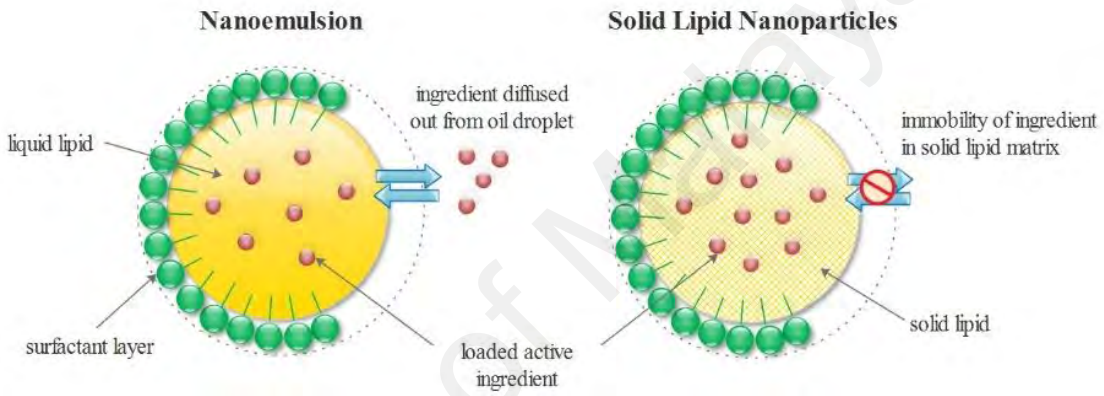

Figure 2.1: Schematic illustration of emulsion droplets and lipid nanoparticles.

A study comparing liposomes and SLN as carrier systems for CoQ10 demonstrated that both SLN and liposomes were biocompatible and suitable for cell proliferation (Gokce *et al.*, 2012). In spite of having smaller particle size and higher drug entrapment efficiency, SLN provided less protection against accumulation of reactive oxygen species. Therefore, liposomes were considered more efficient in terms of topical delivery of CoQ10 for antioxidant purposes.

SLN was also utilized to encapsulate sunscreen agents, which were related to photoallergies, phototoxic reactions and skin irritation. Controlled release of the solar screens from SLN could avoid those side effects, while enabling longer persistence on the skin surface and as such providing prolonged photoprotection. For example, SLN

incorporated with benzophenone-3 (Beck *et al.*, 2011), 2-ethylhexyl-2-cyano-3,3-diphenylacrylate (OCT), 2-ethylhexyl trans-4-methoxycinnamate (OMC) and bis-ethylhexyloxyphenol methoxyphenyl triazine (BEMT) (Lacatusu *et al.*, 2010) did not exhibit allergenic potential and possessed higher sun protector factor (SPF) than the free sunscreen unloaded in any carrier system due to the crystallization of sunscreens inside the lipid core.

Using electron diffraction technique, it was discovered that lipids in the outermost layer of the skin, the stratum corneum, were highly ordered (Pilgram *et al.*, 1999). Despite the hydrophobic nature of SLN, hydrophilic drugs could be loaded in SLN by adsorbing on to the interfacial layer (surfactant) around the nanoparticles. As such, SLN was assumed to increase the penetration and permeation of hydrophilic drugs by carrying to diffusion across the lipid-enriched intercellular regions of the skin barrier. For instances, diclofenac sodium (Liu *et al.*, 2014), isoniazid (Nair *et al.*, 2011; Rohit & Pa, 2013), ciprofloxacin hydrochloride (Shah *et al.*, 2012) and fluorescent dye (Becker Peres *et al.*, 2016) were all loaded in SLN using different methods to ensure high encapsulation efficiency and prolonged release profiles.

Since encapsulated drugs are located within crystal lattice imperfections and between fatty acid chains, the crystalline state of SLN is therefore associated with the risk of gelation, particle growth and potential expulsion of active compounds during storage (Freitas & Müller, 1999; Liu *et al.*, 2007; Mueller *et al.*, 2000).

2.3.2 Nanostructured lipid carriers (NLC)

In order to minimize the limitations of SLN, the second generation of lipid nanoparticles was developed, commonly known as NLC. In NLC, solid lipid and liquid lipid are blended and mixed to increase the loading capacity of SLN. Incorporated liquid

lipid increases the distance between fatty acid chains and therefore generates imperfections within the crystal lattice. These imperfections provide more room to accommodate the guest active molecules (Mehnert & Mäder, 2001; Mueller *et al.*, 2000; Mukherjee *et al.*, 2009).

According to Souto *et al.* (2004), both SLN and NLC were promising carriers for topical delivery of clotrimazole, an antifungal medication. Even though the stability of both systems were similar, NLC exhibited higher entrapment efficiency due to the presence of liquid lipids. NLC showed a faster release and lower occlusive effect compared with SLN with the same lipid content. These results were explained by the physical morphology of the lipid particles. Due to the protective effect of NLC against chemical degradation, NLC was always used to encapsulate antioxidants such as ascorbyl palmitate (Teeranachaideekul *et al.*, 2007) and *β*-carotene (Lacatusu *et al.*, 2012). Natural active compounds including green tea extract (Manea *et al.*, 2014) and *Zingiber zerumbet* oil (Rosli *et al.*, 2015) were also loaded in NLC for enhanced pharmaceutical and nutritional applications. Overall, these active compounds were reported to be more stable and effective in NLC.

Despite the majority of attention being focused on cosmetic and pharmaceutical applications, lipid nanoparticles also have the potential to be developed as a novel carrier for chemotherapeutic drugs. Doktorovova *et al.* (2009) had done a review on the different types of lipid carrier systems for paclitaxel in cancer treatment. Pre-clinical data obtained from the previous studies indicated that SLN, NLC and lipid nanocapsules were promising colloidal carriers to be used in future cancer therapy.

Alternatively, different compositions of NLC were studied to investigate their effect on skin hydration and occlusion (Loo *et al.*, 2013). It was observed that NLCs increased skin hydration significantly, compared with untreated control and high physical

stability, and it could be achieved with the highest amount of lipid and highest concentration of solid lipid. Furthermore, addition of propylene glycol and lecithin into the NLC formulation showed a more pronounced occlusion effect and long term stability. Once again this emphasized the vital role of NLC in topical applications.

In spite of providing good sensory feel upon application, the aqueous medium of a gel formulation can cause problems to the stability of the loaded active ingredients, such as insolubility of the hydrophobic active ingredients and chemical degradation of the sensitive active ingredients. Meanwhile, NLC dispersions, which enhance chemical stability of the loaded active ingredients, are too flowing to be applied on the skin. Therefore, incorporation of NLC into a gel formulation combines their advantages, producing a topical product with good sensory feel, improved stability of the loaded active ingredients and enhanced occlusive properties. Higher viscosity of a gel formulation is also able to prevent the sedimentation of NLC, which is mainly caused by the gravitational effect (Pardeike *et al.*, 2009).

2.4 Lipid nanoparticles in topical formulations

Development of novel topical products is enhanced by the introduction of SLN or NLC into the topical product formulations. SLN and NLC are well-tolerated carrier systems, highly efficient in controlled release of loaded active ingredients besides acting as a protection. In the past decade, there have been numerous studies related to the effect of incorporation of lipid nanoparticles into topical formulations.

Effects of a conventional oil-in-water (o/w) cream and of the same cream enriched with SLN on skin hydration and viscoelastic properties *in vivo* were evaluated (Wissing & Müller, 2003). The results demonstrated that it was possible to incorporate SLN into a cosmetic o/w cream to produce a physically stable formulation. The SLN-cream

showed pronounced skin hydration and viscoelasticity compared to the conventional cream. The increased hydration was assumed to be due to the occlusion properties of SLN, which could help to reduce water loss from the skin's surface. In the study, nanoparticles with high crystallinity were observed to form a dense film on skin upon application, which subsequently contributed to the occlusion effect.

Lipid nanoparticles have always been used to encapsulate water insoluble and chemically unstable compounds such as CoQ10. CoQ10 has potent antioxidant properties which had been shown to have beneficial effects on liver, heart, lung and skin (Kocharian *et al.*, 2009). It was also reported the effect of SLN on skin hydration by comparing a simple cream of CoQ10 with a cream consisting of CoQ10-loaded SLN (Farboud *et al.*, 2011; Pardeike *et al.*, 2010). Both the research groups reported prolonged release of CoQ10 from SLN and improved skin hydration with lower transepidermal water loss. The main reason suggested for the increased skin hydration was the occlusion effect of SLN which further enhanced the penetration of CoQ10 into the stratum corneum. Meanwhile, a good correlation between polymorphic transitions and drug release was observed in a study which investigated the drug release of active ingredient from a hydrogel and an o/w cream containing Vitamin A-loaded SLN (Jenning *et al.*, 2000). Humectants, thickening agents and surfactants used in the hydrogel and o/w cream were found to protect the ß' form of the lipid matrix from transforming into the ß form rapidly. Such system showed slow drug expulsion and hence stabilize the sustained release properties of SLN.

Besides cosmetic compounds, pharmaceutical and therapeutic drugs were also incorporated into lipid nanoparticles to minimize the irritation effect. SLN was reported as a promising carrier for follicular delivery of adapalene (Harde *et al.*, 2015). The drug encapsulated in SLN-gel performed better as an anti-acne agent and also revealed

improved skin tolerability, compared with the conventional gel. Furthermore, poor solubility and low bioavailability of an anti-T cell drug, known as Tacrolimus, were successfully solved by loading the drug into a modified NLC consisting of lipophilic solubilizers (Pople & Singh, 2011). The encapsulation efficiency was increased up to 96.66%. Same as the aforementioned studies, NLC showed advantages in gel formulations with respect to the stability of Tacrolimus and skin localization.

As a conclusion, the literature reported many features of SLN and NLC that were advantageous in topical application for cosmetic and pharmaceutical products. Lipid nanoparticles have assured occlusive properties to enable deep penetration of loaded drugs into the skin. There are several topical products containing lipid nanoparticles found on the market, such as Dr. Rimpler Cutanova Cream Nano Repair Q10 (2005), Beate Johnen NLC Deep Effect Repair Cream (2006), Chemisches Laboratorium Dr. Kurt Richter Nanolipid Q10 CLR (2006), Scholl Regenerationscreme Intensive (2007), Isabelle Lancray SURMER Crème Contour Des Yeux (2008) and Dr. Theiss NanoRemodelante Olivenöl Anti Falten Pflegekonzentrat (2008) (Woo, 2014).

2.5 Rheology in topical application

Rheology is fundamental in the optimization of a topical formulation as it is associated with the flow behavior of a semisolid system under physical deformations, which gives rise to the prediction of spreadability on the skin, dispensing from the packaging and physical stability during storage (Martin, 1993). In particular, the plasticity, viscoelasticity and rigidity of a material under the influence of stress are investigated in rheological tests. These rheological properties are useful in designing the manufacturing processes, packaging materials and even delivery of active ingredients (Gennaro, 2000; Lieberman *et al.*, 1996).

Surfactants are commonly used in topical products. Above the critical concentration, surfactants tend to form micelles, which may appear in spherical or anisometric shapes, such as rods. In contrast to the monodisperse spherical micelles, micelles in rods shape are always polydisperse where the average length rises with the concentration. The viscosity of the surfactant solution can be increased dramatically by adding electrolyte to form thread-like, flexible micelles that overlap and entangle with one another (Hoffmann *et al.*, 1992). Regardless to the application, an oscillation viscometer was employed to investigate the effects of different ionic strength of surfactants and salt on the network of surfactant solutions (Balzer *et al.*, 1995). Aqueous solutions of fatty alcohol ether sulfate and carboxymethylated fatty alcohol ethoxylate (anionic surfactants), when blended with salt or cation surfactants or zwitterionic surfactants, showed viscoelastic properties and Maxwell behavior. In the study, the properties of a liquid thread was related to the balance of elasticity and viscosity.

With respect to the complexity of the nanostructured carriers, which are incorporated in semisolid system, rheological analysis is essential to understand the interactions between the dispersing system, nanoparticles and active ingredients. For example, liposomes (Tan & Misni, 2014), polymeric nanoparticles (Alves *et al.*, 2005; Milao *et al.*, 2003; Terroso *et al.*, 2009) and lipid nanoparticles (Junyaprasert *et al.*, 2009; Pardeike *et al.*, 2009) were incorporated into hydrogels and creams to evaluate their rheological pattern before and after incorporation of active ingredients, loaded or unloaded nanoparticles. It was reported that a wide range of viscosities could be achieved by manipulating the solid content of the nanocarriers.

Junyaprasert *et al.* (2009) and his co-workers had studied the difference between CoQ10-loaded nanoemulsions and CoQ10-loaded NLC in terms of stability, rheology and skin permeation before and after incorporation into a hydrogel. It was observed that

both CoQ10-loaded carrier systems, stored at all temperatures without exposure to light, were stable up to 12 months. After 6 months storage, storage modulus, *G'* of CoQ10-loaded NLC gel slightly increased, explained by the spatial arrangement in lipid matrix of NLC during storage. Alternatively, the incorporation of triamcinolone acetonide acetate-loaded SLN improved the thixotropy properties of a Carbopol gel, compared with the blank gel (Liu *et al.*, 2008). Similar results were obtained in a rheological study of Carbopol gel loaded with NLC containing minoxidil (Silva *et al.*, 2009).

On the basis of rheological studies, distribution of topical products on skin or hair, and their thread-forming behavior can be tailored to meet the consumers' expectations. The literature proved that performance of a topical product can be evaluated via rheological tests prior to *in vivo* tests, and as such, saves the analysis cost.

CHAPTER 3: MATERIALS AND METHOD

3.1 Materials

Stearic acid (95%), oleic acid (99%), Tween 80, *iota*-carrageenan (*ι*-C), phosphotungstic acid hydrate and phosphate buffered saline tablets (pH 7.4) were purchased from Sigma Aldrich (St. Louis, USA). Calcium chloride ($CaCl_2$) anhydrous and methanol (analytical grade) were obtained from Merck and carboxymethyl cellulose (CMC) was supplied by Dai-Ichi Kogyo Seiyaku (Kyoto, Japan), respectively. Lecithin was purchased from Alfa Aesar (Massachusetts, USA) and ethanol 95% was supplied by Bumi-Pharma (Malaysia). Hydroquinone was obtained from BDH Laboratory Supplies (UK) and *alpha*-tocopherol was purchased from Spectrum (New Jersey, USA). All solutions and samples were prepared with deionized water of 18.2 Ω cm^{-1} resistivity, which was supplied from a Barnstead Diamond Nanopure Water Purification unit coupled with a Barnstead Diamond RO unit (Barnstead International, USA).

3.2 Methodology

3.2.1 Preparation of NLC

NLC was prepared by employing the hot homogenization method using a high shear homogenizer (Heidolph Silent Crusher M, Germany). NLC of different concentration of fatty acid and surfactants were prepared to obtain the optimized formulation. Similarly, the speed and time of homogenization were manipulated to obtain the most stable formulation. Nevertheless, the ratio of lipid phase to aqueous phase was remained at 2 to 23. The lipid phase, containing stearic acid and oleic acid was heated in a water bath thermostated at 80 ˚C until the mixture became a clear liquid. Surfactant solution (Tween 80) was pre-heated at the same temperature and dispersed into the lipid phase under strong agitation. The hot emulsion was then poured into cold water, at approximately 2 ˚C under magnetic stirring, where solidification of lipids occurred.

Another series of NLC with different concentration of lecithin were prepared in the same manner as above, whereby lecithin was added into the lipid phase and heated at 80 ˚C. After confirming the optimized formulation from the physicochemical characterization of the NLCs, the active compound was loaded by adding *alpha*-tocopherol or hydroquinone into the molten lipid phase prior to the addition of surfactant solution. The NLC dispersions were stored at 4 ˚C for further investigation.

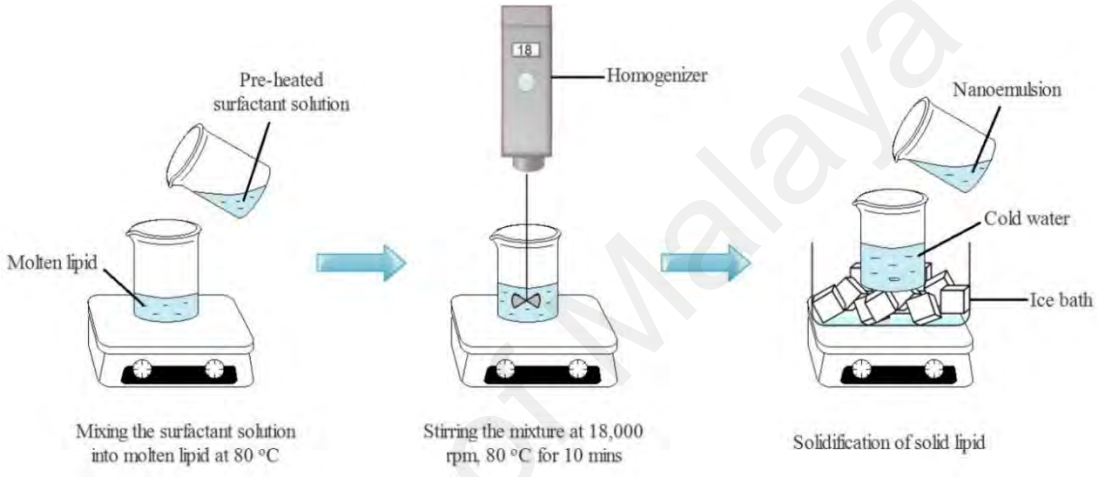

Figure 3.1: Schematic illustration of preparation of NLC using hot homogenization method.

3.2.2 Mean particle size and polydispersity index of NLC

The mean particle size and polydispersity index (PDI) of NLCs were determined by Zetasizer Nano ZS (Malvern Instruments, U.K.) using Dynamic Light Scattering (DLS) technique. The instrument was equipped with a red Helium laser of wavelength 633 nm, capable measuring particle size range from 0.3 nm to 10 μm.

In general, DLS technique measures the Brownian motion of the suspended particles. First, a laser light source is converged by a lens to focus in the sample and the particles of the sample scatter light at all angles. Then, a single detector set at a certain angle collects the scattered light intensity over very short timescale at a rate dependent on the

particle size. The intensity fluctuations yields velocity of Brownian motion known as translational diffusion coefficient by a correlation function, as shown in Eq. 3.1.

$$G(t) = A_c[1 + B\ exp\ (-2\Gamma t)] \quad \text{Eq. 3.1}$$

$$\Gamma = 2Dq^2 \quad \text{Eq. 3.2}$$

Where *G(t)* is the scattered intensity, A_c is the baseline of correlation function, *B* is the intercept of correlation function, Γ is the relaxation time, *D* is the translational diffusion coefficient, *q* is the scattering vector and *t* is the delay time between two intensity measurements.

Since small particles move more rapidly and large particles move more slowly, Stokes-Einstein relationship is then used to correlate the diffusion speed with particle size as shown in the following equation:

$$d = \frac{kT}{3\pi\eta D} \quad \text{Eq. 3.3}$$

Where *d* is the hydrodynamic diameter of particle, *k* is the Boltzmann's constant, *T* is the absolute temperature, η is the viscosity of sample and *D* is the translational diffusion coefficient. This relationship assumes that the particles are spherical and there is no interaction among them. The particle size distribution is obtained from Eq. 3.3 as well. The broadness of the size distribution is then calculated and indicated by PDI, ranges from 0 to 1. PDI that close to 0 reveals a monodisperse sample while PDI close to 1 indicates a polydisperse sample.

The instrument utilizes non-invasive backscatter (NIBS) technology for detection. The light scattered by a sample is measured at a scattering angle of 173˚ to increase the measurement volume where a higher volume of sample is illuminated by laser (Figure 3.2). The effect of large particles such as dust or contaminant can also be minimized in this detection attributed to the fact that large particles scatter light primarily at forward angle. Moreover, the focus lens can be moved to adjust the measurement position within

the cell according to the concentration of the sample. For a dilute sample, measurement at centre of the cell is preferred to minimize the effect of laser flare yet maximizing the measured volume. In contrast, measurement close to cell wall is favourable for a concentrated sample to avoid multi-scattering. In addition, an attenuator can also be used to scale the input intensity of laser where 1 means least laser power for concentrated samples and 11 means full laser power for dilute samples.

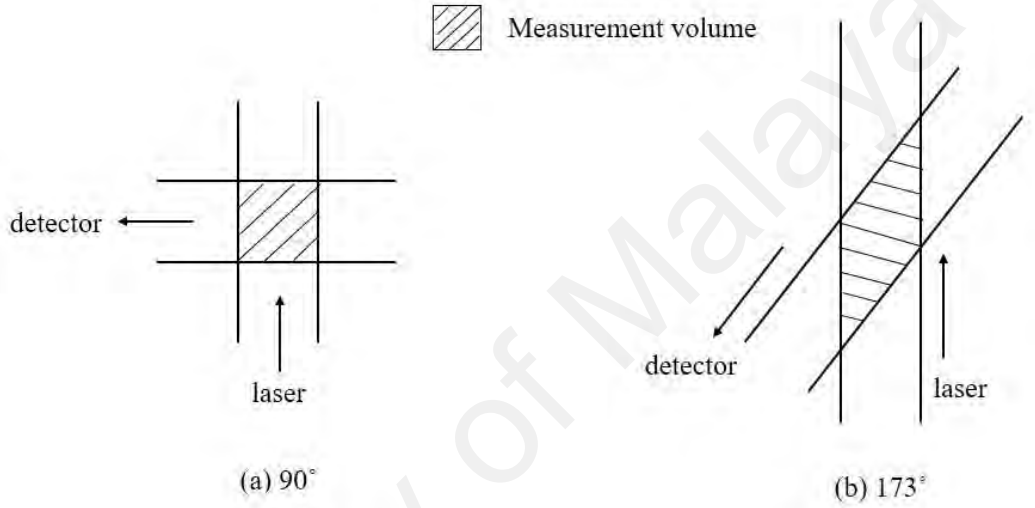

Figure 3.2: Schematic illustration of measurement volume of sample at (a) normal scatter 90˚ and (b) backscatter 173˚.

In this study, NLC dispersions were diluted to an appropriate concentration before being placed into a 1 cm path length quartz cuvette. The sample was then equilibrated at 25 ˚C for 120 seconds prior the analysis. The measurement position and attenuator was set as automatic so that the optimum conditions can be obtained according to the concentration of the sample. Generally, the attenuator values were maintained within range 6 to 9 for consistency so that the concentrations of samples were not differ much. All the measurements were based on Mie theory, which exactly describes how spherical particles of all sizes and optical properties scatter light. Rayleigh theory is not suitable in this case as it fits only particles with diameter less than 1/10 of wavelength, $\lambda/10$, that is 60 nm for the laser used.

3.2.3 Zeta potential of NLC

Zeta potential of NLCs was measured by Zetasizer Nano ZS (Malvern Instruments, U.K.). Electrophoresis and laser Doppler velocimetry techniques are utilized to measure the velocity of a particle moving in liquid when an electric field is applied and zeta potential is calculated using Henry equation (Eq. 3.4) as below:

$$U_E = \frac{2\varepsilon\zeta\, f(ka)}{3\eta} \qquad \text{Eq. 3.4}$$

Where U_E is the electrophoretic mobility or velocity, ε is the electric constant, ζ is the zeta potential, *f(ka)* is the Henry's function where Smoluchowski approximation = 1.5 is applied for polar media while Huckel approximation = 1.0 is applied for non-polar media, and η is the viscosity of the sample.

On the whole, zeta potential is the potential difference exists between the slipping plane of the double layer and dispersing medium (Figure 3.3). It is always used to determine the tendency of particles in a dispersion to flocculate. Regardless of the positive or negative sign, the magnitude of zeta potential indicates the physical stability of a colloidal dispersion. The higher magnitude shows higher repulsion between the particles and hence sedimentation is less likely to occur. In general, surface charge of a particle is originated from the dissociation of surface groups, for instance acidic groups give negatively charged surface. In some cases, adsorption of charged surfactants is also used to modify the surface charge. Zeta potential can be affected by several factors including pH and conductivity of the dispersing medium and the concentration of a formulation component.

In present work, a disposable folded capillary cell (DTS1070) was employed to perform the zeta potential measurement. The diluted sample was added into the folded capillary cell slowly to ensure no formation of bubbles, and then equilibrated at 25 ˚C for 120 seconds before the measurements.

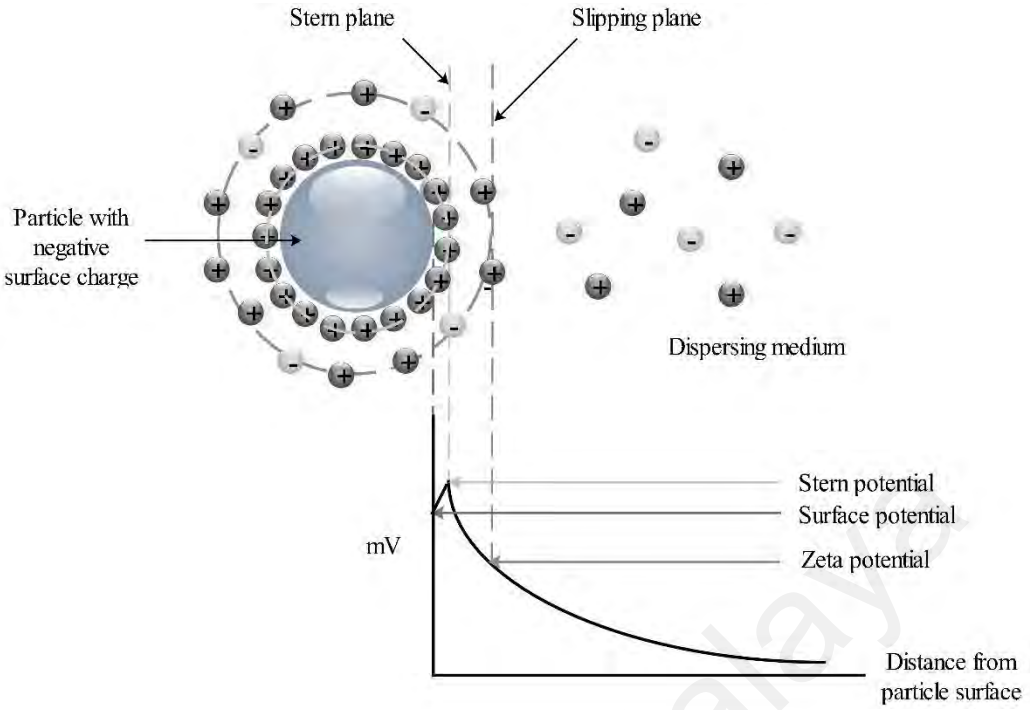

Figure 3.3: Schematic illustration of zeta potential of a particle.

3.2.4 Optical polarizing microscope (OPM)

The morphology of NLC dispersions was observed using Leica Polarizing Microscope (Leica Mycrosystems, Germany). NLC dispersion was placed on a glass slide and covered with a cover glass. The object was then viewed under the microscope. Although OPM is not suitable for viewing nanoparticles, due to its small magnification and low resolution, it can be used to observe any aggregates of NLC or liposomes formed in the NLC dispersions. Lecithin used in an adequate amount can form liposomes or micelles in aqueous dispersing medium. Since liposomes possess optically active properties, resulting from the ordered and concentric arrangement of the phospholipid layer, the presence of liposomes can therefore be determined by using an OPM (Placzek & Kosela, 2016).

OPM, equipped with a heating stage THMS 600 connected to a temperature programmer TMS 91 (Linkam Scientific Instruments Ltd., UK), was employed to observe the phase transitions of dried NLC, such as melting and crystallization. NLC

dispersions were air-dried in a desiccator for 24 hours and then solid form NLC was viewed under OPM. The morphology of each sample was investigated during the heating and cooling processes, from 30 ˚C to 80 ˚C and then back to 30 ˚C, at a rate of 5 ˚C min^{-1}. Additionally, lecithin powder was heated up to 200 ˚C to examine its phase transition during the heating and cooling processes.

3.2.5 Transmission electron microscope (TEM)

Morphology of NLCs was observed by an Energy Filtered TEM model LIBRA 120 (Zeiss, Germany) with an accelerating voltage of 120 kV. TEM is an essential tool in viewing nanoparticles due to its high magnification and resolution power. TEM operates based on the same principle as a light microscope, except that the sample is illuminated by electrons instead of light. The transmitted and scattered primary electrons which pass through the sample are detected to create a sample image. As NLC deflects electrons weakly, staining the sample is necessary to visualize the shape, size and surface structure of the sample.

A drop of NLC dispersion was placed on a 400 mesh copper-coated carbon grid for 1 minute. The excess dispersion was removed by blotting with a piece of filter paper then the sample was negatively stained with 1% (w/w) phosphotungstic acid solution and dried by the same method. The grid was kept in a desiccator for 24 hours before examination under TEM (Eh Suk & Misran, 2017).

3.2.6 Differential scanning calorimetry (DSC)

Thermal analysis of the dried NLC was conducted by utilizing Tzero^{TM} DSC Q20 (TA Instruments, USA). DSC is a convenient and inexpensive method to examine the matrix state and phase behaviour of NLCs. In DSC, energy is supplied independently to reference and sample to maintain constant temperature. The relative heat flow between

the reference and sample is measured and the output is recorded as constant-pressure heat capacity as a function of temperature (Eq. 3.5). As shown in Figure 3.4, phase transitions can then be detected by the distinct deviations from the straight baseline of DSC curve and the area under the integrated curve is known as enthalpy change, calculated by Eq. 3.6.

$$C_P = \left(\frac{dq}{dT}\right)_P = \left(\frac{\partial H}{\partial T}\right)_P \qquad \text{Eq. 3.5}$$

$$\Delta H = \int_{T_1}^{T_2} \left(\frac{\partial H}{\partial T}\right)_P dT = \int_{T_1}^{T_2} C_P \, dT \qquad \text{Eq. 3.6}$$

Where C_p is the heat capacity, q is the heat flow measured, T is absolute temperature and ΔH is the enthalpy change.

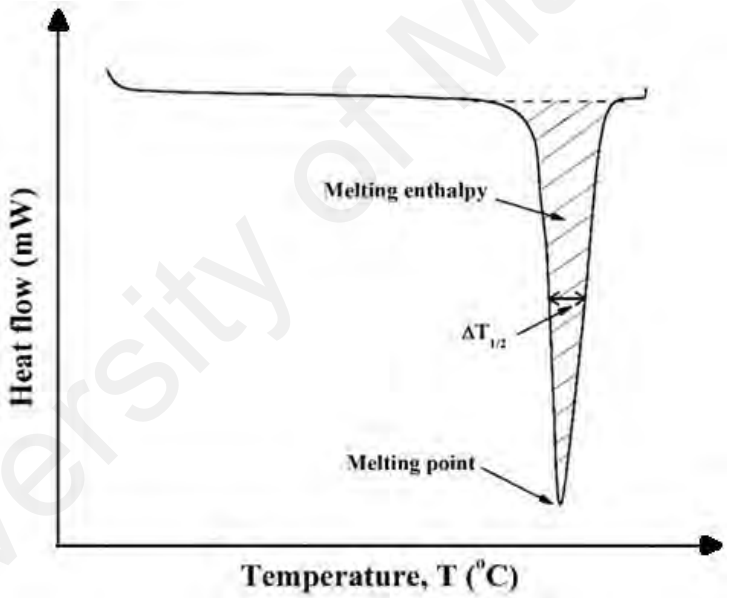

Figure 3.4: Determination of phase transition and enthalpy change from a DSC curve.

The degree of crystallinity of NLC is defined as the percentage of the crystalline state of lipid matrix during the solidification process during NLC preparation (Bunjes & Unruh, 2007). Other than having an influence on hardness, density and diffusion of nanoparticles, it is related to loading capacity, as mentioned in section 2.3.1. The degree of crystallinity of NLC can be determined from the results obtained by the following equation:

$$CD = \left(\frac{\Delta H_{NLC}}{\Delta H_{SA}}\right) \times 100\% \quad \text{Eq. 3.7}$$

Where *CD* is the crystallinity degree, ΔH_{NLC} is the enthalpy change of NLC and ΔH_{SA} is the enthalpy change of bulk stearic acid, respectively.

Dried NLCs were obtained by air-drying the NLC dispersions in a desiccator for 2 days. Approximately 5 mg of the dried sample was weighed and put into an aluminium pan for DSC analysis. An empty aluminium pan was used as reference. The temperature ramp was performed from 30 ˚C to 80 ˚C, at a heating rate of 5 ˚C min^{-1} under continuous flushing of nitrogen gas at the rate of 50 mL min^{-1}. The results were analysed using TA Universal Analysis Software (TA Instruments, USA).

3.2.7 Encapsulation efficiency of active ingredients in NLC

Theoretically, encapsulation efficiency can be calculated by knowing either the amount of encapsulated or free active ingredient, which was separated from the carrier using a centrifuge. However, the nanoparticles were too small to be separated and high centrifugal forces would destroy the carrier. Therefore, a centrifugal filter tube consisting of membrane with 50,000 Da molecular weight cut-off (Vivaspin 6, Sartorius Stedim Biotech, Germany) was utilized to entrap the nanoparticles while water and free ingredients flowed through the membrane and collected in the bottom chamber of the centrifugal tube. In this study, the dispersion was filled into the upper chamber of a centrifugal filter tube and centrifuged at 10,000 rpm for 1 hour utilizing a centrifuge Velocity 18r (Dynamica, UK). After centrifugation of the dispersion, supernatant in the bottom chamber was collected.

For *alpha*-tocopherol loaded NLC, methanol was added to the supernatant and mixed homogeneously. Supernatant of hydroquinone loaded NLC was diluted with deionized water to an appropriate concentration for UV analysis. Both *alpha*-tocopherol and

hydroquinone were then detected spectrophotometrically (Cary 50 UV-Vis Spectrometer, Agilent Technologies, USA) at a wavelength of 290 nm. The concentration of active compounds in each sample was determined from their standard calibration curves respectively. Encapsulation efficiency was calculated with the following equation:

$$EE = \left(\frac{W_T - W_F}{W_T}\right) \times 100\% \qquad \text{Eq. 3.8}$$

Where *EE* is encapsulation efficiency of active compounds in NLC, W_T is the weight of active compounds added during preparation and W_F is the weight of unloaded active compounds detected in filtered aqueous phase, respectively.

3.2.8 Preparation of gel samples for rheological measurements

Ca^{2+} solutions were prepared by adding different weight percentages of $CaCl_2$ salt into a beaker and deionized water was added up to 100 g. They were then being labeled a-e (Table 3.1). A series of mixtures of *ι*-C and CMC was prepared by adding different amounts of *ι*-C powder and CMC powder into 9.80 g of Ca^{2+} solution (Table 3.2). The samples were labeled according to the ratio of *ι*-C to CMC and the concentration of Ca^{2+} ions. For example, *ι*c28b represents a gel mixture of *ι*-C and CMC at ratio 2:8 in 0.02% Ca^{2+} solution. The active ingredient gel was prepared by adding *alpha*-tocopherol or hydroquinone, together with CMC and *ι*-C into the Ca^{2+} solution. All solutions were heated in a water bath thermostated at 80 ˚C until a clear gel was obtained. Samples were then being kept at room temperature for 24 hours before the rheological measurements.

For the preparation of NLC-gel, 30% of NLC dispersion (w/w) was incorporated into the gel system and mixed homogeneously at 8,000 rpm for 1 minute. The NLC-gel was stored at 4 ˚C for 24 hours for further characterization.

Table 3.1: Percentage (% (w/w)) of Ca^{2+} solutions.

Label	Percentage (% w/w) of Ca^{2+}
a	0.00
b	0.02
c	0.04
d	0.06
e	0.08

Table 3.2: Weight fraction (% (w/w)) of the gel mixtures.

Mixture	*ι*-C, g	CMC, g	Ca^{2+} solution, g
*ι*c28	0.04	0.16	9.80
*ι*c37	0.06	0.14	9.80
*ι*c55	0.10	0.10	9.80
*ι*c73	0.14	0.06	9.80
*ι*c82	0.16	0.04	9.80

3.2.9 Rheological characterization of gel samples

Rheology is the science of the flow and deformation of a material. It provides valuable information, including viscosity, viscoelastic properties and transient response of the material. A rotational rheometer, equipped with a suitable measuring geometry, is often utilized to study rheology. There are numerous types of measuring geometry, such as 'cup and bob' for low viscosity materials, 'cone and plate' for viscoelastic materials and 'parallel plate' for thick materials. For geometry cone and plate, different combinations of cone angle and diameter are available. The larger cone angle produces a smaller error but a higher variation of shear rate across the gap and vice versa. Fundamentally, a rheometer controls or measures torque, τ, angular displacement, θ and angular velocity, ω. The desired parameters are then obtained from the calculation as shown in Table 3.3.

Table 3.3: Mathematical functions of rheology parameters.

Parameter	Mathematical function	Unit	
Shear stress, σ	$\sigma = C_1\tau$	Pa	Eq. 3.9
Shear strain, γ	$\gamma = C_2\theta$	-	Eq. 3.10
Shear rate, $\dot{\boldsymbol{\gamma}}$	$\dot{\gamma} = C_2\omega$	s^{-1}	Eq. 3.11
Viscosity, η	$\eta = \frac{\sigma}{\dot{\gamma}} = \frac{\tau}{\omega}\cdot\frac{C_1}{C_2}$	Pa s	Eq. 3.12
Modulus, G	$G = \frac{\sigma}{\gamma} = \frac{\tau}{\theta}\cdot\frac{C_1}{C_2}$	Pa	Eq. 3.13
Stress constant, C_1*	$C_1 = \frac{3}{2\pi r^3}$	m^{-3}	Eq. 3.14
Strain constant, C_2*	$C_2 = \frac{1}{\theta_G}$	rad^{-1}	Eq. 3.15

* *For measuring geometry cone and plate with cone angle θ_G and diameter r.*

A strain rate/stress controlled Rheometer MCR 301 (Anton-Paar, Austria) was employed to carry out the rheological measurements of gel samples: a series of CMC-ι-C gel mixture, NLC-gel, active ingredient gel and active ingredient loaded NLC-gel. All the tests were done at 25 ± 1 ˚C (except for temperature sweep) with a measuring geometry cone and plate of 1˚/50 mm with a gap of 0.100 mm.

3.2.9.1 Viscometry test

A viscometry test was performed at a controlled shear rate, varying from 0.01 to 100 s^{-1}. Generally, gel systems are non-Newtonian fluids and are either pseudoplastics, that exhibit shear thinning behavior, or dilatants, that display shear thickening behavior. In some cases, the polymeric gels show both behaviors under different shear rate. For example, a gel network possessing yield stress, σ_y, shows shear thickening at low shear rate and shear thinning at high shear rate. σ_y is defined as the maximum stress bearable by the structure before deformation occurs and can be obtained from a shear viscosity profile as a function of shear stress (Figure 3.5). In order to study the behavior of a gel, the viscosity profiles were fitted by Power-Law model with the following equation:

$$\eta = K\dot{\gamma}^{n-1} \qquad \text{Eq. 3.16}$$

Where η is the shear viscosity, K is the consistency index, $\dot{\gamma}$ is shear rate and n is the Power-Law index (PLI). PLI is a measure of the degree of deviation from Newtonian behavior, where n = 1 indicates a Newtonian fluid, n < 1 represents shear thinning behavior and n > 1 represents shear thickening behavior. For a system showing n < 0.5, it is considered strong shear thinning (Rauwendaal, 2014).

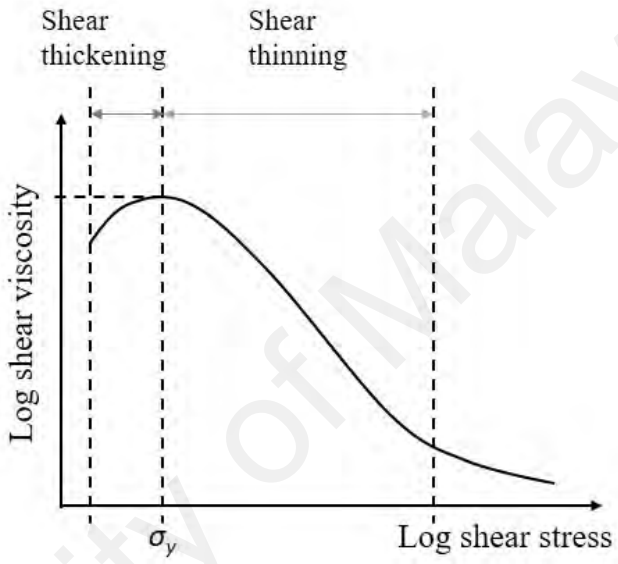

Figure 3.5: Determination of yield stress, σ_y from a shear viscosity-shear stress curve.

3.2.9.2 Oscillatory tests

Oscillatory tests were started with an amplitude sweep in controlled strain mode, with a strain range of 1% to 1000%, at constant frequency 1 Hz, to obtain the linear viscoelastic region (LVR) for frequency and temperature sweep tests. Critical strain, γ_c, can also be acquired from the amplitude sweep curve, as shown in Figure 3.6.

In the frequency sweep, the gel sample was subjected to varying frequency, from 10 to 0.1 Hz under a constant strain of 5%. The slope of storage modulus, *G'*, was obtained from the plot of *G'* as a function of frequency to evaluate the frequency dependency of the gel mixtures. A temperature sweep was then carried out by heating the

thermoresponsive gel mixture from 20 ˚C to 80 ˚C, at a rate of 10 ˚C min^{-1}, single frequency 1 Hz and constant strain 5%. For gel samples incorporated with NLCs and active ingredients, the heating range was decreased to 20 ˚C to 60 ˚C, at a rate of 10 ˚C min^{-1}, to avoid degradation of fatty acids and active ingredients. Solvent traps were used to minimize the evaporation of the sample. The crossover temperature of *G'* and *G''*, T_c, was acquired as shown in Figure 3.7.

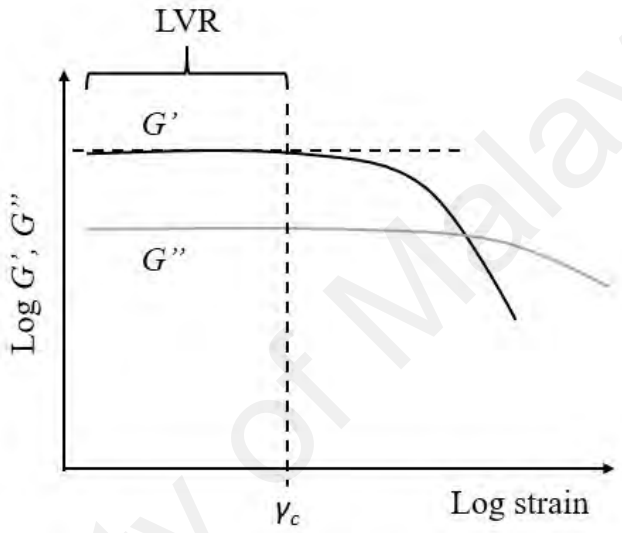

Figure 3.6: Determination of critical strain, γ_c from the storage modulus-strain curve.

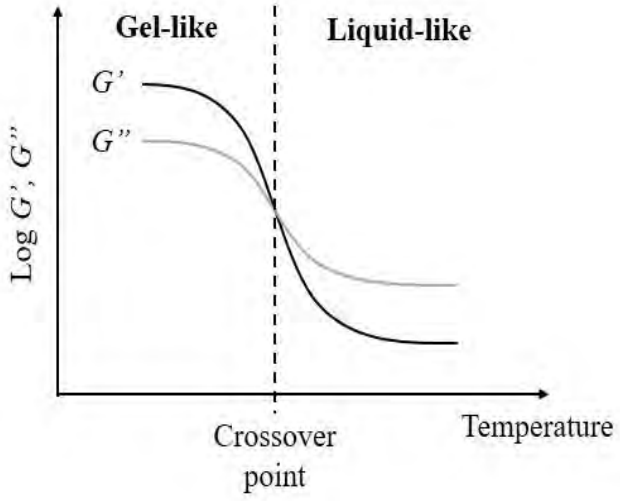

Figure 3.7: Determination of crossover temperature, T_c from the moduli-temperature curve.

3.2.10 Field emission scanning electron microscope (FESEM)

Morphology of the gel sample in solid form was observed under FESEM (Hitachi SU8220 Ultimate Cold Field Emission SEM, Tokyo, Japan) at a low accelerating voltage of 1.0 kV. FESEM differs from TEM due to the construction and principle of operation. Instead of transmission through the sample, the emitted concentrated electron beam scans the sample surface. The emitted secondary electrons, together with the backscattered electrons are then detected, assessing the sample topography to provide a three-dimensional image. As such, it is an excellent method to examine the macrostructure of a gel system. As the FESEM has lower resolution power compared to TEM, due to the low accelerating voltage used, it is not suitable to observe the morphology of nanoparticles (Placzek & Kosela, 2016).

FESEM operates in a high vacuum condition and therefore, it is not suitable to analyze a liquid sample. The aqueous gel mixtures underwent freeze-drying processes by being frozen at -20 ˚C for 24 hours and transferred to the freeze-dryer at -55 ˚C for 72 hours. Prior viewing under FESEM, a layer of carbon paint was put on the sample stage and the gel in solid form was placed onto it.

3.2.11 Preparation of samples for *in vitro* release studies

There were four systems prepared for each active compound. Sample A was *alpha*-tocopherol solution being prepared by dissolving the active ingredient in ethanol 95%: deionized water (80:20 (v/v)). Sample B was diluted *alpha*-tocopherol loaded NLC dispersion and sample C was *alpha*-tocopherol gel, respectively. As prepared in section 3.2.8, sample D was *alpha*-tocopherol loaded NLC-gel.

Samples containing hydroquinone were prepared in the same manner as above except for hydroquinone solution, which was prepared by simply dissolving hydroquinone in deionized water. Hydroquinone solution, diluted hydroquinone loaded NLC, hydroquinone gel and hydroquinone loaded NLC-gel were then denoted as samples E, F, G and H. All samples were kept at 4 ˚C for 24 hours before the experiments.

3.2.12 *In vitro* release

The release rate of active compounds from samples A to H was studied by using an Automated Franz Diffusion Cell System (Microette Plus Autosampling System, Hanson Research Co., USA). Six vertical Franz diffusion cells with diffusate chamber volume of 4 mL and effective diffusion area of 0.636 cm^2 were used. The diffusion cells were water-jacketed and connected to a water bath circulator (PolyScience, USA) to maintain the experiment temperature. A helix spring magnetic stirrer was placed in each cell to ensure medium homogeneity.

The Franz diffusion cells were fitted with pre-hydrated regenerated cellulose membranes with 10,000 Da molecular weight cut-off. A different medium was chosen for different active compounds, according to their solubility. For *alpha*-tocopherol, ethanol 95%: phosphate buffer saline solution (PBS) (80:20 v/v) was filled into the receptor chambers to ensure pseudo-sink conditions by increasing the solubility of active compound in the receiving phase. A similar receptor medium had been used for the study of release of vitamin E in previous studies (Sharipova *et al.,* 2016; Shylaja *et al.,* 2016; Yenilmez *et al.*, 2011). In contrast, receiving medium PBS pH 7.4 was used for hydroquinone. The receiving phase was stirred continuously at 400 rpm and thermostated at 37 ± 1 ˚C. Approximately 1 mL of sample was loaded into each donor chamber with the experiments run for 24 hours. Samples were withdrawn and replaced with fresh medium from reservoir at each predetermined time interval. The temperature

effect on the release of active compounds from samples C, D, G and H were investigated by repeating the experiments at 30 ˚C.

3.2.12.1 Determination of amount of active compound

The amount of active compound was determined from a standard calibration curve by employing Cary 50 UV-Vis Spectrometer (Agilent Technologies, USA). A stock solution of 100 μg mL^{-1} was prepared by adding 10 mg of the active ingredient, *alpha*-tocopherol, into 50 mL of ethanol 95% and PBS solution (80:20 (v/v)), and then made up to the mark 100 mL in a volumetric flask. Next, a series of *alpha*-tocopherol solutions with different concentrations were prepared by diluting the stock solution.

A stock solution of 50 μg mL^{-1} of hydroquinone solution was prepared by dissolving 5 mg of hydroquinone into 50 mL of PBS solution and made up to 100 mL in a volumetric flask. A series of hydroquinone solutions with different concentrations were prepared by diluting the stock solution.

The prepared solutions were measured spectrophotometrically and both the active ingredients were detected at a wavelength of 290 nm. The standard calibration curves of *alpha*-tocopherol and hydroquinone were plotted.

3.2.12.2 Mathematical model evaluations

The release curves of *alpha*-tocopherol and hydroquinone were evaluated by fitting into selected mathematical models using DDSolver software program (China). Mathematical models were applied to represent the active ingredients release kinetics by translating the release curve in the function of different parameters associated with the dosage form. The generic equations that can be deduced from a theoretical analysis of the process are mechanistic such as zero order, first order, Higuchi and Korsmeyer-

Peppas, while in some cases where the theoretical fundament does not exist, an empirical equation such as Peppas-Sahlin is used (Table 3.4). The most widely used criteria for selection of the best fitted mathematical model employs the coefficient of determination, R^2. Nevertheless, a modification is required when comparing models with different parameters, and therefore the adjusted coefficient of determination, $R^2_{adj.}$ was used (Eq. 3.17). Model with the highest $R^2_{adj.}$ is considered the best model in describing the release kinetic properties of the active ingredient.

$$R^2_{adj.} = 1 - \frac{n-1}{n-p}(1 - R^2) \qquad \text{Eq. 3.17}$$

Where n is the number of dissolution data points and p is the number of parameters in the model.

Table 3.4: Mathematical models for drug release characterization (Singhvi & Singh, 2011).

Mathematical model	Equation	
Zero order	$Q_t = Q_0 + K_0 t$	Eq. 3.18
First order	$\log Q_t = \log Q_0 - \frac{K_1 t}{2.303}$	Eq. 3.19
Higuchi	$M_t = K_H t^{1/2}$	Eq. 3.20
Korsmeyer-Peppas	$\frac{M_t}{M} = K_{KP} t^n$	Eq. 3.21
Peppas-Sahlin	$\frac{M_t}{M} = K_d t^m + K_r t^{2m}$	Eq. 3.22

Where Q_t is the amount of drug dissolved in time t, Q_0 is the initial amount of drug, K_0 is the zero order release constant, K_1 is the first order release constant, M_t is the amount of drug released in time t, M is total amount of drug, K_H is the Higuchi release constant, K_{KP} is the Korsmeyer-Peppas release constant, n is the release exponent, K_d is the diffusion constant, K_r is the relaxation constant and m is the purely fickian diffusion exponent for device of any geometrical shape, which exhibit controlled release. Table

3.5 indicates the type of drug transport determined by *n* value of Korsmeyer-Peppas model and *m* value of Peppas-Sahlin model.

Table 3.5: Types of drug transport determined by Korsmeyer-Peppas and Peppas-Sahlin models (Singhvi & Singh, 2011).

Mathematical model	Exponent	Type of drug transport
Korsmeyer-Peppas	$n < 0.45$	Quasi fickian
	$n = 0.45$	Fickian diffusion
	$0.45 < n < 0.89$	Anomalous or non-fickian diffusion
	$0.89 < n < 1$	Case II relaxation or non-fickian case 2
	$n > 1$	Non-fickian super case 2
Peppas-Sahlin	$m < 0.43$	Fickian diffusion
	$0.43 < m < 0.85$	Anomalous transport
	$m > 0.85$	Case II transport

CHAPTER 4: RESULTS AND DISCUSSION

4.1 Physicochemical characterization of NLC

4.1.1 Mean particle size and zeta potential of NLC

The main concerns in formulating a suitable carrier for topical application are suitable size and agglomeration of the particles. The particle size should be small enough to pass through the skin barrier, but not too small to avoid systemic uptake by entering the blood system. Particles within a size range of 3 to 10 μm concentrate in the hair follicles, while particles smaller than 3 μm penetrate both the follicle and stratum corneum via follicular localization (Shekunov *et al.*, 2007). It has been reported that skin penetration of nanoparticles smaller than 200 nm was achieved via follicle localization (Alvarez-Román *et al.*, 2004; Shim *et al.*, 2004). In order to obtain the desired particle size of NLC, the effects of different preparation parameters and composition of NLC on mean particle size, PDI and zeta potential of NLC formed were investigated.

4.1.1.1 Effect of preparation parameters

In emulsion system preparation, energy input is mostly required for a liquid phase to homogeneously disperse in the dispersing medium. In this experiment, the composition of NLC remained constant but variations in homogenization time and speed were manipulated. From the results presented in Table 4.1, it was observed that increasing the homogenization speed from 16,000 rpm to 18,000 rpm successfully reduced the mean particle size and PDI of the NLC as much as 62.7% and 79.16%, respectively. This is attributed to the higher shear force overcoming the interfacial force of the emulsion droplets, which broke down the large droplets into smaller droplets (McClements, 2004). Similarly, the mean particle size decreased with increasing homogenization time, from 8 min to 10 min, where the mean particle size was reduced

36.5% at 16,000 rpm and 5.8% at 18,000 rpm. At the meantime, PDI was reduced 36.5% at 16,000 rpm and 7.3% at 18,000 rpm. These can be explained by longer time available for the droplet breakdown. The difference of mean particle size and PDI at speed 18,000 rpm was less significant compared to 16,000 rpm, indicating that homogenization speed had more effect on the mean particle size and PDI of NLC.

Table 4.1: Effect of production parameters on mean particle size and PDI of NLCs.

Homogenization speed (rpm)	Homogenization time (min)	Mean particle size (nm)	Polydispersity index
16,000	8	578.5 ± 29.8	0.787 ± 0.066
16,000	10	367.4 ± 14.5	0.500 ± 0.064
18,000	8	215.8 ± 0.8	0.164 ± 0.011
18,000	10	203.2 ± 1.7	0.152 ± 0.016

4.1.1.2 Effect of lipid composition

Lipid composition can affect the viscosity of nanoemulsions formed during homogenization and hence influence the particle size and physical stability of NLC. Additionally, lipid composition determines the crystallinity and defects in the particles, and as such the ability to accommodate the guest active ingredient. One lipid used was lecithin, which was a phospholipid that appeared in solid form at room temperature. Lecithin was not only used as a surfactant in forming an emulsion, but also had been used as solid lipid in the formulation of NLC (Otarola *et al.*, 2015). In this study, the lipid composition was varied in terms of ratio of stearic acid to lecithin and also in the ratio of oleic acid to lecithin, as shown in Table 4.2.

Table 4.2: Effect of lipid composition on mean particle size, PDI and zeta potential of NLCs.

Sample	Percentage Composition (% (w/w))				Mean particle size (nm)	PDI	Zeta potential (mV)
	Tween 80	Stearic acid	Oleic acid	Lecithin			
SL1	1.00	4.48	1.60	1.92	599.9 ± 61.41	0.635 ± 0.041	-58.4 ± 0.835
SL2	1.00	5.76	1.60	0.64	373.3 ± 11.87	0.446 ± 0.019	-51.1 ± 0.943
SL3	1.00	5.90	1.60	0.50	230.5 ± 2.273	0.191 ± 0.010	-44.7 ± 0.594
OL1	1.00	5.90	1.80	0.30	237.4 ± 1.337	0.210 ± 0.014	-40.7 ± 0.701
OL2	1.00	5.90	1.90	0.20	232.0 ± 1.549	0.178 ± 0.003	-38.0 ± 0.335

Table 4.2 demonstrated that increased lecithin gave higher mean particle size, PDI and zeta potential. The increment in zeta potential was expected as lecithin was an ionic surfactant. As shown in Figure 4.1, lecithin was a zwitterion surfactant that possessed both positively charged amine group and negatively charged phosphate group. Nevertheless, lecithin gave an overall negative charge as the phosphate group with lower bond dissociation energy, ΔHf_{298} = 596.6 kJ mol^{-1}, tended to dissociate more in the aqueous solution, compared to the amine group with higher bond dissociation energy, ΔHf_{298} = 770.0 kJ mol^{-1} (Cottrell, 1958; Darwent, 1970). Despite the high zeta potential, sedimentation was observed in SL1 after storage for 1 week. This was potentially due to the high concentration of lecithin which produced an emulsion with high viscosity, subsequently forming nanoparticles of high density. The dense particles were easier to form sediment under gravity effect. Additionally, lecithin multilayers plausibly accumulated on the surface of particles, leading to agglomeration and particle growth when fusion of the lecithin bilayers occurred (Schubert & Müller-Goymann, 2005).

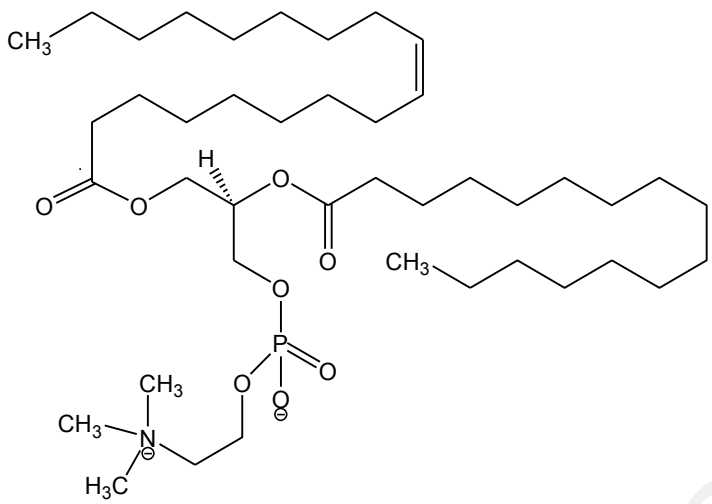

Figure 4.1: Chemical structure of lecithin.

Alternatively, there was no significant difference in mean particle size and PDI of SL3, OL1 and OL2, which indicated that lecithin and oleic acid possessed similar properties within the lipid matrix. Lecithin appeared in solid form at room temperature but did not re-solidify during the rapid cooling process. Instead, it dissolved in the liquid lipid and did not act as solid lipid in NLC. This assumption was further supported by observation under OPM (in section 4.2.1), where lecithin dissolved in oleic acid at room temperature (Figure 4.8) and altered its appearance at approximately 182.8 ˚C (Figure 4.7). Unlike stearic acid, this was an irreversible process and the lecithin remained as liquid when cooled to room temperature. As such, it can be presumed that instead of solid lipid, lecithin could potentially act as a liquid lipid and ionic surfactant, which stabilized the system by contributing high surface charge.

4.1.1.3 Effect of types of nonionic surfactant

As a nonionic surfactant cannot ionize into a charging group in an aqueous system, the surfactant adsorption by its hydroxyl groups can lead it to be negatively charged. Meanwhile, the bulky hydrophilic head groups of the nonionic surfactant provides steric stabilization to stabilize the NLC dispersion. Tweens are hydrophilic surfactants that are

soluble or dispersible in aqueous solutions. The solubility of Tween in water increases with the degree of ethoxylation, but decreases with the number of ester groupings and the molecular weight of the fatty acid. In this study, several Tween surfactants with different hydrophilic-lipophilic balance (HLB) were utilized to select the most suitable one in producing the most stable and smallest NLC dispersion (Table 4.3).

Table 4.3: Types of Tween surfactants.

Surfactant	Chemical identity	Number of carbon	HLB
Tween 40	PEG-20 sorbitan monopalmitate	16	15.6
Tween 60	PEG-20 sorbitan monostearate	18	14.9
Tween 80	PEG-20 sorbitan monooleate	18	15.0

Unlike Tween 40, Tween 60 possesses longer alkyl chains and lower HLB which is more lipophilic and creates unfavorable energy when in contact with water. In order to minimize the unfavorable energy, it is more likely to self-assemble into aggregates at low concentration in aqueous medium, and therefore, form smaller emulsion droplets and consequently smaller particles (Franzetti *et al.*, 2010; Woo, 2014). In this case, Tween 60 yielded small particles after preparation but showed large size increment throughout the storage period as indicated in Figure 4.2. NLC stabilized by Tween 80 exhibited the smallest mean particle size and least increment over the tested period. Tween 80, that had the same chain length with Tween 60, contained unsaturated carbon chain. Unlike the linear structure of Tween 60, the double bond of Tween 80 caused the hydrophobic tail to bend. This structure was presumed to be more compatible with lecithin to form a closely packed surfactant layer by intercalating between the phospholipid monolayer. As a result, increased stability was achieved. Meanwhile, there was no significant difference in PDI between all formulations (less than 0.25) over the

storage period of 30 days, therefore the occurrence of aggregation was least probable to happen.

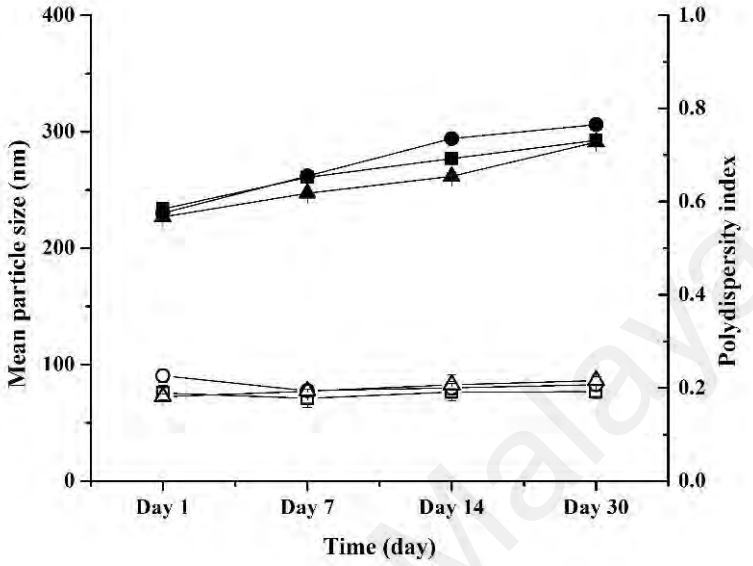

Figure 4.2: Mean particle size (solid symbol) and polydispersity index (open symbol) of T40 (■), T60 (●) and T80 (▲) as a function of storage time, at 25 ˚C.

4.1.1.4 Effect of surfactant ratio Tween 80 to lecithin

The two surfactants used were Tween 80, a nonionic surfactant and lecithin, an ionic surfactant. It was presumed that Tween 80 stabilized the system in term of steric stabilization by presumably coating the NLC, while lecithin provided electrostatic repulsion among the nanoparticles. Due to their amphiphilic character, these surfactants were likely to remain on the particle interface and therefore influenced the particle size and zeta potential. Experiments were carried out to investigate the suitable ratio of the surfactants in stabilizing the system. A range of NLCs with different composition of surfactants (Table 4.4) were labeled as TL1 to TL6 to highlight their variations in concentration of Tween 80 and lecithin. The samples were tested for their stabilities with respect to the mean particle size, PDI and zeta potential for 30 days.

TL2 with only lecithin as surfactant formed large particulates during the rapid cooling process, and as such was not subjected to particle size and zeta potential analysis. During the solidification process, the surface condition changed dramatically from a liquid emulsion droplet to a solid nanoparticle. Surfactants were added to the newly formed particles in order to help stabilize the particles in suspension. When high concentration of lecithin was used alone as a surfactant, it tended to form vesicles in the aqueous medium which therefore slowed down the molecular movement to cover the newly formed naked nanoparticle surface. The particle surface, without protection of a surfactant prone to flocculate due to the intermolecular Van der Waals attractive forces, leading to the failure in nanoparticles formation (Shekhawat, 2013).

Table 4.4: Formulations of NLCs with different surfactant compositions.

Sample	Percentage of ingredient (% (w/w))				
	Stearic acid	**Oleic acid**	**Lecithin**	**Tween 80**	**Deionized water**
TL1	5.9	1.6	0	1.5	91.0
TL2	5.9	1.6	1.5	0	91.0
TL3	5.9	1.6	0.1	1.4	91.0
TL4	5.9	1.6	0.2	1.3	91.0
TL5	5.9	1.6	0.3	1.2	91.0
TL6	5.9	1.6	0.4	1.1	91.0

This work has demonstrated that NLCs with mixed lecithin and Tween 80 surfactants were successfully prepared. In Figure 4.3, the mean particle size decreased from TL1 to TL4, but increased from TL4 to TL6. This could potentially be attributed to lecithin favoring a large oil/water interface which was able to increase the interfacial area, and as such produced a smaller particle. When the curvature radius reached a critical value, further reduction in particle size was disfavored by lecithin (Schubert & Müller-Goymann, 2005). Additionally, lecithin at high concentrations destabilized the system,

which was indicated by the fluctuating mean particle size and PDI of TL6 across the storage period. This could possibly be due to the formation of micelles by lecithin in the aqueous phase, producing a higher PDI. According to Schubert and Müller-Goymann (2005), a monolayer of lecithin at the surface of particle was formed only at a low concentration of lecithin. As such, the amount of lecithin should be minimized to avoid the formation of other structures in the system.

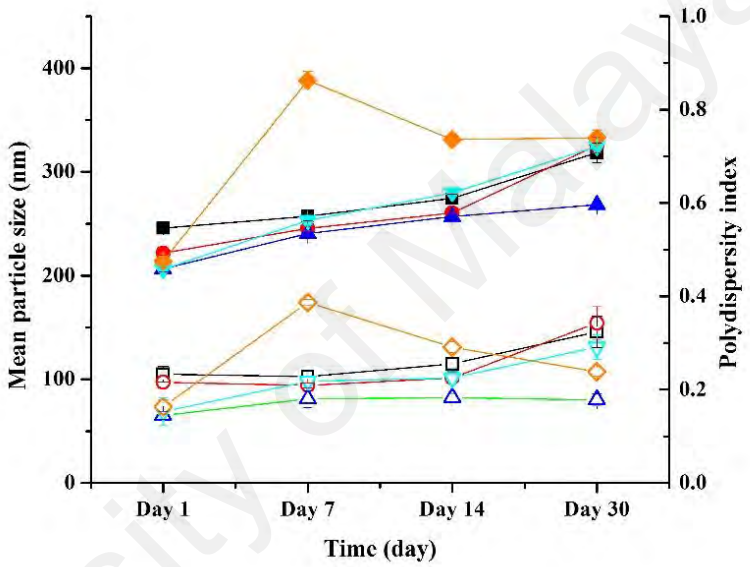

Figure 4.3: Mean particle size (solid symbol) and polydispersity index (open symbol) of TL1 (■), TL3 (●), TL4 (▲), TL5 (▼) and TL6 (♦) as a function of storage time, at 25 ˚C.

In Figure 4.4, there was negligible changes in zeta potential of the NLCs, implying constant interface properties of the particles. This indicated that migration of lecithin molecules into the aqueous system to form vesicles was unlikely to occur (Schubert *et al.*, 2006). TL1 without lecithin had a zeta potential of less than -30 mV, showing increased stability of the stearic acid-nanoparticles. The negative sign of zeta potential was plausibly dominated by the carboxylic groups of stearic acid, phosphate group of lecithin and the hydroxyl adsorption by Tween 80 in the aqueous medium. Incorporation of lecithin enhanced the stability of the system with stronger repulsion forces, indicated

by a higher zeta potential of less than -40 mV. Nonetheless, too much lecithin could lead to aggregation.

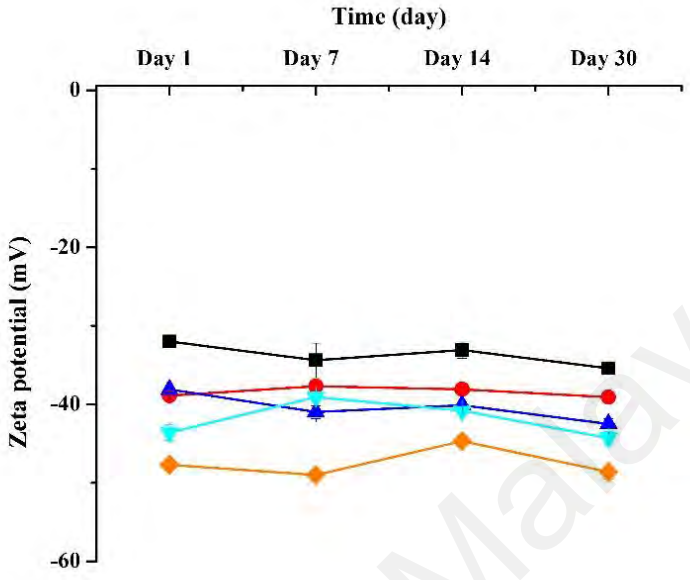

Figure 4.4: Zeta potential of TL1 (■), TL3 (●), TL4 (▲), TL5 (▼) and TL6 (♦) as a function of storage time, at 25 ˚C.

Based on the results obtained from previous experiments, the optimum NLC preparation parameters and compositions as were chosen to prepare a stable NLC dispersion with desired particle size and zeta potential. The optimized preparation parameters were homogenization speed of 18,000 rpm and homogenization time of 10 mins while the optimized formulation was TL4 as stated in Table 4.4.

4.1.1.5 Incorporation of *alpha*-tocopherol

Alpha-tocopherol is a common active ingredient utilized in topical application. The lipophilic property of *alpha*-tocopherol gave rise to its encapsulation within the lipid matrix of NLC. In this study, effect of concentration of *alpha*-tocopherol on particle size of NLCs was investigated. The amount of *alpha*-tocopherol added was found to affect the mean particle size of NLC and the stability of the formulation. As shown in Figure

4.5, mean particle size and PDI of NLCs increased with increasing amount of *alpha*-tocopherol. Sedimentation was observed in NLCs with 0.4% and 0.6% of *alpha*-tocopherol after 21 days, potentially due to the denser particles formed during lipid solidification. High amount of *alpha*-tocopherol produced highly viscous nanoemulsions and formed dense nanoparticles upon solidification. Even though NLCs containing 0.1% and 0.2% of *alpha*-tocopherol were having similar mean particle size after 30 days, 0.1% was considered more stable due to its lower and increasingly more stable increment in mean particle size and PDI. The increasing mean particle size and PDI of *alpha*-tocopherol loaded NLCs across the storage period were probably caused by the expulsion of *alpha*-tocopherol from the lipid matrix, where the free *alpha*-tocopherol could potentially form larger nanoemulsions with excess surfactant and consequently contribute to the higher PDI (Woo *et al.*, 2014).

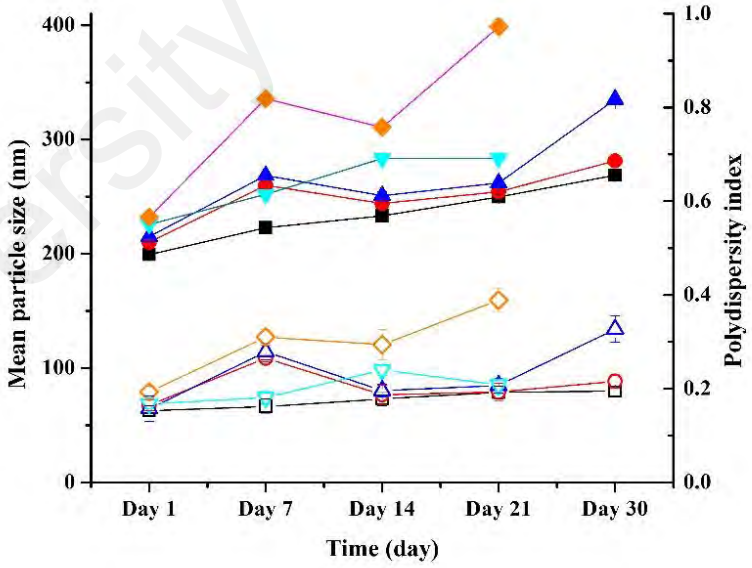

Figure 4.5: Mean particle size (solid symbol) and polydispersity index (open symbol) of NLCs loaded with *alpha*-tocopherol at concentrations of 0.1% (■), 0.2% (●), 0.3% (▲), 0.4% (▼) and 0.6% (♦) as a function of time, at 25 ˚C.

Meanwhile, the *alpha*-tocopherol loaded NLCs showed a negligible difference of average zeta potential with the unloaded NLC and there was also no significant changes across the investigation period. This indicated consistent condition on the surface structure of the particles. Additionally, the zeta potential for all formulations was found to be lower than -30 mV, and as such it was generally accepted as a stable colloidal dispersion (Müller *et al.*, 2001). Nonetheless, the steric stabilizer present in the system was not taken into account in this prediction. For instance, Tween 80 as a nonionic surfactant was able to adsorb onto the surface of particles to provide steric stabilization between the particles (Han *et al.*, 2008).

4.1.1.6 Incorporation of hydroquinone

For studying the ability of NLC to encapsulate active ingredients of different properties, hydroquinone, which is water-soluble, was loaded into NLC in the same manner as *alpha*-tocopherol. Since NLCs loaded with 0.4% and 0.6% of *alpha*-tocopherol were not stable in the previous experiment, the stability test for hydroquinone loaded NLCs was carried out at concentrations of 0.1%, 0.2% and 0.3% only. From the particle size analysis as shown in Figure 4.6, the mean particle size and PDI of NLC were directly proportional to the amount of hydroquinone loaded and the storage time. This phenomena might be explained by the aggregation of particles during storage under the effect of gravity. Nonetheless, all the formulations were considered monodisperse throughout the analysis period, indicated by the low PDI, which was less than 0.25. The low increments in mean particle size and PDI were owing to the hydrophilic nature of hydroquinone, where the hydroquinone molecules that diffused into the dispersing medium preferably stayed in the aqueous system, rather than forming emulsion with the excess surfactant.

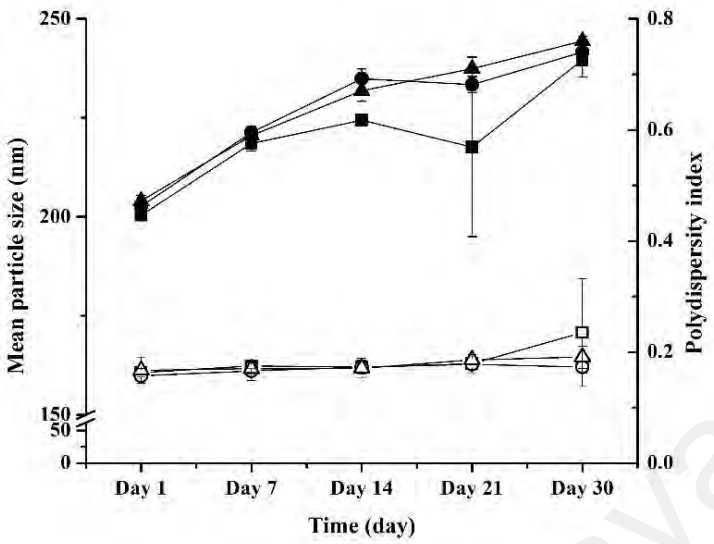

Figure 4.6: Mean particle size (solid symbol) and polydispersity index (open symbol) of NLCs loaded with hydroquinone at concentrations of 0.1% (■), 0.2% (●) and 0.3% (▲) as a function of time, at 25 ˚C.

4.1.2 Morphology of NLC

4.1.2.1 Optical polarizing microscope (OPM)

Although OPM has limited resolution in examining the morphology of NLC, it was employed to investigate the formation of liposomes by lecithin in the aqueous medium. According to Placzek & Kosela (2016), liposomes showed a birefringence effect under polarized light. As the structure could not be found in the NLC dispersion, it was assumed that liposomes did not form in the system. Lecithin appeared as solid at room temperature but did not melt and recrystalize during the heating and cooling processes (Figure 4.7). As shown in Figure 4.8, lecithin dissolved in oleic acid at room temperature, therefore could not be used as a solid lipid in forming the SLN or NLC.

To visualize the crystallization process, NLC was melted and cooled back to room temperature. It was observed that the air-dried NLC melted upon heating and recrystallized upon cooling, ensuring the formation of lipid nanoparticles by stearic acid. This observation was further supported by the thermal analysis of NLC in section 4.1.3.

Crystallization of melted NLC started from the center of the droplet outwards (Figure 4.9). Therefore, active ingredients incorporated in the lipid matrix might be settled around the lipid outer shell. According to Grana *et al.* (2013), this was known as a shell model.

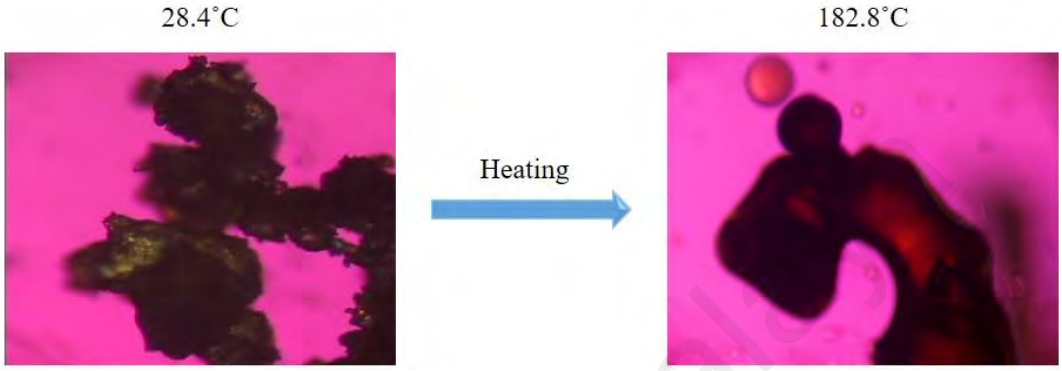

Figure 4.7: Polarizing micrograph of lecithin at 28.4 ˚C and 182.8 ˚C.

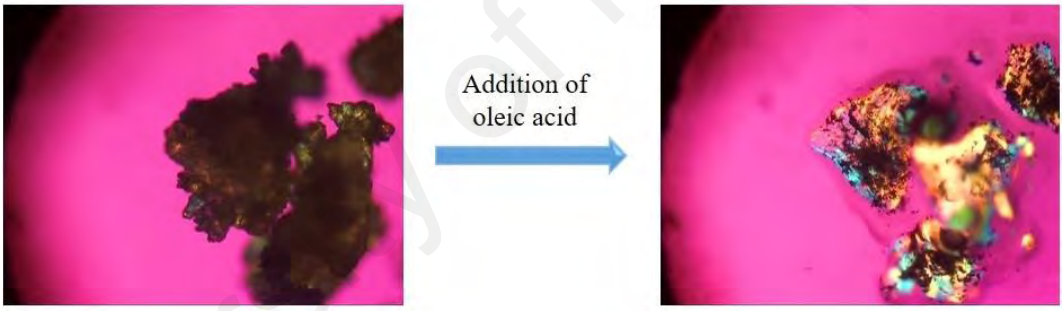

Figure 4.8: Polarizing micrograph of lecithin before and after addition of oleic acid.

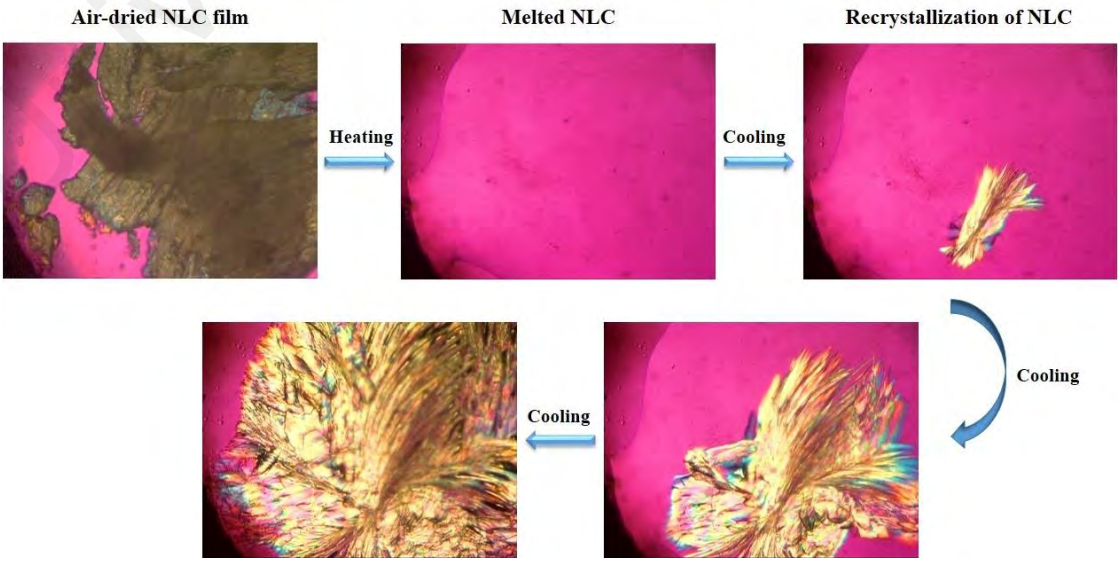

Figure 4.9: The melting and re-crystallization processes of air-dried NLC.

4.1.2.2 Transmission electron microscope (TEM)

The effect of lecithin and the concentration of *alpha*-tocopherol on morphology of NLC was scrutinized using TEM microscopy. TEM micrographs of the NLCs revealed the round shape of particles, which was in agreement with the assumption in particle size measurement. In Figure 4.10 (b), addition of lecithin managed to stabilize the system by electrostatic repulsion forces so that particles stayed distant. In contrast, NLC without lecithin demonstrated particles of different size with potent aggregation (Figure 4.10 (a)). As shown in Figure 4.11 (a), NLC with 0.1% *alpha*-tocopherol had monodisperse particle size and no evident aggregation. Nevertheless, NLC with 0.6% *alpha*-tocopherol in Figure 4.11 (b) were not as solid as NLC with 0.1% *alpha*-tocopherol. NLC particles were smearing due to the high vacuum condition of TEM, indicating that nanoemulsions might instead form rather than nanoparticles. Aggregation was obvious and this explains the occurrence of sedimentation after storage for 21 days.

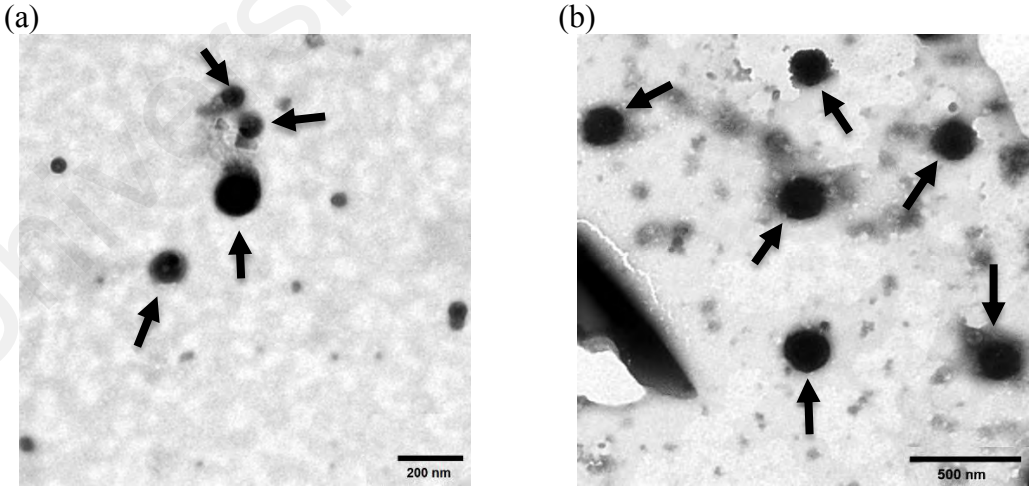

Figure 4.10: TEM micrographs of NLCs (a) without lecithin, TL1 and (b) with lecithin, TL4.

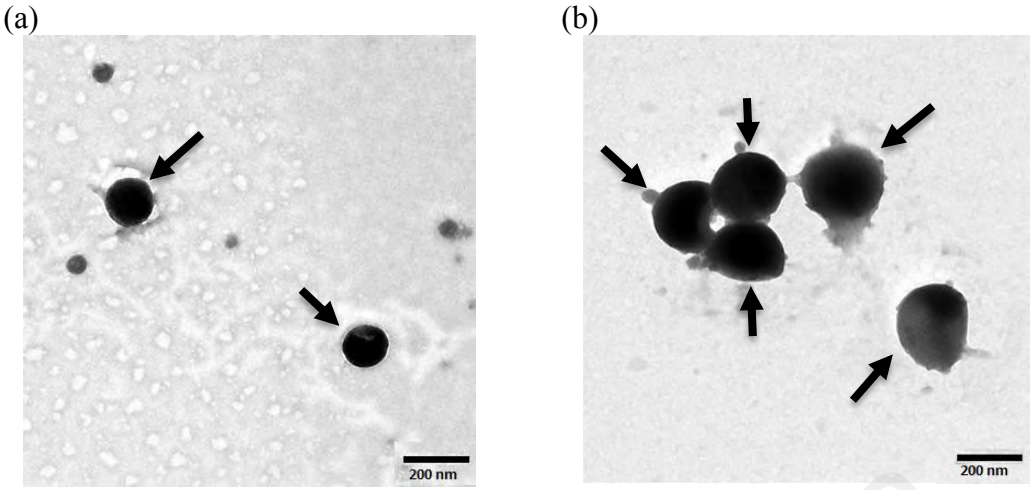

Figure 4.11: TEM micrographs of NLCs loaded with (a) 0.1% and (b) 0.6% *alpha*-tocopherol.

It was noticed that the particle size shown in the TEM micrographs was smaller compared to the mean particle size reported by Zetasizer analysis. This was due to TEM that displayed the image of the particle core as the surfactant layer was too thin to be visualized by electrons, while Zetasizer measured the hydrodynamic diameter of a particle dependent on its surface structure, concentration and type of ions in the medium. Additionally, all particles, including contaminants and dust, present in the sample were taken into account by Zetasizer, influencing the mean particle size obtained.

4.1.3 Thermal analysis of NLC

Thermal properties of NLCs, such as melting point (T_m), peak width at half minimum ($\Delta T_{1/2}$) and melting enthalpy (ΔH), were analyzed by using a DSC. The differences in these thermal properties reflected different molecular packing of the hydrocarbon chains in the crystal lattice. The endotherm of nanoparticles were broadened and shifted to a lower temperature due to the adsorption of surfactant molecules.

Stearic acid is a solid lipid with high crystallinity at both atmospheric and body temperature. In NLC, the incorporated lipidic components had dissimilar structures which caused a mismatch in the hydrocarbon chains and subsequent imperfections in the lipid matrix of stearic acid (Nahak *et al.*, 2015). These lipidic components include

oleic acid and stabilizers used in the system, such as lecithin and Tween 80. In this study, DSC was utilized to shed light on the location of the surfactants. A higher volume of hydrophobic surfactant would penetrate deeper into the lipid core, contributing to a lower crystallinity, while hydrophilic surfactant preferentially resided on the particle's surface. This perturbed the packing of the hydrocarbon chains in the lipid matrix in a smaller extent, and hence, remained the thermal properties.

Figure 4.12 showed the thermogram of stearic acid analyzed by TA Universal Analysis Software. The peak of minimum heat flow represented the melting point, T_m (70.8 ˚C) with the enthalpy change, ΔH (210.1 J g^{-1}) obtained from integration of the shaded area of the endothermic peak. The peak width can also be used to mark the presence of multicrystallinity. A sharp peak with narrow $\Delta T_{1/2}$ (3.6 ˚C) indicated that the pure stearic acid was highly crystalline.

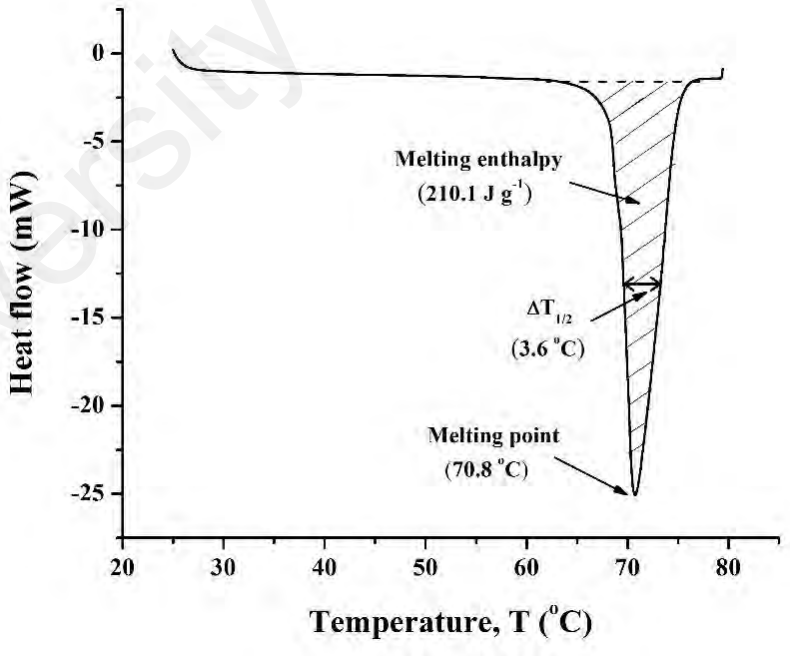

Figure 4.12: Endothermic thermogram of stearic acid.

As shown in Table 4.5 and Figure 4.13, there was no obvious trend in the crystallinity of the NLCs with surfactant content. This indicated that the packing of lecithin and

Tween 80 was different at different concentrations. For example, the crystallinity degree was high when lecithin was used alone as the surfactant. As mentioned in section 4.1.1.4, the nanoemulsions did not form nanoparticles during rapid cooling process. Instead, it formed large particulates containing stearic acid matrix incorporated with only oleic acid, and therefore possessed higher crystallinity. Alternatively, NLC without lecithin had higher crystallinity degree compared to NLCs with low amount of lecithin, suggesting that lecithin was more hydrophobic and penetrated deeper into the lipid core than Tween 80. In addition, lecithin which possessed two hydrophobic tails could potentially induce heterogeneous nucleation caused by the interaction between the lipid melt and the surfactant layer (Bunjes & Unruh, 2007). However, 0.5% of lecithin provided slightly higher crystallinity compared to 0.2% of lecithin. This was in agreement with a previous observation in section 4.1.1.4, where not all lecithin participated in the formation of lipid nanoparticles. Excess lecithin molecules could potentially form other structures in the dispersing medium. Additionally, there were previous studies reporting faster polymorphic transition in lecithin-loaded lipid matrices, and as such lecithin should be used at an appropriate amount to provide low crystallinity and minimize the polymorphic transition rate (Schubert *et al.*, 2006; Schubert & Müller-Goymann, 2005; Schubert *et al.*, 2005).

Table 4.5: Melting point (T_m), peak width at half minimum ($\Delta T_{1/2}$), melting enthalpy (ΔH) and degree of crystallinity of NLCs.

Lecithin content (%)	Tween 80 content (%)	Thermal properties of NLC			
		T_m (°C)	$\Delta T_{1/2}$ (°C)	ΔH (J g^{-1})	Crystallinity degree (%)
0	1.5	65.1	4.7	135.6	64.5
0.2	1.3	65.0	5.4	133.6	63.6
0.5	1.0	65.4	5.2	134.5	64.0
1.5	0	66.4	3.4	136.6	65.0

NLCs were subjected to a heating scan followed by a cooling scan. The recrystallization event was observed by an exothermic peak as demonstrated in Figure 4.14, once again confirmed the reversible phase transition of the stearic acid-nanoparticles. This observation was being consistent with the results shown by OPM. Nevertheless, the recrystallized forms of NLCs did not have a nano structure as the lipid components could potentially fuse upon melting. Therefore, storage and further processing of NLCs must avoid exposure to heat.

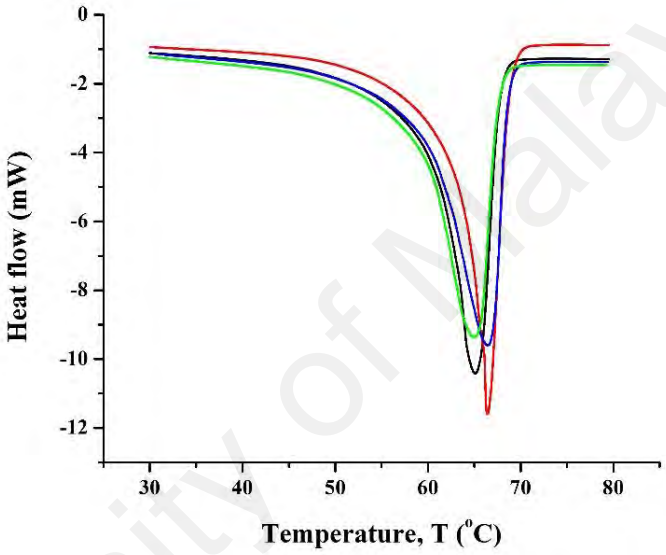

Figure 4.13: Endothermic thermograms of NLCs containing 0% (−), 0.1% (−), 0.2% (−) and 1.5% (−) of lecithin.

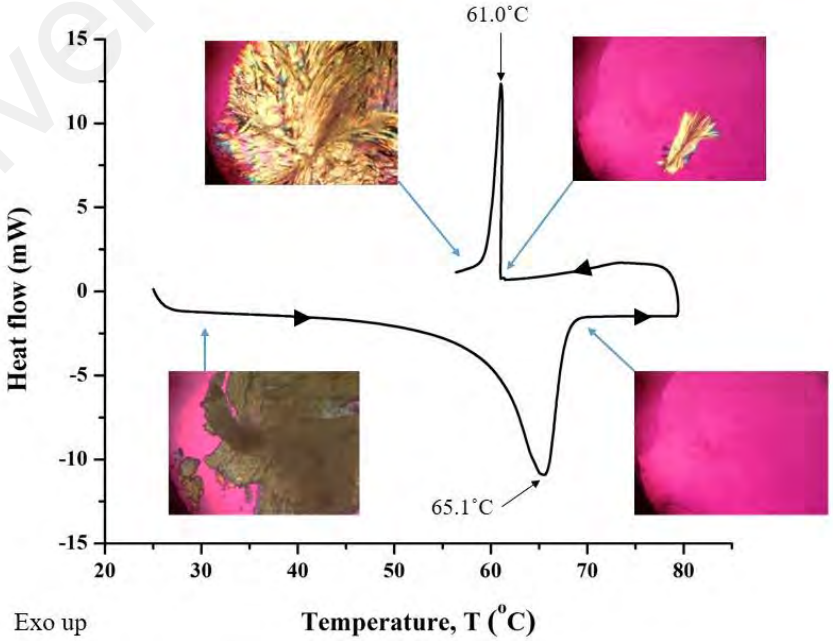

Figure 4.14: Thermogram shows the melting and recrystallization processes of air-dried TL1 upon heating and cooling scans, corresponding to the polarizing micrographs.

4.1.4 Encapsulation efficiency of active ingredients in NLC

For an effective carrier system, it is very important to be aware of the encapsulation efficiency of active ingredients in the carrier to minimize the loss. Only stable NLC formulations, without any appearance of sedimentation, were evaluated for the encapsulation efficiency of *alpha*-tocopherol and hydroquinone.

Incorporation of oleic acid into the solid lipid perturbed the crystalline matrix of the solid lipid matrix, which increased the loading space for the active compound (Woo *et al.*, 20.14). It can be observed in Figure 4.16 that the encapsulation efficiency of *alpha*-tocopherol was inversely proportional to the amount of *alpha*-tocopherol added. The active ingredient could plausibly exceed its maximum capacity in the lipid matrix due to the limited space to accommodate the guest molecules or because it has reached the optimum molecular compatibility in the NLC matrix composition. Nevertheless, the encapsulation efficiency was high overall, more than 90% for all formulations under investigation. This observation might be attributed to the two-membered ring with long hydrocarbon chain of *alpha*-tocopherol, as shown in Figure 4.15, which has higher preference in the lipid matrix compared to the aqueous dispersing medium. As such, the main criteria in selecting the optimum concentration of *alpha*-tocopherol was not only based on the encapsulation efficiency but also on the compatibility of the lipid matrix and also the stability of the formulation during storage, according to the particle size measurement.

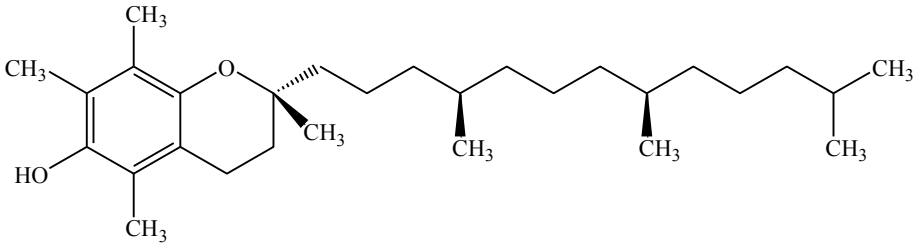

Figure 4.15: Chemical structure of *alpha*-tocopherol.

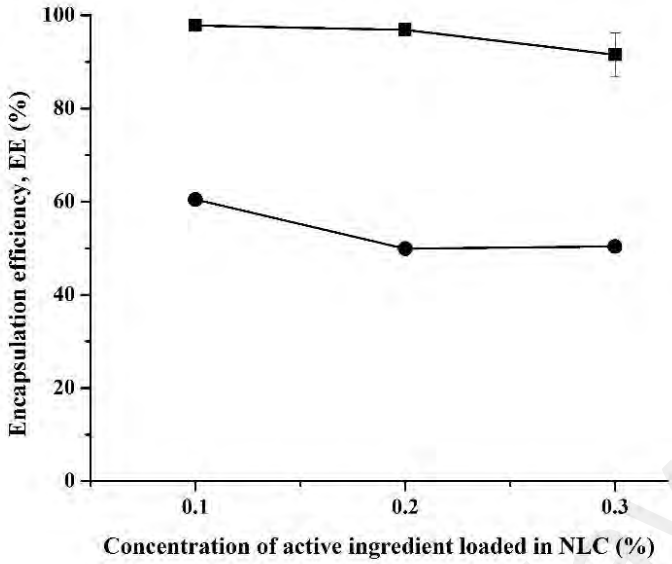

Figure 4.16: Encapsulation efficiency of *alpha*-tocopherol (■) and hydroquinone (●) as a function of concentration of active ingredient loaded in NLC.

In contrast, the encapsulation efficiency of hydroquinone was much lower than that of *alpha*-tocopherol. In Figure 4.16, NLC loaded with 0.1% of hydroquinone exhibited the highest encapsulation efficiency of 60.48%, the number was then decreased significantly to around 50% when 0.2% and 0.3% of hydroquinone were loaded. The low encapsulation of hydroquinone in NLC was probably due to its hydrophilic structure, as shown in Figure 4.17, to disproportionate in the aqueous medium, preferably further apart from the particles. Undoubtedly, the centrifugal ultrafiltration method could potentially give a lower encapsulation efficiency of hydroquinone as the active ingredient was loosely adsorbed on the surface of particle. Consequently, it was easy to be re-dispersed into the aqueous medium under strong centrifugal forces.

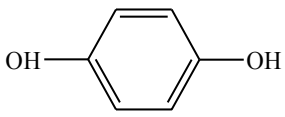

Figure 4.17: Chemical structure of hydroquinone.

Based on the results obtained from the physicochemical characterization of NLCs, formulation TL4 loaded with 0.1% of active ingredients was considered to be the optimized formulation to be incorporated into the gel mixture.

4.2 Characterization of thermoresponsive gel

4.2.1 Rheological characterization

4.2.1.1 Viscometry test

The viscometry test of the plain gel in Figure 4.18 demonstrated that the flow behavior of the gel mixture was influenced by the concentration of *ι*-C and Ca^{2+} ions. Yield stress, σ_y, that represents the maximum shear stress below which no flow will occur, is commonly used to calculate whether a sample is likely to settle at equilibrium and the difficulty to start pumping or stirring. A higher σ_y illustrates a more structured network and therefore higher stability and higher difficulty to be pumped out. Figure 4.18 (a) showed that the σ_y increased with ascending amount of *ι*-C, where there was a huge gap between *ι*c37 and *ι*c73, indicating the more entangled structure caused by *ι*-C. However, only σ_y of *ι*c55 was dependent on the concentration of Ca^{2+} ions.

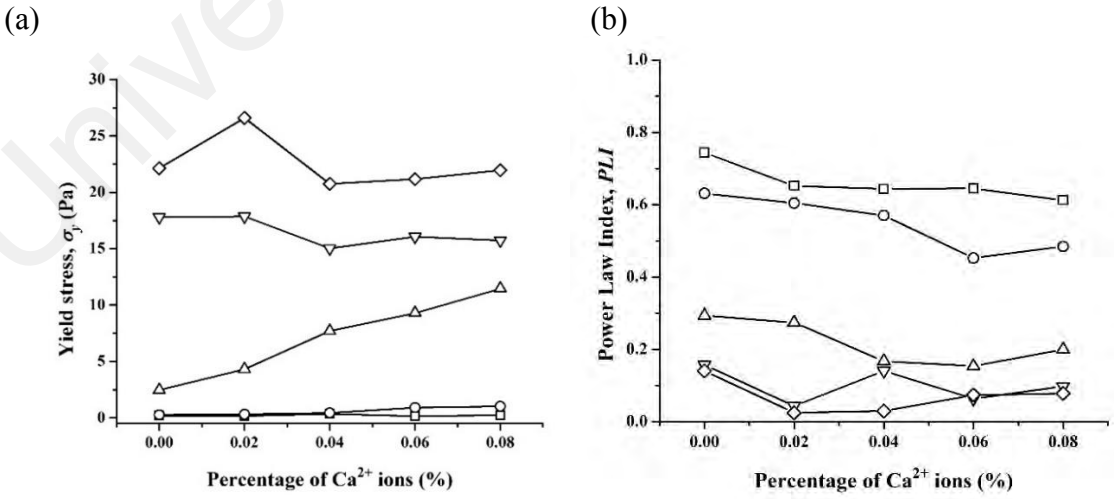

Figure 4.18: (a) Yield stress, σ_y and (b) Power-Law index, *n* of gel mixtures *ι*c28 (□), *ι*c37 (○), *ι*c55 (△), *ι*c73 (▽) and *ι*c82 (◊) as a function of percentage concentration of Ca^{2+} ions, at 25 °C.

In Figure 4.18 (b), all the gel mixtures exhibited shear thinning behavior, indicated by Power-Law index where $n < 1$, with the behavior more pronounced in gel mixtures containing high amount of *ι*-C, such as *ι*c55, *ι*c73 and *ι*c82, in which $n < 0.5$. Shear thinning was due to the disentanglement of the polymer coils which then orientated to the flow direction resulting from the externally imposed shear. The effect of added cations on the viscosity, η, of the gel was limited to a certain critical cation concentration. As shown in Figure 4.19 (a), η of *ι*c55 increased markedly from 0.02% to 0.04% of Ca^{2+} ions, but the η remained constant for 0.06% and 0.08% of Ca^{2+} ions. Additionally, η of the gel mixture *ι*c73 (Figure 4.19 (b)) and *ι*c82 did not seem to be influenced by the concentration of Ca^{2+} ions. This was attributed to the limited free volume in the gel system, where the polymer chains were packed closely enough to crosslink and entangle, reducing the role of Ca^{2+} ions in entanglement of the polymers.

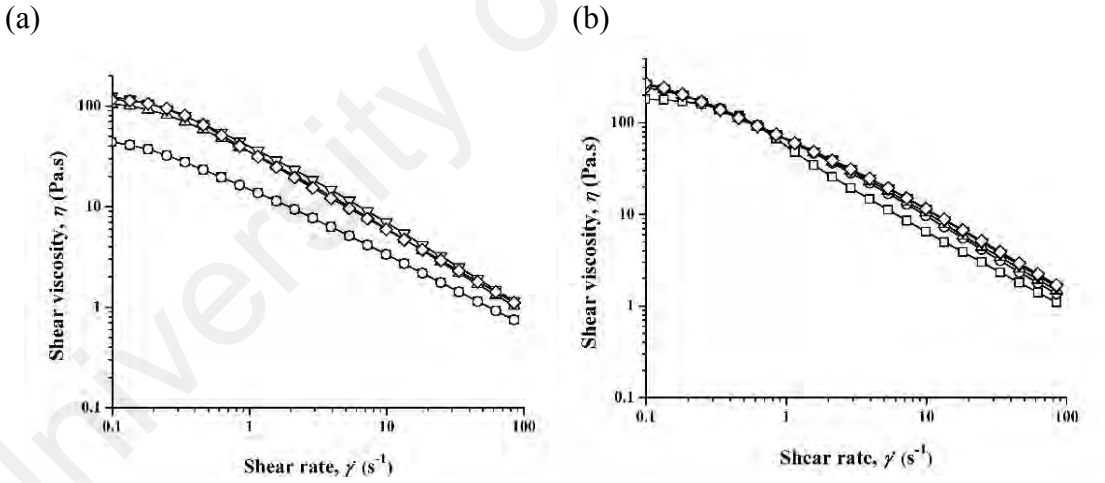

Figure 4.19: Shear viscosity, η of gel mixtures (a) *ι*c55 and (b) *ι*c73 in 0% (□), 0.02% (○), 0.04% (△), 0.06% (▽) and 0.08% (◊) of Ca^{2+} ion solutions as a function of shear rate, at 25 ˚C.

In contrast to *ι*-C, the CMC gel strength was affected by the pH of a medium. Low pH was favorable in strong gel formation as the Na^+ ion was replaced by the H^+ ion which formed inter-chain hydrogen bonds, decreasing the solubility of CMC in water (Gulrez & Al-Assaf, 2011). As such, CMC in the neutral system displayed liquid-like

behavior with limited intrinsic viscosity and strength (Yang *et al.*, 2009). CMC gel was too weak to hold and stabilize the lipid nanoparticles in the gel system, while *ι*-C gel was too rigid to spread evenly on the skin. As such, a mixture of CMC and *ι*-C was a promising combination to provide an adequate flowing profile under shear and at the same time maintain its rigidity in storage.

4.2.1.2 Linear viscoelastic behavior

Amplitude sweep delivers comprehensive information, such as linear viscoelastic region (LVR), storage modulus, *G'*, loss modulus, *G''* and critical strain, γ_c, of the viscoelastic sample. LVR is of main interest as it is associated with the configuration of the polymer, which does not change substantially from the equilibrium structure of the gel system. The point at γ_c is the maximum strain before the gel structure breaks beyond the linear region. After this critical point, the entangled molecule chains start to reorganize and align with the flow direction (Aho, 2011). Frequency sweep and temperature ramp are then carried out under the strain within the LVR to ensure non-destructive conditions so that the structure will not be disrupted as it does in the continuous shear technique (Shekhawat, 2013).

In Figure 4.20, it was noteworthy that γ_c of gel mixtures in 0% to 0.04% Ca^{2+} solutions was constant until a significant increment was observed at 0.06% of Ca^{2+} ions. Concurrently, γ_c of the gel mixtures was increased with increased concentration of *ι*-C. Addition of *ι*-C strengthened the gel system and hence caused a higher resistance against deformation, owing to the formation of increasingly entangled, and a subsequently more flexible network structure.

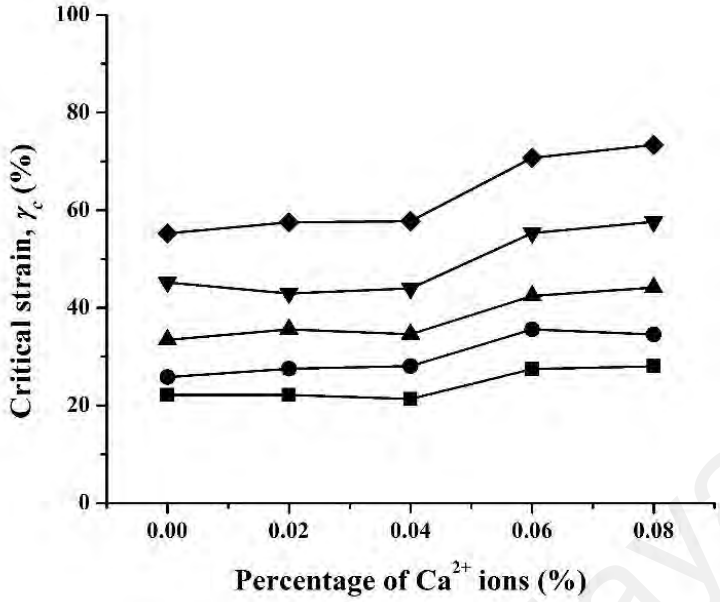

Figure 4.20: Critical strain, γ_c of gel mixtures *ι*c28 (■), *ι*c37 (●), *ι*c55 (▲), *ι*c73 (▼) and *ι*c82 (♦) as a function of percentage of Ca^{2+} ions, at 25 ˚C.

For a viscoelastic material, *G'* obtained from the measurement denotes the elasticity of the system, while *G''* demonstrates the viscous component. As previously shown in Figure 4.19, Ca^{2+} ions participated in the increased *G'* of gel mixtures with low content of *ι*-C, yet its presence was less important for those with high content of *ι*-C. As shown in Figure 4.21 (a), gel mixture *ι*c37 with 0% to 0.04% Ca^{2+} ions was dominant in the viscous component, while gel mixtures with 0.06% and 0.08% Ca^{2+} ions displayed increased gel strength with the elastic component dominating. Meanwhile for *ι*c73, as shown in Figure 4.21 (b), all the gel mixtures with and without Ca^{2+} ions exhibited solid-like properties, where $G' >> G''$. The crossover of *G'* and *G''* was shifted to a higher strain from approximately 40% to 120% when the concentration of *ι*-C increased from *ι*c37 to *ι*c73. This revealed a stronger network formed by *ι*-C which was able to endure a higher deformation.

(a)

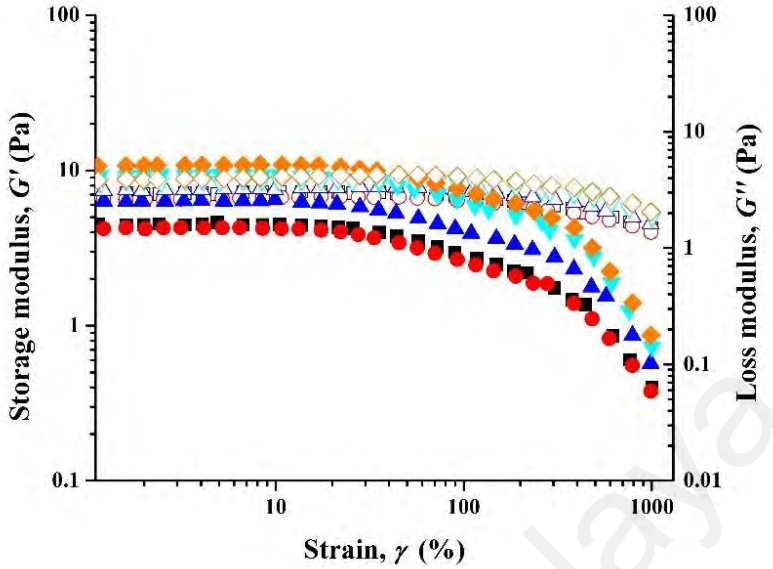

(b)

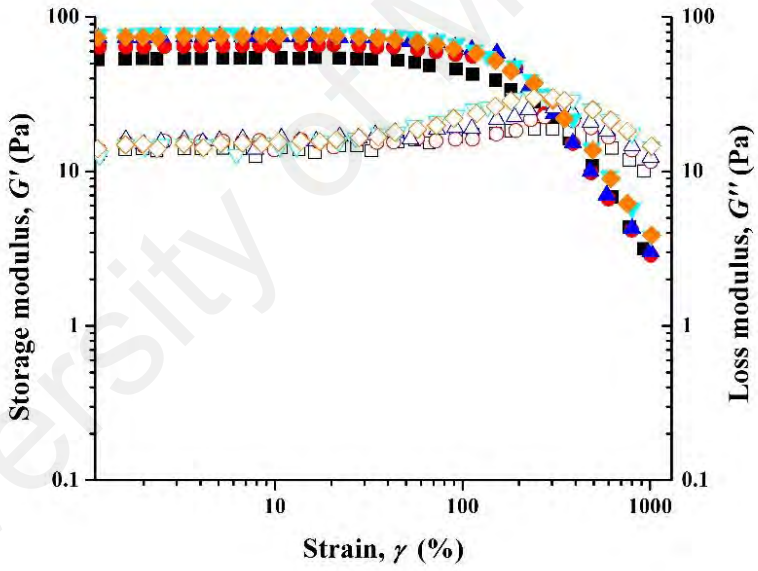

Figure 4.21: Storage modulus, *G'* (solid symbol) and loss modulus, *G''* (open symbol) of gel mixtures (a) *ι*c37 and (b) *ι*c73 in 0% (■), 0.02% (●), 0.04% (▲), 0.06% (▼) and 0.08% (♦) of Ca^{2+}solutions as a function of strain, at 25 ˚C.

4.2.1.3 Isothermal frequency sweep test

Frequency sweep is utilized to predict the behavior of a gel at long and short time scales, with respect to the low and high frequencies. The results obtained are then related to the gels condition during storage and application. In Figure 4.22, the gel mixtures

containing high amount of *ι*-C, such as *ι*c55, *ι*c73 and *ι*c82, were stable at stationary, yet had relatively poor spreadability as $G' > G''$ across the tested frequency range. In contrast, *ι*c28 with $G' < G''$ demonstrated increased spreadability with possibility processed a runny behavior. The crossover of G' and G'' in the moduli curves of *ι*c37d was worth noting as it indicated the relaxation time of the gel network. Relaxation time is the time required for a system to return to equilibrium in response to a sudden disturbance. The crossover also implied that the system behaved like a solid at low frequencies, but started to flow when high shear was applied at higher frequencies. As such, it was presumed that the system possessed increased stability during storage and good spreadability upon application.

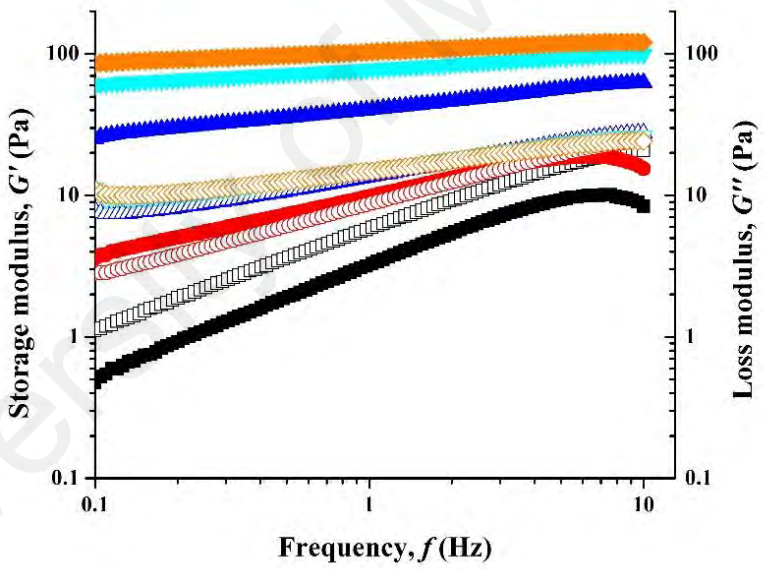

Figure 4.22: Storage modulus, G' (solid symbol) and loss modulus, G'' (open symbol) of gel mixtures (a) *ι*c28 (■), *ι*c37 (●), *ι*c55 (▲), *ι*c73 (▼) and *ι*c82 (♦) in 0.06% Ca^{2+} solution, at 25 ˚C.

In general, the *ι*-C helices are unable to aggregate due to charge repulsion between the sulfate groups, however the cations (Ca^{2+} ions) reduce the repulsion by forming electrostatic interactions with the sulfate groups (Janaswamy & Chandrasekaran, 2008). In accordance with the viscometry test in section 4.2.1.1, there was an unexpected

behavior shown by the gel mixtures *ι*c73 (Figure 4.23) and *ι*c82, where their *G'* were highest with 0.04% Ca^{2+} ions instead of 0.08% Ca^{2+} ions. This was plausibly attributed to the limited space available in the system with a high amount of *ι*-C, which lead to the restriction of movement and entanglement of the polymer molecules by the extra Ca^{2+} ions. Consequently, the system lost its elasticity.

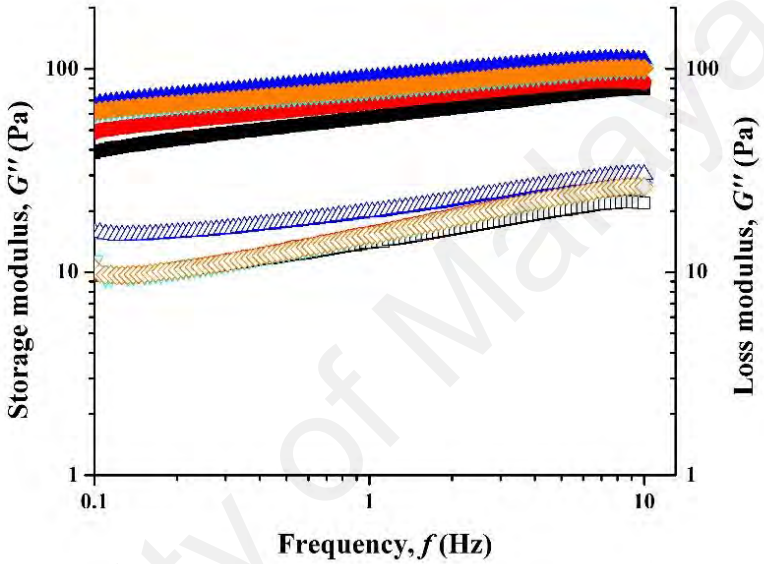

Figure 4.23: Storage modulus, *G'* (solid symbol) and loss modulus, *G''* (open symbol) of gel mixture *ι*c73 in 0% (■), 0.02% (●), 0.04% (▲), 0.06% (▼) and 0.08% (♦) of Ca^{2+} solutions as a function of frequency, at 25 ˚C.

Small strain oscillatory frequency sweep is also employed to characterize the rheological properties of the gel mixtures in term of frequency dependency of *G'*, indicated by its slope. A weak gel shows frequency dependent *G'*, while a strong gel has *G'* that is independent on frequency (Garrec & Norton, 2013). From Figure 4.24, it was proven that *ι*-C affected the gel strength of the gel mixtures more significantly compared to Ca^{2+} ions. The slope of *G'* was found to decrease with the increased concentration of *ι*-C and Ca^{2+} ions, indicating that *ι*-C contributed more in the elastic component compared with CMC, while the cations were interacting with the polymer chains to form a rigid network.

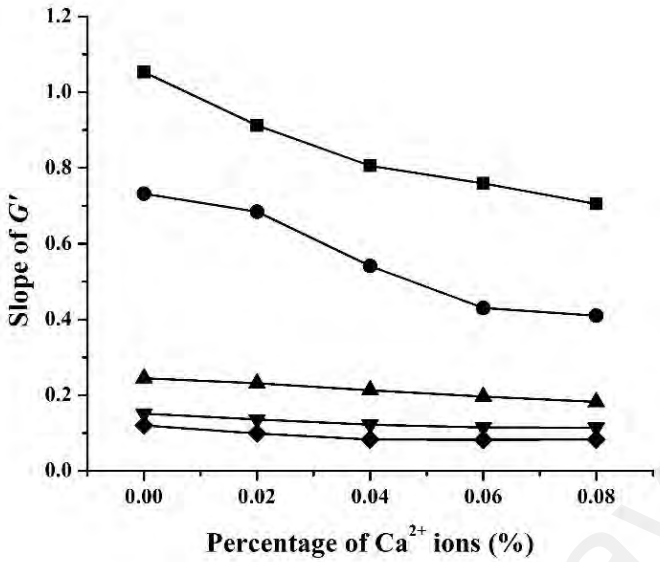

Figure 4.24: The slope of *G'* of gel mixtures *ι*c28 (■), *ι*c37 (●), *ι*c55 (▲), *ι*c73 (▼) and *ι*c82 (♦) as a function of percentage of Ca^{2+} ions, at 25 ˚C.

4.2.1.4 Temperature ramp test

Temperature ramp testing provides insight into the microscopic structure changes of a viscoelastic sample in response to temperature change. *G'* and *G''* from the heating and cooling curves demonstrate the changing structure of the gel system in response to the manufacturing processes and storage conditions. For example, heating mimics the application process while cooling can be used to design the suitable conditions for production and packaging. With transition temperature approximate to the temperature of the human body, the system is ideal for personal care and cosmetic application.

Phase transition of a gel mixture to solution was determined from the *G'* and *G''* curves generated during the heating and cooling process. There was a steep slope observed in the curves of Figure 4.25, indicating the structure lost its energy within a short temperature range and became predominant in the viscous component. According to the previous study, the structure of *ι*-C transformed from a double helix conformation to a coil conformation upon heating (Rees *et al.*, 1982). The crossover point of *G'* and

G'', T_c, was commonly known as the rheological gelling point as the structure changed from solid-like to liquid-like and vice versa. From Table 4.6, it can be noted that the gel mixtures did not gel at low concentration of *ι*-C and Ca^{2+} ions and T_c was enhanced with increasing concentrations of *ι*-C and Ca^{2+} ions. Nonetheless, the crossover point could not represent the gelling point for all gel mixtures. The crossover points of *G'* and *G''* in the heating curves of *ι*c73d (Figure 4.25), *ι*c73e, *ι*c82c, *ι*c82d and *ι*c82e were found lower than that in the cooling curves. This unpredicted phenomenon was plausibly due to entanglement and crosslinking of the concentrated polymer chains immediately after the supply of heat was stopped. As rheology can be affected by a small degree of crosslinking, *G'* became dominant against *G''*, even at temperatures higher than the gelling point. The difference between T_c and gelling point was also reported by Winter (1987), depending on the cross-linker.

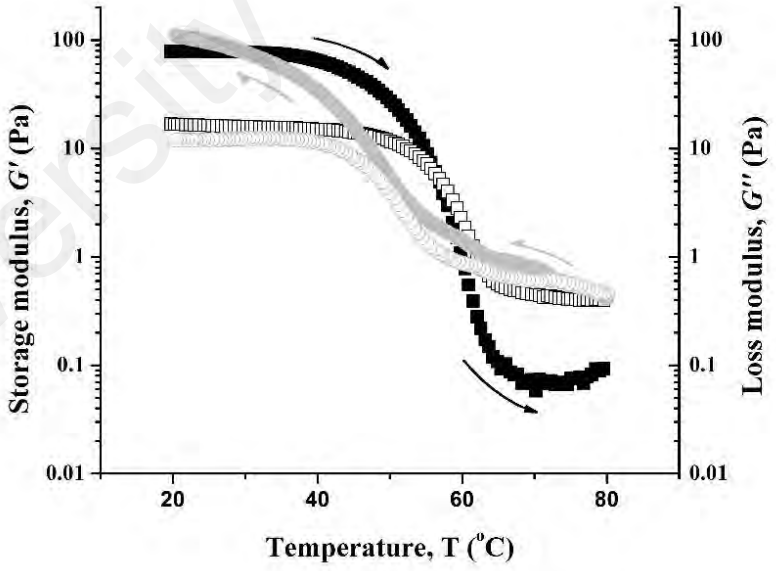

Figure 4.25: Storage modulus, *G'* (solid symbol) and loss modulus, *G''* (open symbol) of gel mixture *ι*c73d as a function of temperature during heating (■) and cooling (●) processes.

Table 4.6: Crossover temperature, T_c (˚C) of gel mixtures.

	***ι*c28**	***ι*c37**	***ι*c55**	***ι*c73**	***ι*c82**
a	-	-	42.5	48.9	52.0
b	-	-	44.7	51.8	54.2
c	-	-	47.8	53.2	57.1
d	-	38.0	50.5	56.3	59.7
e	-	43.0	52.7	58.5	61.3

Phase angle, δ could also be used to observe the occurrence of phase transition in the gel systems as the phase transition corresponds to a sudden change or maximum peak in δ, which is a measure of elasticity, where $0^\circ < \delta < 45^\circ$ indicates elastic character, while $45^\circ < \delta < 90^\circ$ indicates viscous character. As shown in figures, *ι*c28d (Figure 4.26 (a)) remained as a flowing solution with high δ over the tested temperature range, while an abrupt change in δ can be clearly observed in the rigid gelling system such as *ι*c55d in Figure 4.26 (b).

(a)

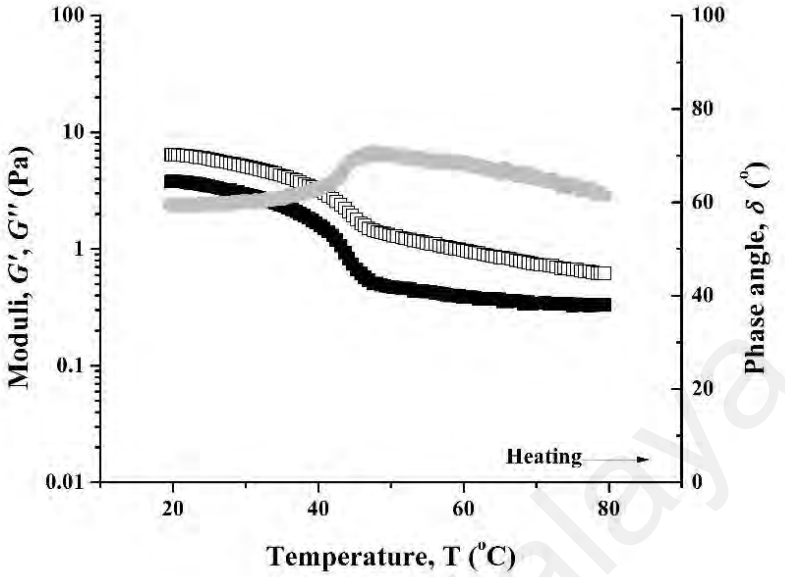

(b)

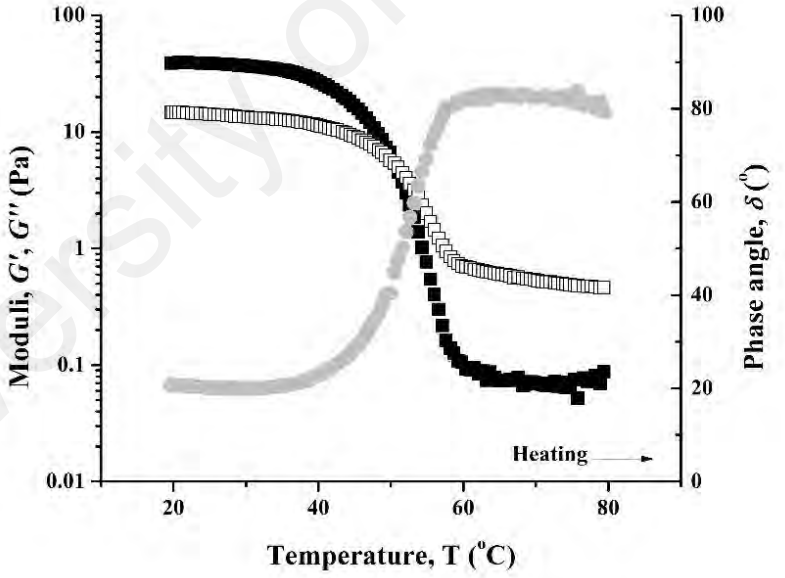

Figure 4.26: Storage modulus, *G'* (■), loss modulus, *G''* (□) and phase angle, δ (●) of gel mixtures (a) *ι*c28d and (b) *ι*c55d as a function of temperature during heating process.

Another interesting event was noticed in the systems where *G'* decreased as temperature increased, and this might fit the Arrhenius equation:

$$G' = G'_o \exp\left[{}^{E_a}/_{RT}\right] \quad \text{Eq. 4.1}$$

$$\ln G' = \left({}^{E_a}/_{RT}\right) + \ln G'_o \quad \text{Eq. 4.2}$$

Where E_a is the activation energy of the phase transition from gel to solution; R is universal gas constant, 8.31 J mol^{-1} K^{-1} and T is absolute temperature in Kelvin, K. Therefore, E_a of the phase transition can be calculated by obtaining the slope of graph ln *G'* as a function of 1/*T*.

During the heating process, aggregation of *ι*-C helices lost interactions, turning into double helixes and then into random coils (Tari *et al.*, 2011). The reduction of connectivity of polymer chains in the gel system was reflected by the decreasing *G'* with rising temperature. As reported by Janaswamy and Chandrasekaran (2002), *ι*-C molecules formed inter-chain hydrogen bonds to stabilize the double helix conformation, while Ca^{2+} ions and water molecules enhanced the 'helix-helix' interactions by connections with the sulfate groups of the polymer. Figure 4.27 illustrates the potential connection between *ι*-C molecules and Ca^{2+} ions via electrostatic interactions.

Despite the tendency of CMC to flow and dissipate energy under applied shear, the elastic component of pure CMC solution could also be raised by adding Ca^{2+} ions. As such, it could be assumed that CMC molecules were bound by interactions between carbonyl groups of CMC, COO^- and cations Ca^{2+} as illustrated in Figure 4.28. However, the solution still exhibited liquid-like behavior.

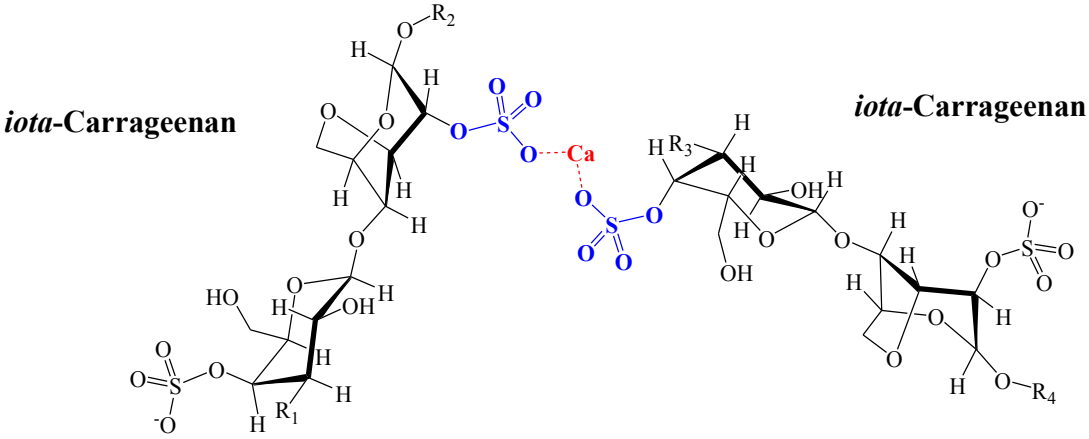

Figure 4.27: Proposed electrostatic interactions formed between Ca^{2+} ion and the negatively charged center oxygen on sulfate functional groups of *ι*-C molecules.

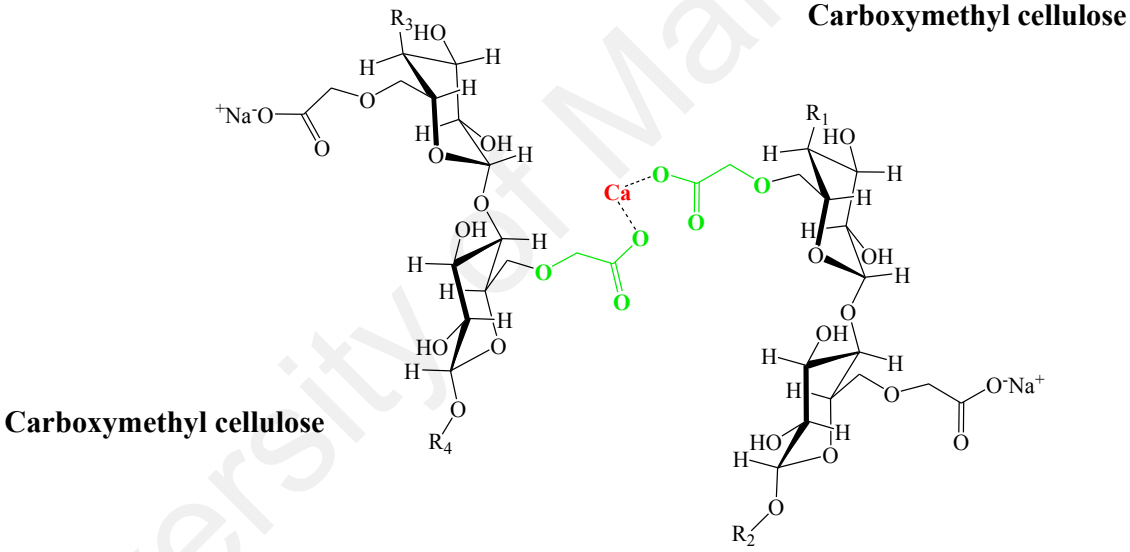

Figure 4.28: Proposed electrostatic interactions formed between Ca^{2+} ion and the negatively charged center oxygen on carbonyl functional groups of CMC molecules.

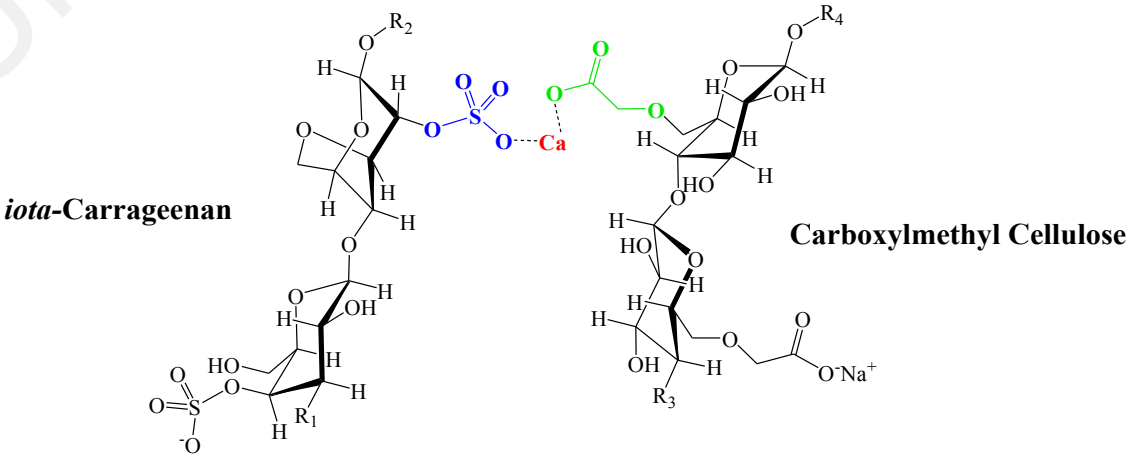

Figure 4.29: Proposed linkage between CMC and *ι*-C molecules by forming electrostatic interactions with Ca^{2+} ion respectively.

Similarly, CMC in the gel mixture was potentially linked to *ι*-C by Ca^{2+} ions, as shown in Figure 4.29. Gel mixtures can generally be classified into four types of networks, which are single polymer network entrapping the second polymer, interpenetrating networks formed by separate polymer networks, a phase-separated network and coupled network formed by interacting polymers (Cairns *et al.*, 1987). From the results obtained in the rheological measurements, the mixed gels of CMC and *ι*-C were supposed to form coupled networks by interacting with Ca^{2+} ions. Due to the growing molecular motion with ascending temperature, the hydrogen bond strength and electrostatic interaction became lesser, subsequently increasing the solubility of *ι*-C in water. As such, the rigid gel transformed into a flowing solution during the heating process and vice versa during the cooling process (Figure 4.30).

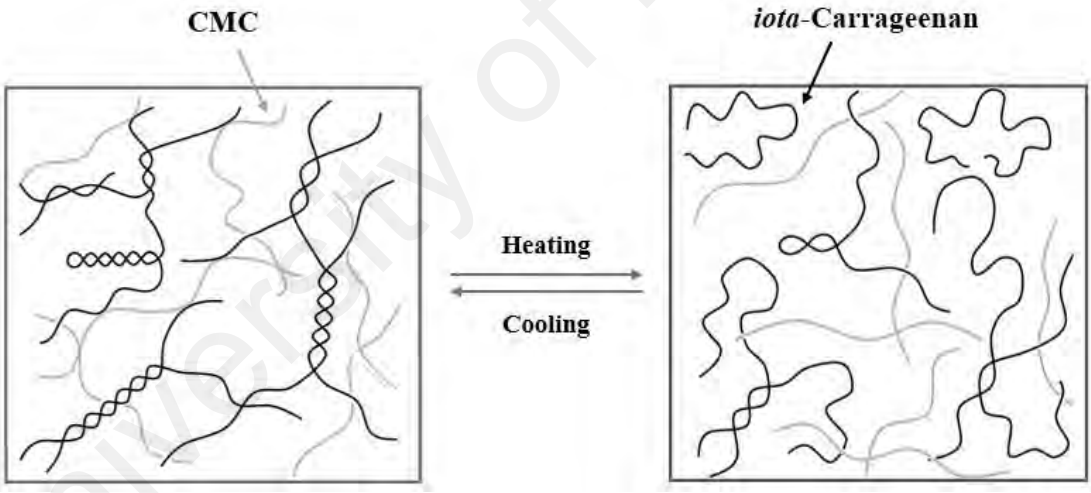

Figure 4.30: Coupled network formed between double helices of *ι*-C and CMC molecules, producing a rigid gel at low temperature. The double helices transform into coils upon heating, losing the gel network and therefore the solution starts flowing.

4.2.2 Morphology of thermoresponsive gel

Despite the volume shrinkage caused by the removal of water during the freeze-drying process, the gel samples were freeze-dried to maintain their structure and network, which would then be examined under the FESEM (He *et al.*, 2014). Figures 4.31 (a) and (b) show the micrographs of gel mixtures *ι*c73a without Ca^{2+} ions and *ι*c73c

with 0.04% Ca^{2+} ions. Both the gel mixtures possessed porous structures, however the gel with Ca^{2+} ions displayed reduced porous size compared to the one without. This was in accordance with the proposed mechanism that the formation of electrostatic interactions between the cations Ca^{2+} with the sulfate groups of *ι*-C and carbonyl groups of CMC was able to hold the polymer chains more strongly.

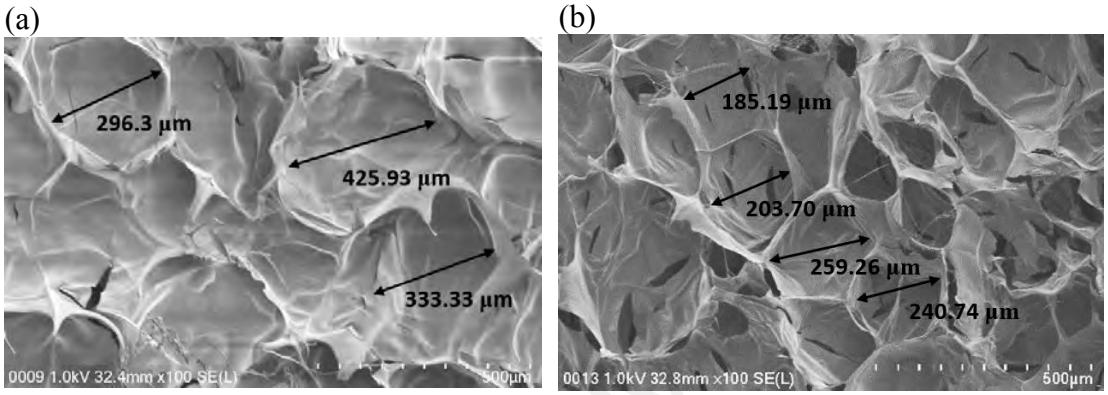

Figure 4.31: FESEM micrographs of freeze-dried gel mixture (a) *ι*c73a and (b) *ι*c73c.

4.3 Characterization of NLC-gel

4.3.1 Rheological characterization of gel samples

From the rheological properties reported in section 4.2.1, *ιc*37d was selected as the optimum gel base for incorporation with NLC. The optimized gel formulation was not too rigid to provide adequate spreadability and efficient delivery of the active ingredient, yet it was not flowing at low shear to hold the incorporated NLC and consequently achieved enhanced stability during storage. The active ingredients gel, NLC-gel and active ingredients loaded NLC-gel were then subjected to a series of rheological tests to provide understanding on diffusion of the active ingredients as rheology reveals the microstructure changes and mobility of a semisolid system.

4.3.1.1 Viscometry test

As shown in Figure 4.32, η for all gel samples decreased with increasing shear rate, showing shear thinning behavior of the gel systems. There was no obvious difference in flowing curves of *alpha*-tocopherol-gel and the blank gel, implying that *alpha*-tocopherol did not have any interaction with the polysaccharides. In contrast, η for hydroquinone gel was lower than that of the blank gel, which indicated possible interaction between hydroquinone and the polymer chains. As each hydroquinone molecule contained two hydroxyl groups, hydroquinone molecules were plausibly forming hydrogen bonds with the polysaccharides, and therefore reduced the interactions among the polysaccharides. However, when hydroquinone was loaded in NLC, the hydroquinone loaded NLC-gel exhibited similar flowing profile with the empty NLC-gel. As η was unaffected by the presence of hydroquinone, hydroquinone was assumed to adsorb on to the particles, and as such was unable to interrupt the gel network. Shear thinning behavior is favorable to provide slow flow from the packaging material and easy distribution on the skin (Islam *et al.*, 2004). This is most probably due to the disentanglement of polymer chains at high shear rate and subsequently the active compound entrapped being able to diffuse following the direction of flow.

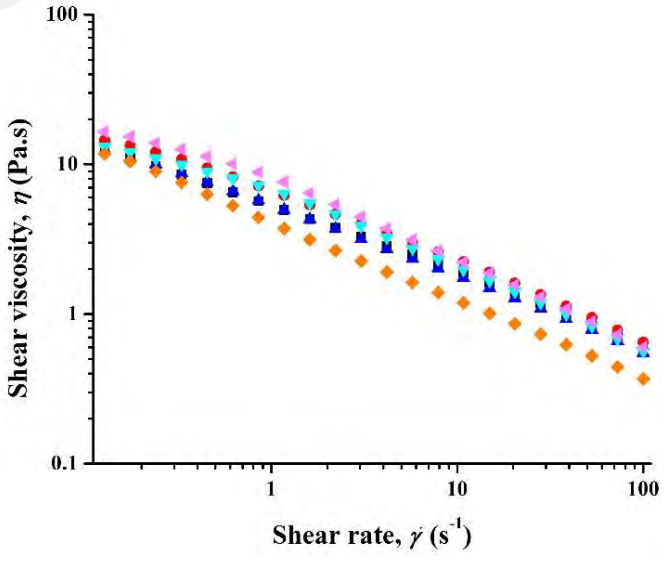

Figure 4.32: Viscosity, η of gel samples ıc37d (■), NLC-gel (●), *alpha*-tocopherol gel (▲), *alpha*-tocopherol loaded NLC-gel (▼), hydroquinone gel (♦) and hydroquinone loaded NLC-gel (◄) as a function of shear rate, at 25 °C.

4.3.1.2 Oscillatory tests

Amplitude sweep was performed to obtain LVR of the gel samples to investigate the strain bearable by the structure before it collapsed. Overall, the elastic component was predominant against the viscous component at low strain, but the samples started flowing at approximately 30% of the observed strain (Figure 4.33 (a)). Therefore, 5% of strain was selected for frequency sweep and temperature ramp tests to ensure non-destructive conditions of samples for applied shear. Being consistent with the viscometry test, hydroquinone gel had the lowest elasticity due to the interaction between hydroquinone and the polysaccharides. This also explains the higher *G'* of NLC-gel compared with hydroquinone loaded NLC-gel, where free hydroquinone molecules in the system might disturb the gel matrix.

The frequency sweep indicated that all the gel samples behaved similarly, as their moduli were frequency dependent. The gel systems were solid-like at low frequency, indicating adequate stability during storage. Nevertheless, *G''* increased more steeply with frequency and consequently $G'' > G'$ at higher frequency, illustrating adequate spreadability of the gels at short time scales, i.e. upon application on the skin. From Figure 4.33 (b), a minimum of *G'* occurred at high frequencies for all gel samples and was most pronounced in the hydroquinone-gel. The minima could potentially be induced by a partial breakage of the interconnected network, which was destructed by the increasingly frequent deformation at high frequency (Shekhawat, 2013). Furthermore, NLC-gel possessed slightly higher *G'* compared with the blank gel, as a result of the incorporation of NLC. This proposed that the lipid nanoparticles were rigid and able to store energy in their elastic components when shear was applied (Tan & Misni, 2014). Besides the rigidity of the particles, NLC potentially interacted with the polymer molecules to enhance the elasticity. It was suggested by previous studies that the oxygen atoms of the fatty acid could probably form hydrogen bonds with the

hydroxyl groups (O-H) at the backbone of the polymer chains in the gel matrix (Chieng & Chen, 2010; Tan & Misni, 2014).

(a)

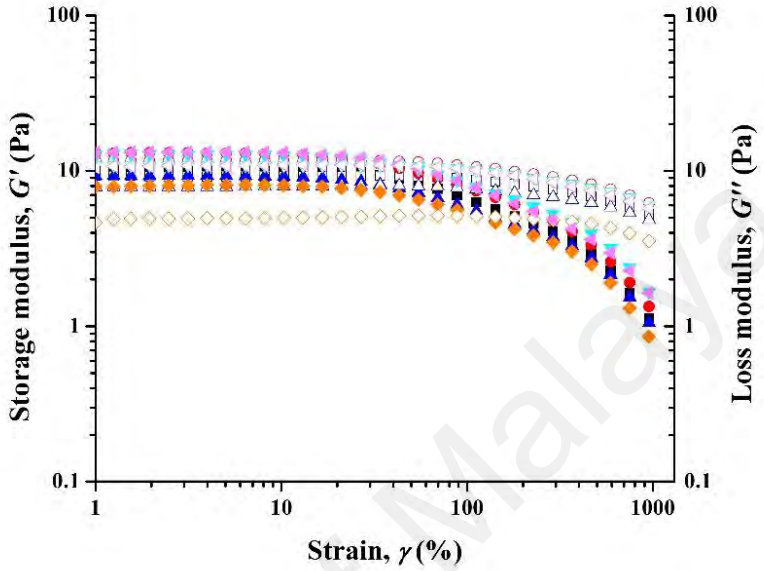

(b)

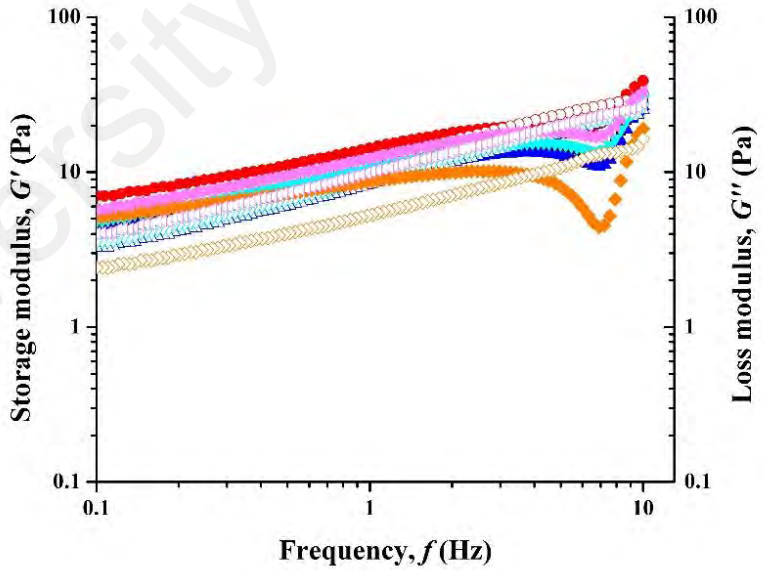

Figure 4.33: Storage modulus, *G'* (solid symbol) and loss modulus, *G''* (open symbol) of gel samples *ι*c37d (■), NLC-gel (●), *alpha*-tocopherol gel (▲), *alpha*-tocopherol loaded NLC-gel (▼), hydroquinone gel (♦) and hydroquinone loaded NLC-gel (◄) as a function of (a) strain in amplitude sweep and (b) frequency in frequency sweep, at 25 ˚C.

Despite the slight difference of rheological properties, the crossover temperature of *G'* and *G''* for all the gel samples occurred at the desired temperature, which was in the vicinity of body temperature (Figure 4.34). The phase transition from gel-like to liquid-like at approximately 37 ˚C improved the spreadability of the gel upon application on the skin, thus promoting delivery of the loaded active ingredients. The rheological measurements revealed that *alpha*-tocopherol had no effect on the rheological properties of the gel systems, while hydroquinone could potentially be forming hydrogen bonds with the polymer molecules, interrupting the gel network, and therefore lowering η and *G'* obtained. However, NLC could reduce the effect of hydroquinone. In spite of the presence of free hydroquinone in the system, the hydroquinone loaded NLC-gel showed similar flowing behavior and elasticity compared to the empty NLC-gel. This prediction was supported by the appearance of the hydroquinone gel and hydroquinone loaded NLC-gel as shown in Figure 4.35. The gel incorporated with hydroquinone was clear with brown coloration, while hydroquinone loaded NLC-gel was opaque with milky white coloration, which was the same as the NLC-gel. In fact, hydroquinone gel should be clear and colorless. The brown color indicated oxidation of hydroquinone into complexes in the gel system (Mijangos *et al.*, 2006). Therefore, it was proven that NLC managed to protect the sensitive active ingredient against degradation in the aqueous medium.

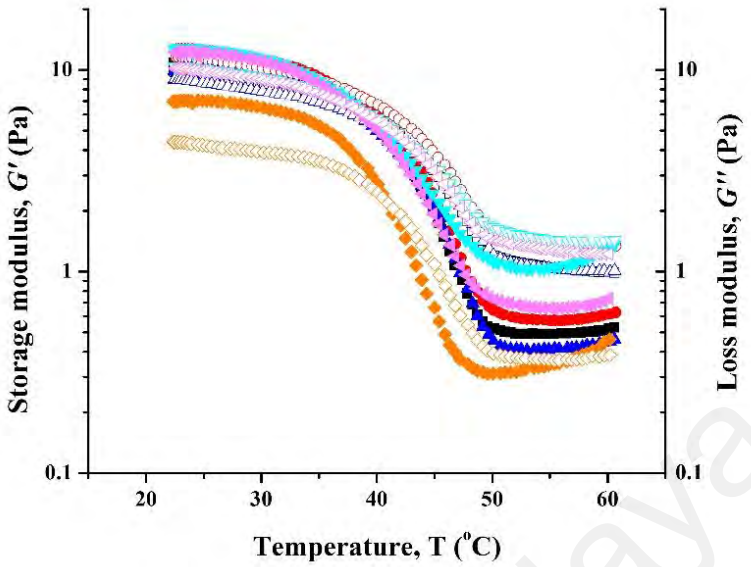

Figure 4.34: Storage modulus, *G'* (solid symbol) and loss modulus, *G''* (open symbol) of gel samples *ι*c37d (■), NLC-gel (●), *alpha*-tocopherol gel (▲), *alpha*-tocopherol loaded NLC-gel (▼), hydroquinone gel (♦) and hydroquinone loaded NLC-gel (◄) as a function of temperature.

Figure 4.35: Images of hydroquinone loaded NLC-gel (left) and hydroquinone gel (right).

4.3.2 *In vitro* release

In vitro release of *alpha*-tocopherol and hydroquinone from the samples, as described in section 3.2.11, were examined by Franz Diffusion Cell system. Figures 4.36 (a) and (b) show the cumulative release of the active ingredient plotted as a function of time release to compare the effect of different suspended environments on release rate.

(a)

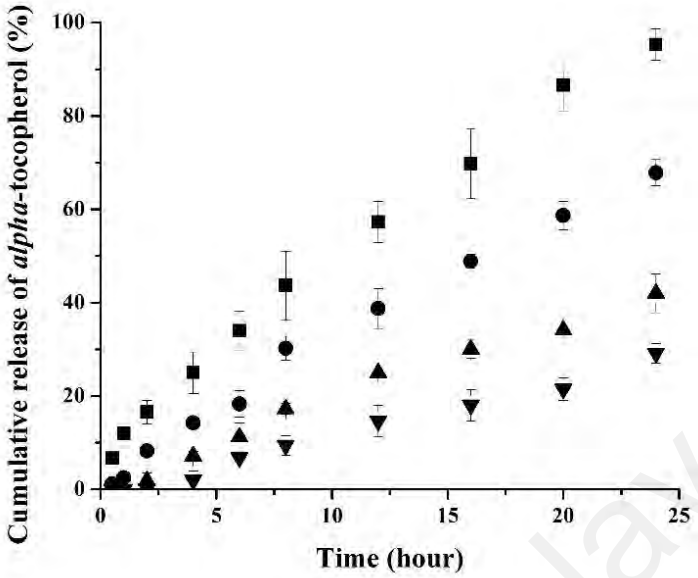

(b)

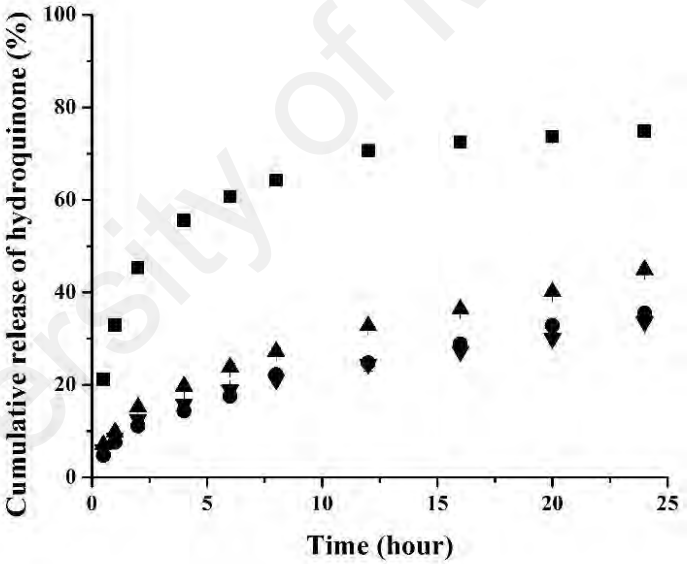

Figure 4.36: Cumulative release of active ingredients from active ingredient solution (■), active ingredient loaded NLC dispersion (●), active ingredient gel (▲) and active ingredient loaded NLC-gel (▼) for (a) *alpha*-tocopherol and (b) hydroquinone as a function of time, at 37 ˚C.

From Figure 4.36 (a), it can be observed that almost all *alpha*-tocopherol molecules in sample A (*alpha*-tocopherol solution) diffused though the membrane after 24 hours, whereas samples B (*alpha*-tocopherol loaded NLC dispersion) showed slower release

rate owing to the limited mobility of the active ingredient in the lipid matrix of NLC. *Alpha*-tocopherol was expected to be released from the lipid phase of NLC due to its poor solubility in the aqueous medium (Jenning *et al.*, 2000). NLC prepared by a hot homogenization method was proposed to be the shell enrichment model, where the active ingredient settled at the outer shell of the particles instead of the lipid core (Üner & Yener, 2007). This was in accordance with the previous OPM observation, shown in section 4.1.2.1, in which crystallization of particles started from the center outwards. This caused the release rate of *alpha*-tocopherol from NLC to be significantly higher compared to that from the gel system of sample C (*alpha*-tocopherol gel). Additionally, the hydrophobic ingredient had increased difficulty diffusing the aqueous gel matrix compared to the lipid matrix. High viscosity of the gel system could also delay the diffusion of the active ingredient. As such, it was not surprising that sample D (*alpha*-tocopherol loaded NLC-gel) gave the lowest cumulative release as *alpha*-tocopherol needed to diffuse through both the lipid matrix and aqueous gel network before reaching the receiving phase.

Unexpectedly, Figure 4.36 (b) shows that the cumulative amount of hydroquinone released from hydroquinone solution (sample E) was less than 80% after 24 hours. This could probably be explained by the hydroquinone molecules binding to the regenerated cellulose membrane pores, which possessed a hydrophilic structure, to interact with the hydroxyl groups of hydroquinone. Subsequently, the release curve of sample E showed a triphasic pattern, where the compound became increasingly difficult to pass through the blocked membrane after a period of time. Meanwhile, there was a significant gap between the release curves of the free solution and hydroquinone gel. This indicated a significant delay in diffusion of the active compound in the gel network. Nevertheless, the amount of hydroquinone released from sample G (hydroquinone gel) was slightly higher than that from sample F (hydroquinone loaded NLC dispersion) and sample H

(hydroquinone loaded NLC-gel), indicating that the hydrophilic compound diffused easier through the aqueous gel matrix. The slower release of hydroquinone from NLC and NLC-gel could potentially result from the adsorption of hydroquinone on the surface of particles. As expected, sample H, which had a double barrier, gave the lowest cumulative release of hydroquinone after 24 hours. Similarly, triphasic patterns were observed in the release curves of sample F, G and H. The initial fast release rate was presumably caused by the free hydroquinone present in the dispersing medium, whereas the slower release rate in the second phase was determined by the diffusion rate of hydroquinone molecules from the particles. The release rate became increasingly slower when membrane pores were blocked by the hydroquinone molecules.

Alternatively, *in vitro* release studies conducted at different temperatures provided comprehensive information on how release rate of active ingredients were affected by the thermoresponsive behavior of the gel system. In Figures 4.37 (a) and (b), it was noticed that the cumulative release of both *alpha*-tocopherol and hydroquinone at 30 ˚C was significantly lower than that at 37 ˚C, illustrating the network structure of the gel at different temperatures. At a higher temperature, reduced interactions were observed among the polysaccharide molecules, lowering the viscosity of the gel system and reducing the barrier for the active ingredients to diffuse towards the receiving chamber. In contrast, gel at a lower temperature was too rigid for the active ingredients to diffuse through. The difference in rigidity was previously discussed in the rheology study in section 4.3.1.2, where the gel was predominantly solid-like at 30 ˚C and became liquid-like at 37 ˚C. The reduced viscosity of the gel at 37 ˚C suggests enhanced spreadability upon application and therefore more efficient delivery of the active ingredients.

(a)

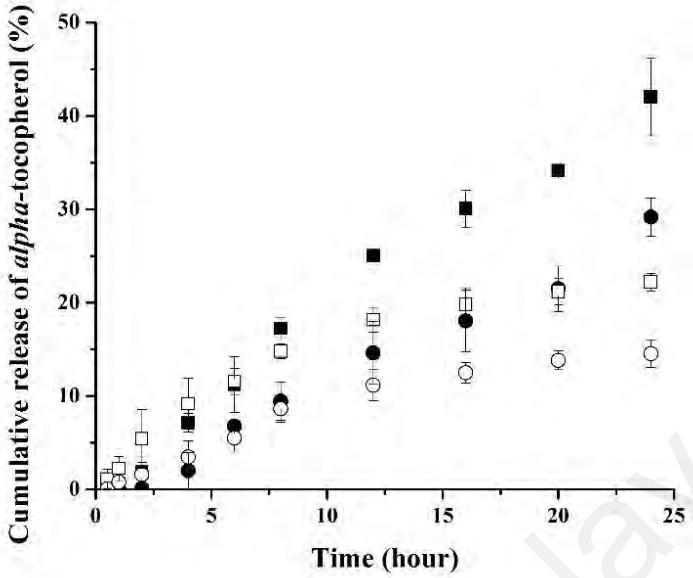

(b)

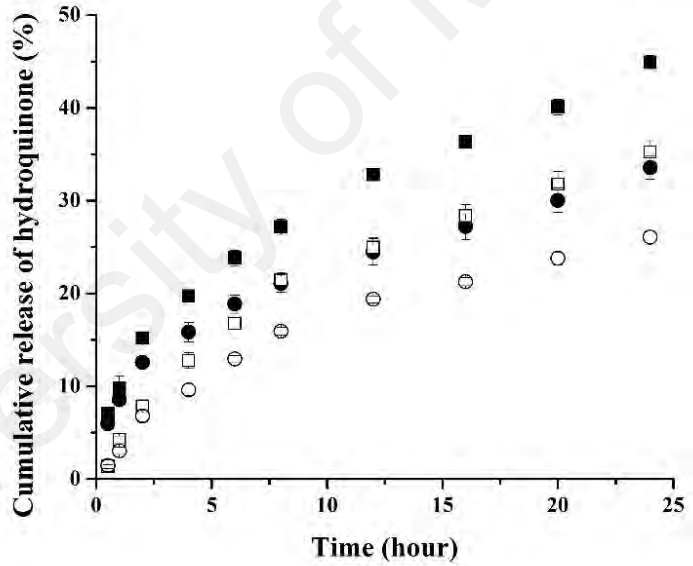

Figure 4.37: Cumulative release of active ingredients from active ingredient gel (■) and active ingredient loaded NLC-gel (●) for (a) *alpha*-tocopherol and (b) hydroquinone as a function of time, at 37 ˚C (solid symbol) and 30 ˚C (open symbol).

The results obtained from the *in vitro* release studies indicate that NLC possessed slow release properties for both hydrophobic (*alpha*-tocopherol) and hydrophilic (hydroquinone) active ingredients. Owing to the hydrophobic nature of *alpha*-tocopherol, it was highly possible that the compound molecules were trapped within the

lipid matrix, forming a shell model NLC, where the active ingredient settled at the outer shell of the particles. Even though there was less attempt to encapsulate hydrophilic compounds in lipid nanoparticles due to their poor compatibility in the lipid phase, it could potentially be assumed that the hydrophilic molecules were adsorbed on the surface of the particles by interacting with the hydrophilic head of the surfactant or solid lipid (Rohit & Pa, 2013). Figure 4.38 demonstrates the schematic illustrations of active ingredients loaded NLCs in the current study.

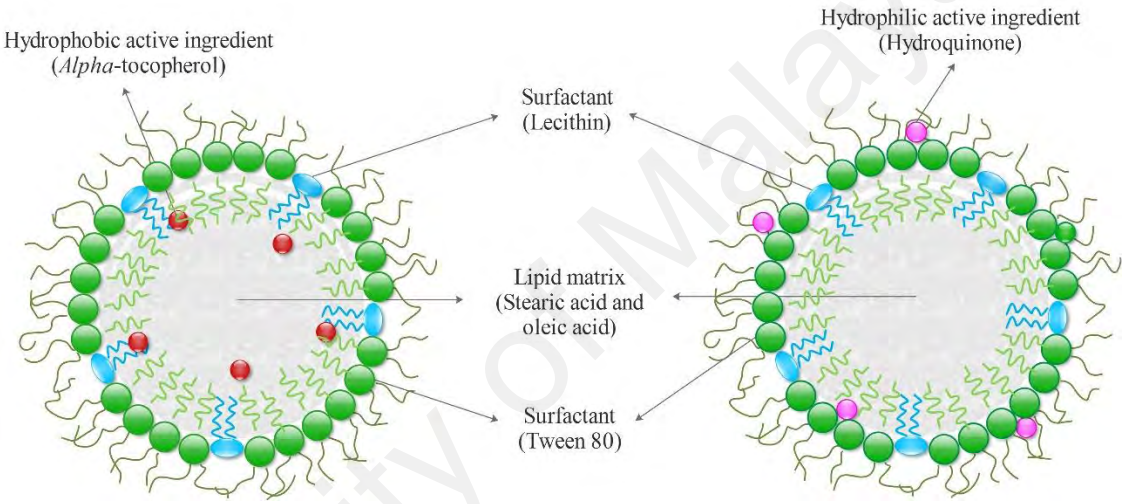

Figure 4.38: Schematic illustrations of *alpha*-tocopherol and hydroquinone loaded NLCs, respectively.

4.3.2.1 Mathematical model evaluations

In order to describe the release kinetic of *alpha*-tocopherol and hydroquinone from different carrier systems, the release profiles for NLCs (sample B and F), gels (sample C and G) and NLC-gels (sample D and H) were fitted with selected mathematical models. The release curves of *alpha*-tocopherol and hydroquinone from the respective carrier systems had different patterns. A triphasic pattern was observed for all release curves of hydroquinone. As such, model fitting of the release curves of hydroquinone was carried out by phase. Due to the restriction of the Peppas-Sahlin model, which

requires a minimum of 4 data points, it is not suitable to fit to the release curves of hydroquinone by phase.

As shown in Table 4.7, *alpha*-tocopherol loaded samples B, C and D demonstrated a best fit to the Peppas-Sahlin equation, with $R^2_{adj.} > 0.98$. As $m < 0.430$ for all samples, the active compounds were proposed to be dominantly released by fickian diffusion rather than polymer relaxation. Fickian diffusion related the diffusive flux to the concentration of molecules under the assumption of steady state (Bokstein *et al.*, 2005). Therefore, the release of *alpha*-tocopherol became slower when its concentration in the receiving phase increased.

Table 4.7: Mathematical model evaluations of *alpha*-tocopherol released from samples B, C and D at 37 ˚C.

Mathematical model		Sample		
		B	**C**	**D**
Zero order	K_0	2.989	1.809	1.148
	$R^2_{adj.}$	0.9846	0.9838	0.9801
First order	K_1	0.044	0.022	0.013
	$R^2_{adj.}$	0.9955	0.9897	0.9727
Higuchi	K_H	12.044	7.214	4.489
	$R^2_{adj.}$	0.9114	0.8734	0.8066
Korsmeyer-Peppas	K_{KP}	4.856	2.318	0.755
	n	0.833	0.915	1.144
	$R^2_{adj.}$	0.9960	0.9847	0.9833
Peppas-Sahlin	K_d	-8.586	-9.574	-2.881
	K_r	11.837	9.825	2.593
	m	0.322	0.300	0.428
	$R^2_{adj.}$	0.9981	0.9931	0.9861

Alternatively, Tables 4.8, 4.9 and 4.10 indicate that all phases of the release curves of hydroquinone were of best fit with the Korsmeyer-Peppas model, which described drug release from a polymeric system, including sample F (NLC dispersion). As Tween

80 was a polymer that could adsorb on the surface of NLC, this observation was in agreement with the previous assumption that hydroquinone was loaded on the surface of particles by interaction with the hydrophilic head groups of Tween 80. However, the release curve of sample F had a best fit with the Higuchi model when it was fitted directly without the need to separate the sample into different phases. Despite the Higuchi model being predominantly used to describe drug release from a granular matrix by Fick diffusion, it is not applicable in this case as the active compound was not encapsulated in the lipid matrix (Dash *et al.*, 2010). Additionally, the *n* value of the Korsmeyer-Peppas model indicated that hydroquinone was released by non-fickian diffusion where $0.45 < n < 0.89$.

Table 4.8: Mathematical model evaluations of hydroquinone released from sample F at 37 ˚C.

Mathematical model		**Sample F**			
		0.5 – 2 h	**4 – 8 h**	**12 – 24 h**	**0.5 – 24 h**
Zero order	K_0	6.131	2.937	1.649	1.764
	$R^2_{adj.}$	0.6825	0.7232	0.3007	0.6652
First order	K_1	0.065	0.033	0.020	0.022
	$R^2_{adj.}$	0.7344	0.8322	0.6982	0.7742
Higuchi	K_H	7.620	7.480	7.252	7.310
	$R^2_{adj.}$	0.9759	0.9334	0.9951	0.9961
Korsmeyer-Peppas	K_{KP}	7.406	5.762	6.708	7.516
	n	0.592	0.642	0.527	0.489
	$R^2_{adj.}$	0.9945	0.9568	0.9963	0.9959
Peppas-Sahlin	K_d	-	-	-	7.521
	K_r	-	-	-	-0.076
	m	-	-	-	0.505
	$R^2_{adj.}$	-	-	-	0.9953

Table 4.9: Mathematical model evaluations of hydroquinone released from sample G at 37 ˚C.

Mathematical model		Sample G			
		0.5 – 2 h	**4 – 8 h**	**12 – 24 h**	**0.5 – 24 h**
Zero order	K_0	8.332	3.788	2.075	2.229
	$R^2_{adj.}$	0.6327	-0.1440	-0.2145	0.5623
First order	K_1	0.091	0.044	0.027	0.030
	$R^2_{adj.}$	0.7075	0.3021	0.5276	0.7310
Higuchi	K_H	10.371	9.707	9.143	9.298
	$R^2_{adj.}$	0.9804	0.9937	0.9761	0.9923
Korsmeyer-Peppas	K_{KP}	10.137	10.401	10.361	10.489
	n	0.574	0.462	0.457	0.454
	$R^2_{adj.}$	0.9902	0.9999	0.9763	0.9978
Peppas-Sahlin	K_d	-	-	-	10.537
	K_r	-	-	-	-0.201
	m	-	-	-	0.480
	$R^2_{adj.}$	-	-	-	0.9976

Table 4.10: Mathematical model evaluations of hydroquinone released from sample H at 37 ˚C.

Mathematical model		Sample H			
		0.5 – 2 h	**4 – 8 h**	**12 – 24 h**	**0.5 – 24 h**
Zero order	K_0	6.987	2.976	1.552	1.682
	$R^2_{adj.}$	0.5335	-0.7241	-0.1968	0.4028
First order	K_1	0.075	0.033	0.019	0.021
	$R^2_{adj.}$	0.6094	-0.2387	0.3620	0.5530
Higuchi	K_H	8.727	7.641	6.841	7.065
	$R^2_{adj.}$	0.9937	0.9561	0.9795	0.9724
Korsmeyer-Peppas	K_{KP}	8.611	8.974	7.709	8.852
	n	0.544	0.412	0.459	0.413
	$R^2_{adj.}$	0.9992	0.9982	0.9804	0.9964
Peppas-Sahlin	K_d	-	-	-	8.912
	K_r	-	-	-	-0.112
	m	-	-	-	0.426
	$R^2_{adj.}$	-	-	-	0.9959

Hydroquinone gel (sample G) and hydroquinone loaded NLC-gel (sample H) also demonstrated a best fit of the Korsmeyer-Peppas model. In these samples, the active compound was presumably released from the gel network. The Korsmeyer-Peppas model predominantly characterized diffusion of hydroquinone through the polymeric gel matrix by non-fickian diffusion for samples G and H as $0.45 < n < 0.89$. Nonetheless, there was an exception where the second phase of sample H described the release of hydroquinone molecules by quasi fickian diffusion, with $n < 0.45$. The slight difference between samples G and H was probably due to the presence of NLC in sample H.

CHAPTER 5: CONCLUSION

In this study, the hot homogenization method was employed to prepare the lecithin-fatty acid nanoparticles for topical delivery purposes. The preparation parameters and composition of NLC have been proven to affect the characteristic of the NLCs produced. The optimized conditions obtained were homogenization of mixture at 18,000 rpm for 10 minutes, in water bath thermostated at 80 ˚C. It was demonstrated that incorporation of lecithin at an adequate amount was necessary to achieve smaller particle size and stable dispersion. NLC with desired mean particle size (< 500 nm) and PDI (< 0.3) was successfully prepared by using surfactants of 0.2% of lecithin and 1.3% of Tween 80.

Encapsulation efficiency of active ingredients which were *alpha*-tocopherol and hydroquinone of different water solubility into NLCs was studied. The encapsulation efficiency for the hydrophobic compound *alpha*-tocopherol was high for all formulations, due to its higher compatibility to the lipid matrix. As such, the optimum concentration of *alpha*-tocopherol was determined from its stability profile according to its mean particle size and PDI after storage for 30 days. Alternatively, the concentration of hydroquinone directly influenced its encapsulation efficiency in NLC, with high amounts of hydroquinone having lower encapsulation efficiency. As such, 0.1% of the active ingredients were incorporated into the NLCs.

Furthermore, a series of thermoresponsive gel mixtures, consisting of CMC and *ι*-C, was prepared. Gel systems with high rigidity were produced with high amount of *ι*-C, while CMC mostly contributed to the flow properties. Addition of Ca^{2+} ions successfully increased the gel strength to a higher extent. Ca^{2+} ions could potentially participate in the formation of a strong gel network by connecting the negatively charged oxygen atoms on the sulfate groups of *ι*-C and carbonyl groups of CMC. Furthermore, the temperature effect on flowing behavior of gel mixture was investigated. The phase

transition from gel to solution was illustrated by the crossover point of *G'* and *G''*. The gel mixture that possessed T_c at approximately the body temperature was chosen as the optimized formulation to incorporate the loaded NLCs.

Despite the minor increase in rigidity of NLC-gel, incorporation of NLC did not show a significant effect on the rheological properties of the gel mixture. All the gel samples incorporated with NLCs exhibited shear thinning behavior and thermally activated phase transition from gel to liquid at temperatures in the vicinity of 37 ˚C. These features are advantageous in topical application as they achieve enhanced spreadability upon application.

In vitro release studies confirmed the slow release properties of NLC by comparing the release profile of NLC dispersion and active ingredient solution. However, the solubility of the active ingredients influenced the release rate from the gel matrix. The cumulative release of *alpha*-tocopherol and NLC-gel was low due to their limited mobility in the aqueous system, while diffusion of hydroquinone was controlled by NLC. Additionally, gel samples release both active ingredients at a slower rate at 30 ˚C compared to 37 ˚C, implying the improved flowing behavior of the gels at higher temperature and hence more efficient delivery of the active ingredients.

The obtained results indicated that the thermoresponsive gel mixture had great potential in topical application, while NLC is a promising carrier system for *alpha*-tocopherol and hydroquinone.

REFERENCES

Agorku, E. S., Kwaansa-Ansah, E. E., Voegborlo, R. B., Amegbletor, P., and Opoku, F. (2016). Mercury and hydroquinone content of skin toning creams and cosmetic soaps, and the potential risks to the health of Ghanaian women. *SpringerPlus, 5*, 319.

Aho, J. (2011). *Rheological characterization of polymer melts in shear and extension: Measurement reliability and data for practical processing*. Finland: Tampere University of Technology.

Akbarzadeh, A., Rezaei-Sadabady, R., Davaran, S., Joo, S. W., Zarghami, N., Hanifehpour, Y., Samiei, M., Kouhi, M., and Nejati-Koshki, K. (2013). Liposome: Classification, preparation, and applications. *Nanoscale Research Letters, 8*(1), 102.

Albanes, D., Heinonen, O. P., Huttunen, J. K., Taylor, P. R., Virtamo, J., Edwards, B. K., Haapakoski, J., Rautalahti, M., Hartman, A. M., and Palmgren, J. (1995). Effects of *alpha*-tocopherol and *beta*-carotene supplements on cancer incidence in the *alpha*-tocopherol *beta*-carotene cancer prevention study. *The American Journal of Clinical Nutrition, 62*(6), 1427S-1430S.

Alvarez-Román, R., Naik, A., Kalia, Y. N., Guy, R. H., and Fessi, H. (2004). Skin penetration and distribution of polymeric nanoparticles. *Journal of Controlled Release, 99*(1), 53-62.

Alves, P. M., Pohlmann, A. R., and Guterres, S. S. (2005). Semisolid topical formulations containing nimesulide-loaded nanocapsules, nanospheres or nanoemulsions: Development and rheological characterization. *Pharmazie, 60*(12), 900-904.

Aulton, M. E., and Taylor, K. M. G. (Ed.). (2013). *Aulton's Pharmaceutics: The design and manufacture of medicines* (4th ed.). Netherlands: Elsevier Health Sciences.

Balzer, D., Varwig, S., and Weihrauch, M. (1995). Viscoelasticity of personal care products. *Colloids and Surfaces A: Physicochemical and Engineering Aspects, 99*(2), 233-246.

Beaurline, J. M., Roddy, P. J., and Tomai, M. A. (1999). Gel formulations for topical drug delivery *(pp. US5939090 A)*: Google Patents.

Beck, R., Guterres, S., and Pohlmann, A. (Eds.). (2011). *Nanocosmetics and Nanomedicines.* Berlin: Springer-Verlag.

Becker Peres, L., Becker Peres, L., de Araújo, P. H. H., and Sayer, C. (2016). Solid lipid nanoparticles for encapsulation of hydrophilic drugs by an organic solvent free double emulsion technique. *Colloids and Surfaces B: Biointerfaces, 140*, 317-323.

Bokstein, B. S., Mendeleev, M. I., and Srolovitz, D. J. (2005). *Thermodynamics and kinetics in materials science: A short course*. Oxford: Oxford University Press.

Bromberg, L. E., and Ron, E. S. (1998). Temperature-responsive gels and thermogelling polymer matrices for protein and peptide delivery. *Advanced Drug Delivery Reviews, 31*(3), 197-221.

Bunjes, H., and Unruh, T. (2007). Characterization of lipid nanoparticles by differential scanning calorimetry, X-ray and neutron scattering. *Advanced Drug Delivery Reviews, 59*(6), 379-402.

Cairns, P., Miles, M. J., Morris, V. J., and Brownsey, G. J. (1987). X-Ray fibre-diffraction studies of synergistic, binary polysaccharide gels. *Carbohydrate Research, 160*, 411-423.

Chenite, A., Chaput, C., Wang, D., Combes, C., Buschmann, M. D., Hoemann, C. D., Leroux, J. C., Atkinson, B. L., Binette, F., and Selmani, A. (2000). Novel injectable neutral solutions of chitosan form biodegradable gels *in situ*. *Biomaterials, 21*(21), 2155-2161.

Chieng, Y. Y. and Chen, S. B. (2010). Rheological study of hydrophobically modified hydroxyethyl cellulose and phospholipid vesicles. *Journal of Colloid and Interface Science, 349*(1), 236-245.

Cottrell, T. L. (1958). *The strengths of chemical bonds* (2nd ed.). London: Butterworth.

Couteau, C., and Coiffard, L. (2016). Overview of skin whitening agents: Drugs and cosmetic products. *Cosmetics, 3*(3), 27.

Darwent, B. deB. (1970). *National standard reference data series* (no. 31). Washington: National Bureau of Standards.

Dash, S., Murthy, P. N., Nath, L., and Chowdhury, P. (2010). Kinetic modeling on drug release from controlled drug delivery systems. *Acta Poloniae Pharmaceutica-Drug Research, 67*(3), 217-223.

Doktorovova, S., Lopes, C. M., and Souto, E. B. (2009). Lipid nanoparticle mediated drug delivery for safer cancer treatment: Example of paclitaxel. *Revista da Faculdade de ciencias da Saude*, 84-93.

Doshi, N., Zahr, A. S., Bhaskar, S., Lahann, J., and Mitragotri, S. (2009). Red blood cell-mimicking synthetic biomaterial particles. *Proceedings of the National Academy of Sciences of the United States of America, 106*(51), 21495-21499.

Eh Suk, V. R. and Misran, M. (2017). Preparation, characterization and physicochemical properties of DOPE-PEG2000 stabilized oleic acid-soy lecithin liposomes (POLL). *Colloids and Surfaces A: Physicochemical and Engineering Aspects, 513*, 267-273.

Farboud, E. S., Nasrollahi, S. A., and Tabbakhi, Z. (2011). Novel formulation and evaluation of a Q10-loaded solid lipid nanoparticle cream: *In vitro* and *in vivo* studies. *International Journal of Nanomedicine, 6*, 611-617.

Fedorchak, M. V., Little, S. R., Schuman, J. S., and Cugini, A. (2014). Thermoresponsive hydrogel containing polymer microparticles for noninvasive ocular drug delivery *(pp. WO2014138085 A1)*: Google Patents.

Franzetti, A., Gandolfi, I., Bestetti, G., and Banat, I. (2010). (Bio)surfactant and bioremediation, successes and failures. In I. G. Plaza (Ed.), *Trending in bioremediation and phytoremediation* (pp. 145-156). Kerala, India: Research Signpost.

Freitas, C., and Müller, R. H. (1999). Correlation between long-term stability of solid lipid nanoparticles (SLN™) and crystallinity of the lipid phase. *European Journal of Pharmaceutics and Biopharmaceutics, 47*(2), 125-132.

Gandra, S. C. R., Nguyen, S., Nazzal, S., Alayoubi, A., Jung, R., and Nesamony, J. (2015). Thermoresponsive fluconazole gels for topical delivery: Rheological and mechanical properties, *in vitro* drug release and anti-fungal efficacy. *Pharmaceutical Development and Technology, 20*(1), 41-49.

Garrec, D. A., and Norton, I. T. (2013). Kappa carrageenan fluid gel material properties. Part 2: Tribology. *Food Hydrocolloids, 33*(1): 160-167.

Garud, A., Singh, D., and Navneet, G. (2012). Solid lipid nanoparticles (SLN): Method, characterization and applications. *International Current Pharmaceutical Journal, 1*(11), 384-393.

Gennaro, A. R. (Ed.). (2000). *Rheology in Remington: The science and practice of pharmacy* (20th ed.). Philadelphia: University of the Sciences in Philadelphia.

Ghanbarzadeh, S., Hariri, R., Kouhsoltani, M., Shokri, J., Javadzadeh, Y., and Hamishehkar, H. (2015). Enhanced stability and dermal delivery of hydroquinone using solid lipid nanoparticles. *Colloids and Surfaces B: Biointerfaces, 136*, 1004-1010.

Gokce, E. H., Korkmaz, E., Tuncay-Tanrıverdi, S., Dellera, E., Sandri, G., Bonferoni, M. C., and Ozer, O. (2012). A comparative evaluation of coenzyme Q10-loaded liposomes and solid lipid nanoparticles as dermal antioxidant carriers. *International Journal of Nanomedicine, 7*, 5109-5117.

Gulrez, S. K. H., and Al-Assaf, S. (2011). Hydrogels: Methods of preparation, characterisation and applications. *Progress in Molecular and Environmental Bioengineering - From Analysis and Modeling to Technology Applications*, Prof. Angelo Carpi (Ed.): InTech.

Han, F., Li, S., Yin, R., Liu, H., and Xu, L. (2008). Effect of surfactants on the formation and characterization of a new type of colloidal drug delivery system: Nanostructured lipid carriers. *Colloids and Surfaces A: Physicochemical and Engineering Aspects, 315*(1–3), 210-216.

Hapiot, F., Menuel, S., and Monflier, E. (2013). Thermoresponsive hydrogels in catalysis. *ACS Catalysis, 3*(5), 1006-1010.

Harde, H., Agrawal, A. K., Katariya, M., Kale, D., and Jain, S. (2015). Development of a topical adapalene-solid lipid nanoparticle loaded gel with enhanced efficacy and improved skin tolerability. *RSC Advances, 5*, 43917-43929.

He, X., Fan, J., Zhang, F., Li, R., Pollack, K. A., Raymond, J. E., Zou, J., and Wooley, K. L. (2014). Multi-responsive hydrogels derived from the self-assembly of tethered allyl-functionalized racemic oligopeptides. *Journal of Materials Chemistry B, 2*(46), 8123-8130.

Hoffmann, H., Rehage, H., and Rauscher, A. (Eds.). (1992). *Structure and dynamics of strongly interactive colloids and supramolecular aggregates in solution*. The Netherlands: Kluwer Academic.

Islam, M. T., Rodriguez-Hornedo, N., Ciotti, S. and Ackermann, C. (2004). Rheological characterization of topical carbomer gels neutralized to different pH. *Pharmaceutical Research, 21*(7), 1192-1199.

Janaswamy, S., and Chandrasekaran, R. (2002). Effect of calcium ions on the organization of *iota*-carrageenan helices: An X-ray investigation. *Carbohydrate Research, 337*(6), 523-535.

Janaswamy, S., and Chandrasekaran, R. (2005). Cation-induced polymorphism in *iota*-carrageenan. *Carbohydrate Polymers, 60*(4), 499-505.

Janaswamy, S., and Chandrasekaran, R. (2008). Heterogeneity in *iota*-carrageenan molecular structure: Insights for polymorph II→III transition in the presence of calcium ions. *Carbohydrate Research, 343*(2), 364-373.

Janaswamy, S., and Youngren, S. R. (2012). Hydrocolloid-based nutraceutical delivery systems. *Food and Function, 3*(5), 503-507.

Jenning, V., and Gohla, S. H. (2001). Encapsulation of retinoids in solid lipid nanoparticles (SLN). *Journal of Microencapsulation, 18*(2), 149-158.

Jenning, V., Schäfer-Korting, M., and Gohla, S. (2000). Vitamin A-loaded solid lipid nanoparticles for topical use: Drug release properties. *Journal of Controlled Release, 66*(2–3), 115-126.

Jeong, B., Kim, S. W., and Bae, Y. H. (2002). Thermosensitive sol–gel reversible hydrogels. *Advanced Drug Delivery Reviews, 54*(1), 37-51.

Junyaprasert, V. B., Teeranachaideekul, V., Souto, E. B., Boonme, P., and Müller, R. H. (2009). Q10-loaded NLC versus nanoemulsions: Stability, rheology and *in vitro* skin permeation. *International Journal of Pharmaceutics, 377*(1–2), 207-214.

Kara, S., Arda, E., and Pekcan, Ö. (2007). Monovalent and divalent cation effects on phase transitions of ι-carrageenan. *Journal of Bioactive and Compatible Polymers, 22*(1), 42-61.

Klouda, L., and Mikos, A. G. (2008). Thermoresponsive hydrogels in biomedical applications. *European Journal of Pharmaceutics and Biopharmaceutics, 68*(1), 34-45.

Kocharian, A., Shabanian, R., Rafiei-Khorgami, M., Kiani, A., and Heidari-Bateni, G. (2009). Coenzyme-Q10 improves diastolic function in children with idiopathic dilated cardiomyopathy. *Cardiology in the Young, 19*(5), 501-506.

Lacatusu, I., Badea, N., Murariu, A., Bojin, D., and Meghea, A. (2010). Effect of UV sunscreens loaded in solid lipid nanoparticles: A combinated SPF assay and photostability. *Molecular Crystals and Liquid Crystals, 523*(1), 247-259.

Lacatusu, I., Badea, N., Ovidiu, O., Bojin, D., and Meghea, A. (2012). Highly antioxidant carotene-lipid nanocarriers: Synthesis and antibacterial activity. *Journal of Nanoparticle Research, 14*(6), 902.

Lawrence, M. J., and Rees, G. D. (2000). Microemulsion-based media as novel drug delivery systems. *Advanced Drug Delivery Reviews, 45*(1), 89-121.

Lieberman, J. A., Rieger, M. M., and Banker, G. S. (Eds.). (1996). *Pharmaceutical dosage forms: Disperse systems* (2nd ed.): New York.

Liu, D., Chen, L., Jiang, S., Zhu, S., Qian, Y., Wang, F., Li, R., and Xu, Q. (2014). Formulation and characterization of hydrophilic drug diclofenac sodium-loaded solid lipid nanoparticles based on phospholipid complexes technology. *Journal of Liposome Research, 24*(1), 17-26.

Liu, J., Hu, W., Chen, H., Ni, Q., Xu, H., and Yang, X. (2007). Isotretinoin-loaded solid lipid nanoparticles with skin targeting for topical delivery. *International Journal of Pharmaceutics, 328*(2), 191-195.

Liu, W., Hu, M., Liu, W., Xue, C., Xu, H., and Yang, X. (2008). Investigation of the carbopol gel of solid lipid nanoparticles for the transdermal iontophoretic delivery of triamcinolone acetonide acetate. *International Journal of Pharmaceutics, 364*(1), 135-141.

Loo, C., Basri, M., Ismail, R., Lau, H., Tejo, B., Kanthimathi, M., Hassan, H., and Choo, Y. (2013). Effect of compositions in nanostructured lipid carriers (NLC) on skin hydration and occlusion. *Internatonal Jornal of Nanomedicine, 8*, 13-22.

Lopaciuk, A., and Loboda, M. (2013). *Global beauty industry trends in the 21st century*. Zadar, Croatia: International Conference 2013.

Lucks, S., and Muller, R. (1998). Medication vehicles made of solid lipid particles (solid lipid nanospheres-sln) *(pp. CA2119253 A2119251)*: Google Patents.

Manea, A.-M., Vasile, B. S., and Meghea, A. (2014). Antioxidant and antimicrobial activities of green tea extract loaded into nanostructured lipid carriers. *Comptes Rendus Chimie, 17*(4), 331-341.

Martin, A. (Ed.). (1993). *Rheology in physical pharmacy: Physical chemical principles the pharmaceutical sciences* (4th ed.). Philadelphia: Lippicott Williams & Wilkins.

McClements, D. J. (2004). *Food emulsions: Principles, practices, and techniques* (2nd ed.). United States: CRC Press.

Mehnert, W., and Mäder, K. (2001). Solid lipid nanoparticles: Production, characterization and applications. *Advanced Drug Delivery Reviews, 47*(2–3), 165-196.

Mijangos, F., Varona, F., and Villota, N. (2006). Changes in solution color during phenol oxidation by Fenton reagent. *Environmental Science and Technology, 40*(17), 5538-5543.

Milao, D., Knorst, M. T., Richter, W., and Guterres, S. S. (2003). Hydrophilic gel containing nanocapsules of diclofenac: Development, stability study and physico-chemical characterization. *Pharmazie, 58*(5), 325-329.

Mueller, R., Maeder, K., Lippacher, A., and Jenning, V. (2000). Lipid particles based on matrix comprising solid and liquid lipid, useful in diagnostics and for controlled release of active agents, especially pharmaceuticals *(pp. DE19945203 A19945201)*: Google Patents.

Mukherjee, S., Ray, S., and Thakur, R. S. (2009). Solid lipid nnoparticles: A modern formulation approach in drug delivery system. *Indian Journal of Pharmaceutical Sciences, 71*(4), 349-358.

Müller, R. H., Jacobs, C., and Kayser, O. (2001). Nanosuspensions as particulate drug formulations in therapy: Rationale for development and what we can expect for the future. *Advanced Drug Delivery Reviews, 47*(1), 3-19.

Müller, R. H., Jenning, V., Mäder, K., and Lippacher, A. (2000). Lipid particles on the basis of mixtures of liquid and solid lipids and the method for producing same. *(pp. 8,663,692)*: US Patents.

Naeem, S., Kiew, L. V., Chung, L. Y., Teo, Y. Y., and Misran, M. (2015). Drug delivery and innovative pharmaceutical development in mimicking the red blood cell membrane. *Reviews in Chemical Engineering, 31*(5), 491-508.

Nahak, P., Karmakar, G., Roy, B., Guha, P., Sapkota, M., Koirala, S., Chang, C. H., and Panda, A. K. (2015). Physicochemical studies on local anaesthetic loaded second generation nanolipid carriers. *RSC Advances, 5*, 26061-26070.

Nair, R., Priya, K. V., Kumar, K. S. A., T.Md.Badivaddin, and M, S. (2011). Formulation and evaluation of solid lipid nanoparticles of water soluble drug: Isoniazid. *Journal of Pharmaceutical Sciences and Research, 3*(5), 1256-1264.

Necas, J., and Bartosikova, L. (2013). Carrageenan: A review. *Veterinární Medicína, 58*(4), 187-205.

Nishinari, K. (2009). Some thoughts on the definition of a gel. In M. Tokita and K. Nishinari (Eds.). *Gels: Structures, properties, and functions: Fundamentals and applications* (pp. 87-94). Berlin: Springer-Berlin Heidelberg.

Otarola, J., Lista, A. G., Band, B. F., and Garridon, M. (2015). Capillary electrophoresis to determine entrapment efficiency of a nanostructured lipid carrier loaded with piroxicam. *Journal of Pharmaceutical Analysis, 5*(1), 70-73.

Pardeike, J., Hommoss, A., and Müller, R. H. (2009). Lipid nanoparticles (SLN, NLC) in cosmetic and pharmaceutical dermal products. *International Journal of Pharmaceutics, 366*(1–2), 170-184.

Pardeike, J., Schwabe, K., and Muller, R. H. (2010). Influence of nanostructured lipid carriers (NLC) on the physical properties of the Cutanova Nanorepair Q10 cream and the in vivo skin hydration effect. *International Journal of Pharmaceutics, 396*(1-2), 166-173.

Paudel, K. S., Milewski, M., Swadley, C. L., Brogden, N. K., Ghosh, P., and Stinchcomb, A. L. (2010). Challenges and opportunities in dermal/transdermal delivery. *Therapeutic Delivery, 1*(1), 109-131.

Peppas, N. A., Bures, P., Leobandung, W., and Ichikawa, H. (2000). Hydrogels in pharmaceutical formulations. *European Journal of Pharmaceutics and Biopharmaceutics, 50*(1), 27-46.

Pilgram, G. S. K., Marjolein Engelsma-van Pelt, A., Koerten, H. K., and Bouwstra, J. A. (1999). Electron diffraction provides new information on human stratum corneum lipid organization studied in relation to depth and temperature. *Journal of Investigative Dermatology, 113*(3), 403-409.

Placzek, M., and Kosela, M. (2016). Microscopic methods in analysis of submicron phospholipid dispersions. *Acta Pharmaceutica, 66*, 1-22.

Podda, M., and Grundmann-Kollmann, M. (2001). Low molecular weight antioxidants and their role in skin ageing. *Clinical and Experimental Dermatology, 26*(7), 578-582.

Pople, P. V., and Singh, K. K. (2011). Development and evaluation of colloidal modified nanolipid carrier: Application to topical delivery of tacrolimus. *European Journal of Pharmaceutics and Biopharmaceutics, 79*(1), 82-94.

Puri, A., Loomis, K., Smith, B., Lee, J.-H., Yavlovich, A., Heldman, E., and Blumenthal, R. (2009). Lipid-based nanoparticles as pharmaceutical drug carriers: From concepts to clinic. *Critical Reviews in Therapeutic Drug Carrier Systems, 26*(6), 523-580.

Qiu, Y., and Park, K. (2001). Environment-sensitive hydrogels for drug delivery. *Advanced Drug Delivery Reviews, 53*(3), 321-339.

Rao, J. P., and Geckeler, K. E. (2011). Polymer nanoparticles: Preparation techniques and size-control parameters. *Progress in Polymer Science, 36*(7), 887-913.

Rauwendaal, C. (2014). Chapter 5 - Fundamental principles. *Polymer Extrusion* (5th ed.) (pp. 147-189). Germany: Hanser.

Rees, D. A., Williamson, F. B., Frangou, S. A., and Morris, E. R. (1982). Fragmentation and modification of *r*-carrageenan and characterisation of the polysaccharide order-disorder transition in solution. *European Journal of Biochemistry, 122*(1), 71-79.

Richter, F., and Steiger, M. (1999). Pharmaceutical composition *(pp. US5856355 A)*: Google Patents.

Rizvi, S., Raza, S. T., Ahmed, F., Ahmad, A., Abbas, S., and Mahdi, F. (2014). The role of vitamin E in human health and some diseases. *Sultan Qaboos University Medical Journal, 14*(2), e157-e165.

Rohit, B., and Pa, K. I. (2013). A method to prepare solid lipid nanoparticles with improved entrapment efficiency of hydrophilic drugs. *Current Nanoscience, 9*(2), 211-220.

Rosli, N. A., Hasham, R., Aziz, A. A., and Aziz, R. (2015). Formulation and characterization of nanostructured lipid carrier encapsulated *Zingiber zerumbet* oil using ultrasonication technique. *Journal of Advanced Research in Applied Mechanics, 11*(1), 16-23.

Shekunov, B. Y., Chattopadhyay, P., Tong, H. H. Y., and Chow, A. H. L. (2007). Particle size analysis in pharmaceutics: Principles, methods and applications. *Pharmaceutical Research, 24*(2), 203-227.

Shim, J., Kang, H. S., Park, W.-S., Han, S.-H., Kim, J., and Chang, I.-S. (2004). Transdermal delivery of mixnoxidil with block copolymer nanoparticles. *Journal of Controlled Release, 97*(3), 477-484.

Schmaljohann, D. (2006). Thermo- and pH-responsive polymers in drug delivery. *Advanced Drug Delivery Reviews, 58*(15), 1655-1670.

Schubert, M. A., Harms, M., and Müller-Goymann, C. C. (2006). Structural investigations on lipid nanoparticles containing high amounts of lecithin. *European Journal of Pharmaceutical Sciences, 27*(2–3), 226-236.

Schubert, M. A., and Müller-Goymann, C. C. (2005). Characterisation of surface-modified solid lipid nanoparticles (SLN): Influence of lecithin and nonionic emulsifier. *European Journal of Pharmaceutics and Biopharmaceutics, 61*(1–2), 77-86.

Schubert, M. A., Schicke, B. C., and Müller-Goymann, C. C. (2005). Thermal analysis of the crystallization and melting behavior of lipid matrices and lipid nanoparticles containing high amounts of lecithin. *International Journal of Pharmaceutics, 298*(1), 242-254.

Shah, M., Agrawal, Y. K., Garala, K., and Ramkishan, A. (2012). Solid lipid nanoparticles of a water soluble drug, ciprofloxacin hydrochloride. *Indian Journal of Pharmaceutical Sciences, 74*(5), 434-442.

Sharipova, A. A., Aidarova, S. B., Grigoriev, D., Mutalieva, B., Madibekova, G., Tleuova, A. and Miller, R. (2016). Polymer-surfactant complexes for microencapsulation of Vitamin E and its release. *Colloids and Surfaces B: Biointerfaces, 137*, 152-157.

Shekhawat, P. B. (2013). Preparation and evaluation of clotrimazole nanostructured lipid carrier for topical delivery. *International Journal of Pharma and Bio Sciences, 4*(1), 407-416.

Shi, F., Zhao, J. H., Liu, Y., Wang, Z., Zhang, Y. T., and Feng, N. P. (2012). Preparation and characterization of solid lipid nanoparticles loaded with frankincense and myrrh oil. *International Journal of Nanomedicine, 7*, 2033-2043.

Shylaja, P. A., and Mathew, M. M. (2016). Preparation and Characterization of *alpha*-tocopherol loaded solid lipid nanoparticles by hot homogenization method. *International Journal of Pharmacy & Pharmaceutical Research. Human Journals, 7*(1), 437-448.

Silva, A. C., Santos, D., Ferreira, D. C., and Souto, E. B. (2009). Minoxidil-loaded nanostructured lipid carriers (NLC): Characterization and rheological behaviour of topical formulations. *Pharmazie, 64*(3), 177-182.

Singhvi, G., and Singh, M. (2011). Review: *In-vitro* drug release characterization models *International Journal of Pharmaceutical Studies and Research, II*(I), 77-84.

Souto, E. B., and Müller, R. H. (2008). Cosmetic features and applications of lipid nanoparticles (SLN®, NLC®). *International Journal of Cosmetic Science, 30*(3), 157-165.

Souto, E. B., Wissing, S. A., Barbosa, C. M., and Müller, R. H. (2004). Development of a controlled release formulation based on SLN and NLC for topical clotrimazole delivery. *International Journal of Pharmaceutics, 278*(1), 71-77.

Tan, H. W., and Misni, M. (2014). Effect of chitosan-modified fatty acid liposomes on the rheological properties of the carbohydrate-based gel. *Applied Rheology, 24*, 34839-34847.

Tari, Ö., Kara, S., and Pekcan, Ö. (2011). Study of thermal phase transitions in *iota*-carrageenan gels via fluorescence technique. *Journal of Applied Polymer Science, 121*(5), 2652-2661.

Teeranachaideekul, V., Müller, R. H., and Junyaprasert, V. B. (2007). Encapsulation of ascorbyl palmitate in nanostructured lipid carriers (NLC) - Effects of formulation parameters on physicochemical stability. *International Journal of Pharmaceutics, 340*(1–2), 198-206.

Teeranachaideekul, V., Souto, E. B., Junyaprasert, V. B., and Müller, R. H. (2007). Cetyl palmitate-based NLC for topical delivery of Coenzyme Q10 – Development, physicochemical characterization and *in vitro* release studies. *European Journal of Pharmaceutics and Biopharmaceutics, 67*(1), 141-148.

Terroso, T., Külkamp, I. C., Jornada, D. S., Pohlmann, A. R., and Guterres, S. S. (2009). Development of semi-solid cosmetic formulations containing coenzyme Q10-loaded nanocapsules. *Latin American Journal of Pharmacy, 28*(6), 819–826.

Üner, M., and Yener, G. (2007). Importance of solid lipid nanoparticles (SLN) in various administration routes and future perspectives. *International Journal of Nanomedicine, 2*(3), 289-300.

Vijayan, V., Aafreen, S., Sakthivel, S., and Reddy, K. R. (2013). Formulation and characterization of solid lipid nanoparticles loaded Neem oil for topical treatment of acne. *Journal of Acute Disease, 2*(4), 282-286.

Weiss, S. C. (2011). Conventional topical delivery systems. *Dermatologic Therapy, 24*(5), 471-476.

Winter, H. H. (1987). Can the gel point of a cross-linking polymer be detected by the $G' - G''$ crossover? *Polymer Engineering & Science, 27*(22), 1698-1702.

Wissing, S. A., and Müller, R. H. (2003). The influence of solid lipid nanoparticles on skin hydration and viscoelasticity – *In vivo* study. *European Journal of Pharmaceutics and Biopharmaceutics, 56*(1), 67-72.

Woo, J. O. (2014). *Stearic-oleic acid nanocarriers for cream formulation.* Master Thesis, University of Malaya, Kuala Lumpur, Malaysia.

Woo, J. O., Misran, M., Lee, P. F., and Tan, L. P. (2014). Development of a controlled release of salicylic acid loaded stearic acid-oleic acid nanoparticles in cream for topical delivery. *The Scientific World Journal, 2014*, 7.

Yang, F., Li, G., He, Y.-G., Ren, F.-X., and Wang, G.-x. (2009). Synthesis, characterization, and applied properties of carboxymethyl cellulose and polyacrylamide graft copolymer. *Carbohydrate Polymers, 78*(1), 95-99.

Yenilmez, E., Basaran, E. and Yazan, Y. (2011). Release characteristics of Vitamin E incorporated chitosan microspheres and *in vitro-in vivo* evaluation for topical application. *Carbohydrate Polymers, 84*(2), 807-811.

Yuguchi, Y., Urakawa, H., and Kajiwara, K. (2003). Structural characteristics of carrageenan gels: Various types of counter ions. *Food Hydrocolloids, 17*(4), 481-485.

Zhang, Y., Bai, Y., Jia, J., Gao, N., Li, Y., Zhang, R., Jiang, G., and Yan, B. (2014). Perturbation of physiological systems by nanoparticles. *Chemical Society Reviews, 43*(10), 3762-3809.

zur Mühlen, A., Schwarz, C., and Mehnert, W. (1998). Solid lipid nanoparticles (SLN) for controlled drug delivery – Drug release and release mechanism. *European Journal of Pharmaceutics and Biopharmaceutics, 45*(2), 149-155.

LIST OF PUBLICATIONS

Lim, Q. Y. and Misran, M. (2017). Rheological and physicochemical characterization of *alpha*-tocopherol loaded lipid nanoparticles in thermoresponsive gel for topical application. *Malaysian Journal of Fundamental and Applied Science, 13*(3), 248-252.

Lim, Q. Y. and Misran, M. (2017). Thermoresponsive gel mixture carboxymethyl cellulose and *iota*-carrageenan for topical delivery of hydroquinone. *Polymer Science.* (Accepted)

MJFAS MALAYSIAN JOURNAL OF FUNDAMENTAL AND APPLIED SCIENCES
PRINT ISSN: 2289-5981 | ONLINE ISSN: 2289-599X

RESEARCH ARTICLE

Rheological and physicochemical characterization of *alpha*-tocopherol loaded lipid nanoparticles in thermoresponsive gel for topical application

Lim Qian Ying and Misni Misran*

Department of Chemistry, Faculty of Science, University of Malaya, 50603 Kuala Lumpur, Malaysia

* *Corresponding author: misni@um.edu.my*

Article history
Received 18 February 2017
Accepted 4 July 2017

Abstract

Features of a thermoresponsive gel are advantageous for topical application. Lipid nanoparticles is incorporated as a carrier for a hydrophobic active ingredient which is not stable in the aqueous gel system. In this work, a thermoresponsive gel mixture consists of carboxymethyl cellulose (CMC) and *iota*-carrageenan (*ι*-C) was prepared. Nanostructured lipid carriers (NLC) made of fatty acids and lecithin was incorporated into the gel formulation as a carrier for *alpha*-tocopherol. Temperature effect on the rheological behavior of the prepared gel mixture was investigated. The NLC was evaluated for its mean particle size, zeta potential, morphology, encapsulation efficiency and *in vitro* drug release. Physicochemical characterization showed that *alpha*-tocopherol loaded NLC being stored at 4˚C was stable for 1 month and encapsulation efficiency of *alpha*-tocopherol was more than 90% for all formulations due to its hydrophobicity to stay in the lipid matrix. *In vitro* release studies proved that NLC was able to provide slow release of loaded *alpha*-tocopherol. On the other hand, the phase transition from gel-like to liquid-like of the formulated gel mixture was proven to be activated by temperature changes. The rheological gelling point of the gel mixture was represented by the crossover point of storage modulus, *G'* and loss modulus, *G"* which was obtained in the vicinity of body temperature 37˚C. This property is useful in topical application for its better spreadability on skin upon usage and hence better penetration for the *alpha*-tocopherol loaded NLC across the skin barrier. Prolong release of *alpha*-tocopherol with enhanced stability is favored as *alpha*-tocopherol is commonly known for its potent antioxidant activities. These results suggested that gel mixture of CMC and *ι*-C is a good candidate to be developed as a thermoresponsive gel while lipid nanoparticles is a promising carrier system for *alpha*-tocopherol in topical use.

Keywords: Rheology, thermoresponsive gel, lipid nanoparticles, topical application

INTRODUCTION

Topical drug delivery represents a promising route mainly for treatment of localized skin diseases and cosmetic use. A gel is commonly defined as a phase dispersed in another continuous phase forming a three-dimensional network by chemical covalent bond or physical interactions (Nishinari, 2009). It is one of the most general semisolid formulations used in topical application for its good stability against separation and lack of greasiness upon usage. However, active compounds tend to degrade in the dispersing aqueous medium of the gel during storage, thus greatly reduces the effectiveness of the product. Moreover, active compounds are difficult to penetrate across our skin barrier. In fact, skin being the organ most exposed to the environment prevents most external substances penetrating into our body (Friberg, 1990). In order to enhance the penetration and stability of active compounds, a carrier system is incorporated into the gel formulation to provide a more efficient drug delivery.

Colloidal carrier systems had been widely employed to overcome the limitations of conventional dermal formulations in pharmaceutical and cosmetics industries. As an alternative to emulsions, liposomes and polymeric nanoparticles, lipid nanoparticles such as solid lipid nanoparticles (SLN) and nanostructured lipid carriers (NLC) were developed not only to provide improved features but also to meet the industrial needs including low cost and easiness for large scale production. Those features found in lipid nanoparticles are advantageous for dermal products for instances occlusive properties, modified release profile and avoidance of systemic uptake (Beck *et al.*, 2011). Lipid nanoparticles are mainly utilized to load hydrophobic drug in its lipid core or lipid outer shell depending on the production method (Üner *et al.*, 2007). The encapsulated drug is therefore protected against chemical degradation caused by the surrounding environment and dispersing medium such as light, oxidation and hydrolysis by water. In addition, the nanoparticles provide prolong release of drug to enhance its effectiveness and avoid irritation to the skin (Dingler *et al.*, 1999; Grana *et al.*, 2013).

Alpha-tocopherol is a form of lipid-soluble vitamin E with potent antioxidant properties essential for health. Oxidation is always related to numerous diseases especially cancer and aging, therefore daily intake of vitamin E is necessary (Podda *et al.*, 2001; Rizvi *et al.*, 2014). Besides dietary intake either from food or supplements, vitamin E can be applied topically to nourish our skin with the main purpose to prevent aging. Shylaja *et al.* (2016) had shown the enhanced stability and slow release property of vitamin E loaded in SLN.

In this study, *alpha*-tocopherol was loaded in lecithin-fatty acid nanoparticles which were then incorporated into a thermoresponsive gel mixture. The aim of employing a thermoresponsive gel instead of a

Thermoresponsive Gel Mixture Carboxymethyl Cellulose and *iota*-Carrageenan for Topical Delivery of Hydroquinone

Q.Y. Lim[a], M. Misran[a*]

[a] *Department of Chemistry, Faculty of Science, University of Malaya, 50603 Kuala Lumpur, Malaysia*

[*]*Corresponding author, e*-mail*: misni@um.edu.my*

Abstract Property of a gel that responses to heat change contributes many advantages in topical application where the rheological properties illustrate stability of gel during storage and its spreadability upon application. In this work, a gel mixture consists of carboxymethyl cellulose (CMC) and *iota*-carrageenan (*ι*-C) was prepared and its rheological properties under temperature and Ca^{2+} ions effect were evaluated. Subsequently, hydroquinone was incorporated into the optimized gel formulation to study its *in vitro* release at 30 °C and 37 °C. Higher concentration of cation Ca^{2+} was proven to increase the gel strength, however there was a limit where the concentration of cation does not affect the viscosity, η and storage modulus, G' of the system anymore. The phase transition of the gel mixture from solid-like to liquid-like was thermally activated and reversible. The gel mixture with gelling point in the vicinity of body temperature was selected as the optimized formulation. *In vitro* release revealed the effect of thermoresponsive behavior of gel on delivery of active ingredient. The formulation showed flowing behavior at 37 °C where it provided enhanced release of hydroquinone. These results suggested that gel mixture of CMC and *ι*-C is a good candidate to be developed as a thermoresponsive gel for topical delivery of hydroquinone.

Keywords: polysaccharides, thermoresponsive gel, topical delivery, viscoelastic properties

[1] This work was supported by Fundamental Research Grant Scheme (FRGS), Grant no. FP013-2015A and Postgraduate Research Grant (PPP), Grant no. PG114-2016A from University of Malaya, Malaysia.